SEISMIC ENERGY DISSIPATION, SELF-CENTERING, AND SETTLEMENT OF ROCKING FOUNDATIONS: ANALYSIS OF EXPERIMENTAL DATA WITH COMPARISONS TO NUMERICAL MODELING

A Thesis
Submitted to the Graduate Faculty
of the
North Dakota State University
of Agriculture and Applied Science

By

Sujitha Soundararajan

In Partial Fulfillment of the Requirements
for the Degree of
MASTER OF SCIENCE

Major Department:
Civil Engineering

August 2019

Fargo, North Dakota

North Dakota State University
Graduate School

Title

SEISMIC ENERGY DISSIPATION, SELF-CENTERING, AND SETTLEMENT OF ROCKING FOUNDATIONS: ANALYSIS OF EXPERIMENTAL DATA WITH COMPARISONS TO NUMERICAL MODELING

By

Sujitha Soundararajan

The Supervisory Committee certifies that this ***disquisition*** complies with North Dakota State University's regulations and meets the accepted standards for the degree of

MASTER OF SCIENCE

SUPERVISORY COMMITTEE:

Dr. Mijia Yang
Advisor

Dr. Sivapalan Gajan
Co-Advisor

Dr. Zhibin Lin

Dr. Zhili Gao

Approved:

08/19/2019
Date

Dr. David R. Steward
Department Chair

ABSTRACT

The major objective of this study is to correlate the rocking foundation performance parameters with their capacity parameters and earthquake demand parameters using the results obtained from 142 centrifuge and shaking table experiments. It is found that seismic energy dissipation and permanent settlement of rocking foundations correlate well with rocking coefficient and Arias intensity of the earthquake, whereas the maximum moment and peak rotation of the foundation correlate well with peak ground acceleration. A numerical model, using the contact interface model available in OpenSees, is developed to simulate the performance of rocking foundations, and it is validated using experimental results. Though the numerical model predicts the moment capacity, seismic energy dissipation, and tipping-over stability of rocking foundations reasonably well, the model appears to overpredict the settlement of foundations. Furthermore, a parametric study showed that settlement reduces as initial vertical stiffness increases and is directly proportional to peak ground displacement.

ACKNOWLEDGEMENTS

I would like to thank my advisors Dr. Mijia Yang and Dr. Sivapalan Gajan, for their guidance and support, without whom this research would have been impossible.

I would also like to thank my respective graduate committee, Dr. Zhibin Lin and Dr. Zhili Gao, for their invaluable input and guidance to complete this work.

I am thankful to my colleagues at my office, and also my friends Amritha, Subha, Sunoj and Saravanan (Anna) for their continuous support towards my completion of this thesis.

And finally, to the Department of Civil and Environmental Engineering at North Dakota State University for giving me the opportunity to complete this master's degree and also ND – EPSCoR for the funding in my last year of master's program.

DEDICATION

To my Parents, Vijay, Sruthi, and Tarun

TABLE OF CONTENTS

LIST OF TABLES

LIST OF FIGURES

1. INTRODUCTION AND LITERATURE REVIEW

1.1. Research Background

One of the major changes in the traditional seismic design procedures, adopted in the design guidelines of National Earthquake Hazard Reduction Program (NEHRP) in 2000, was that by allowing rocking behavior of foundations and mobilization of the ultimate capacity, the force and ductility demands transmitted to structures can be reduced (FEMA 2000). This is a beneficial consequence of dissipation of seismic energy below foundation by yielding of soil. In fact, it has been shown that "soil failure" (yielding of soil) can be used for seismic protection of structures (Anastasopoulos et al. 2010). In addition, it has been observed that after some earthquakes in Japan, a number of structures resting on spread footings responded to seismic excitation by rocking on their foundations and thus avoiding failure (Mergos and Kawashima 2005). However, concerns about rocking induced permanent settlement of foundation due to plastic shearing of soil and excessive rotation of the foundation that could possibly lead to tipping-over failure of the structure have hindered use of foundation rocking as an efficient and effective energy dissipation mechanism to reduce/eliminate damage in structures in civil engineering practice.

1.1.1. Background on experimental analysis

Recently many researchers have conducted centrifuge and shaking table experiments to examine both the beneficial and detrimental effects of rocking foundations (for e.g., Gajan et al. 2005; Gajan and Kutter 2008a and 2009a; Drosos et al. 2012; Deng et al. 2012; Deng and Kutter 2012; Hakhamaneshi et al. 2012; Anastasopoulos et al. 2013; Tsatsis and Anastasopoulos 2015; Antonellis et al. 2015). Their major findings reveal that shallow foundations, with controlled rocking, possess many desirable characteristics such as well-defined capacity, excellent ductility,

isolation, and excellent self-centering characteristics. Despite all these experimental and field case history evidence, foundation rocking and soil yielding still remain as an unreliable/unproven energy dissipation mechanism for reducing ductility demands on the structure.

1.1.2. Background on numerical analysis

Non-linear cyclic load-displacement response of soil-foundation systems subjected to seismic loading can be modeled using beam on non-linear Winkler foundation model (BNWF), macro-element model, and finite-element/finite-difference model (modeling superstructure, foundation and soil in detail). The BNWF model captures the settlement-rotation response of the footing based on input acceleration (Houlsby et al., 2005; Harden and Hutchinson, 2006; Raychowdhury and Hutchinson, 2009). However, in BNWF model, the moment capacity and shear capacity are not coupled, instead modeled as individual springs. In this study, a macro-element model is adopted, which captures the moment-rotation and settlement-rotation of the footing effectively by coupling the vertical, horizontal, and moment capacity. In the macro-element model chosen for this study, the entire soil-foundation system is considered as a single element and modeled as contact interface model (CIM) (Gajan and Kutter, 2008b; Gajan and Kutter 2009a).

1.2. Scope of the Research

1.2.1. Objective

This study analyzes the results of 142 centrifuge and shake table experiments conducted in US, Greece and Italy. The intention of this research is to combine and make sense of the results obtained by the previous researchers involving a wide range of soil, foundation, and structure properties through correlating several key parameters of rocking systems. In order to achieve this goal, an extensive analysis of experimental results was carried out and a numerical

model is developed using CIM available in OpenSees to effectively capture the nonlinear load-deformation behavior in the soil-footing interface of shear wall and bridge-pier supported by rocking foundations and validated against experimental results to measure the accuracy of the model.

The primary objectives of this study are,

- To summarize, in meaningful engineering parameters, the results obtained from 142 centrifuge and shaking table experiments on rocking foundations that involve a wide range of soil, foundation, and structure properties, and varying magnitudes of earthquake shakings.
- To explore possible correlations between rocking system capacity parameters (rocking coefficient, critical contact area ratio, and slenderness ratio), earthquake demand parameters (Arias intensity and peak ground acceleration), and rocking system performance parameters (moment capacity, seismic energy dissipation, permanent settlement, and self-centering ability).
- To develop a numerical model using the soil-foundation contact interface model (CIM), available in OpenSees finite element platform, that captures the essential features of rocking shallow foundations, and to validate the numerical model performance using experimental results.
- To perform a parametric study to evaluate the combined effects of initial vertical stiffness and peak ground displacement on permanent settlement of rocking foundations using the numerical model developed in this study

1.2.2. Methodology

The major goal of this research is to highlight the potential benefits of rocking behavior of shallow foundations in terms of energy dissipation, permanent rotation, self-centering characteristics, and stability against tip-over failure. Therefore, the correlation of performance parameters with capacity and demand parameters using experimental analysis and numerical model was a paramount task. The collected 142 experimental data was summarized and analyzed to compute the performance parameters, and the correlation of capacity parameters, demand parameters, and performance parameters was achieved by grouping different range of rocking coefficient and aspect ratio of the structure-footing system. Further, a reliable numerical model was developed using CIM available in OpenSees to effectively capture the nonlinear load deformation behavior of shear wall and bridge-pier supported with rocking foundation. Initially, the model was developed using theoretical values, validated with the experimental results, and further used to compute the performance parameters for selected events.

As the numerical model was overpredicting the settlement values for certain experimental data, a simple parametric study was carried out to study the effects of initial vertical stiffness and peak ground displacement on settlement using two earthquake events (Kobe 1995, and Gazli 1975). The initial vertical stiffness is varied by changing shear modulus values and the corresponding permanent settlement was determined using numerical model developed in this study. Also, the effects of friction angle of sand and shear strength of clay on moment capacity compared to bearing capacity was also studied to reinforce the previous research findings by varying vertical factor of safety (FS_v) and critical contact area ratio (A/A_c) in conventional bearing capacity equations.

1.3. Organization of the Thesis

This thesis consists of six chapters and the following summarizes the content of each chapter,

- Chapter 1: Introduction and the previous research which include background to the experimental analysis, background to the numerical analysis, objectives, and thesis organization.
- Chapter 2: Discussion on rocking system parameters which includes capacity parameters such as rocking coefficient and base shear coefficient; demand parameters such as Arias intensity and maximum acceleration; performance parameters such as cyclic rotation, energy dissipation, permanent settlement, self-centering ability, and tipping-over stability.
- Chapter 3: Summarization of extensive experimental analysis on centrifuge and shake table tests conducted in US, Greece and Italy and effect of rocking coefficient on energy dissipation and permanent settlement.
- Chapter 4: Development and validation of the shear wall and bridge-pier model using OpenSees and filling the parameter gaps in experimental results using the validated numerical model.
- Chapter 5: Evaluation of moment capacity on friction angle of sand or shear strength of clay and the effects of initial vertical stiffness and maximum acceleration on permanent settlement.
- Chapter 6: Conclusions and recommendations for future work.

2. ROCKING SYSTEM PARAMETERS

2.1. Introduction

In this chapter, the rocking system parameters such as capacity parameters, demand parameters, and performance parameters used for the analysis are presented, and the relation between the rocking system parameters are discussed.

2.2. Capacity Parameters

The following capacity parameters such as, critical contact area ratio, rocking coefficient, slenderness ratio and base shear coefficient are discussed below.

2.2.1. Critical contact area ratio

The critical contact area ratio (A/A_c) is defined as the ratio of total base area of the footing (A) to the minimum footing contact area with the soil required to support the applied vertical loads on the foundation (A_c) (which can be calculated from conventional bearing capacity equation and the associated shape and depth factors (Gajan and Kutter, 2008a); (given in chapter 4).

The bearing capacity factors, shape factors, and depth factors (Terzaghi, 1943, De Beer, 1970, and Hansen, 1970) indicate that A/A_c is different from FS_v, as contact geometry changes during foundation rocking (Equation 2.2).

$$FS_v = \frac{V_{ult}}{V} \tag{2.1}$$

$$\frac{A}{A_c} \neq FS_v \tag{2.2}$$

2.2.2. Rocking coefficient and slenderness ratio

The rocking coefficient (C_r) of a soil-foundation system is defined as the ratio of ultimate moment capacity (M_{ult}) of the foundation to the applied vertical load on the foundation (V or P_{st}) normalized by the effective height of the structure (height from the base center point of the

footing to the center of gravity of the structure, h). By considering equilibrium equations and the moment capacity of soil-foundation system, the following equation can be obtained for C_r,

$$C_r = \frac{L}{2.h}.\left[1 - \frac{A_c}{A}\right] \quad (2.3)$$

C_r is a non-dimensional, normalized ultimate moment capacity of the soil-foundation system that combines the effects of A/A_c (or FS_v) and the slenderness ratio of the structure-foundation system (h/L). Note that C_r is defined the same way as the base shear coefficient (C_y) for a structural (reinforced concrete) column.

2.2.3. Base shear coefficient

C_y is defined as the ratio of yield moment capacity of column (M_{cy}) to the product of weight (V) of the structure and the effective height of the structure (h):

$$C_y = \frac{M_{cy}}{V.h} \quad (2.4)$$

The relative values of C_y and C_r of a soil-foundation-structure system dictate whether the overall system's behavior during seismic loading would be structural-yield dominated or foundation-soil-yield dominated (rocking). In conventional seismic design of foundations (fixed-base), typically C_y is smaller than C_r, and hence structural yielding is encouraged while relative movement between soil and footing is restricted or prohibited during intense earthquake shaking. However, Deng et al. (2012), for example, using centrifuge experiments, showed that plastic hinging can be forced to occur at foundation soil during rocking by making sure that C_r is smaller than C_y. Similarly, Anastasopoulos et al. (2010), for example, using numerical simulations, showed how soil yielding (mobilization of ultimate bearing capacity) during foundation rocking ($C_r < C_y$) can be used for seismic protection of structures. Godagama (2016) showed how the beneficial effects of foundation rocking can be utilized while minimizing the detrimental effects of rocking by appropriately selecting C_r values in design. Conceivably, the

hinging mechanism ("fuse") can be forced to occur either at structural elements or foundation soil by appropriately designing C_r and C_y values.

2.3. Demand Parameters

The demand parameters such as Arias intensity and acceleration transmitted to the superstructure and its relation with capacity parameters are presented below.

2.3.1. Arias intensity

In addition to peak ground motion parameters such as maximum ground displacement and acceleration (a_{max}), another way of quantifying the intensity of an earthquake is Arias intensity (Kramer, 1996). Arias intensity (I_a) combines the magnitude, frequency content, and duration of shaking, and is defined as,

$$I_a = \frac{\pi}{2.g} \int_0^{\infty} [a(t)]^2 \, dt \tag{2.5}$$

where g is the gravitational acceleration and a(t) is the shaking acceleration time history.

2.3.2. Acceleration transmitted to structure

By comparing the maximum moment transmitted to the soil-foundation interface due to the inertial forces from the structure to the ultimate moment capacity of the foundation, the following relationships can be obtained,

$$M_{ult} \geq \left[\frac{V}{g}.a_{max,str}.h + V.h.sin(\theta)\right] \tag{2.6}$$

$$\frac{a_{max,str}}{g} \leq \frac{B}{2.h}.\left[1 - \frac{A_c}{A}\right] - \theta \tag{2.7}$$

where $a_{max,str}$ is the maximum horizontal acceleration transmitted to the center of gravity of the structure. Note that θ is in radians in Equation 2.7 and sin (θ) is approximately equal to θ for relatively small values of θ (θ < 0.1 rad.). If P-Δ effect (θ, effect of lateral eccentricity of the vertical load on foundation) is neglected, then Equation 2.7 can simply be written as,

$$\frac{a_{max,str}}{g} \leq C_r \quad (2.8)$$

Note that $a_{max,str}$ is also proportional to the maximum base shear force experienced by the structure during shaking and hence it is a good parameter to gauge the earthquake induced force demands on the structure. Acceleration amplification ratio (AAR) of a rocking foundation is defined as,

$$AAR = \frac{a_{max,str}}{a_{max,base}} \quad (2.9)$$

2.4. Performance Parameters

The performance parameters such as moment capacity, maximum rotation, permanent settlement, energy dissipation, self-centering ability and tipping-over stability are discussed below.

2.4.1. Foundation (moment or rocking) capacity

The theoretical ultimate moment capacity (M_{ult}) of a rocking shallow foundation can be obtained using equilibrium equations of soil-foundation system and expressed as (Gajan and Kutter, 2008a),

$$M_{ult} = \frac{P_{st}.L}{2}.\left[1 - \frac{A_c}{A}\right] \quad (2.10)$$

where, P_{st} is the total applied vertical load on the foundation (this may include weight of the structure, weight of footing, and weight of soil above footing), L is the length of the footing in the direction of shaking, and A_c/A is the inverse of critical contact area ratio of the soil-foundation system. The first term (P_{st}.L/2) represents the moment capacity of a foundation supported by rigid base.

Due to the interaction between applied shear and moment at soil-foundation interface, the maximum moment that the foundation can resist is smaller than what Equation 2.10 predicts. However, the reduction in M_{ult} due to the presence of shear is negligible when the aspect ratio of

the structure-foundation system (h/L) is greater than one, which is commonly the case for rocking dominated systems (as opposed to sliding-dominated) (Gajan and Kutter, 2009).

It should be noted that the above equation for M_{ult} (Equation 2.10) assumes a uniform ultimate bearing stress distribution under the footing-soil contact area and ignores the effects of passive resistance in front of the footing and side resistance of soil adjacent to the footing. Gajan and Kutter (2008b) showed that the relative error in M_{ult} by ignoring the side friction and passive resistance of soil is up to about 5% for relatively shallow embedded ($D \leq B$) foundations, where D is the depth of embedment of the footing. It has been shown (also evident from Equation 2.10) that the moment capacity of a rocking footing is well defined and, unlike bearing capacity, moment capacity is less sensitive to the uncertainty in soil properties as A/A_c increases. Gajan and Kayser (2017) showed that M_{ult} of the soil-foundation system is more sensitive to (about 75% or more) the applied vertical load on the foundation (P_{st}) than any soil properties.

2.4.2. Cyclic rotation

It is postulated (also found from experimental evidence) that the rocking induced maximum rotation of the foundation is primarily a function of aspect ratio of the structure-foundation system (h/L) and maximum acceleration of the earthquake (a_{max}).

$$\theta_{peak} = f\left(\frac{h}{L}, a_{max}\right) \tag{2.11}$$

Gajan and Kayser (2017), using parametric studies of numerical simulations, showed that the maximum rotation of a rocking foundation depends mainly on a_{max} rather than P_{st} or FS_v or the vertical stiffness of the soil-foundation system (K_v). The magnitude rocking induced rotation of the structure also depends on the aspect ratio (h/L), as h/L predominantly controls the applied moment-to-shear ratio (M/(h.L)) at the footing soil interface (Gajan and Kutter, 2009) (Equation 2.12).

$$\frac{M}{H.L} \approx \frac{h}{L} \tag{2.12}$$

For relatively rigid structures supported by rocking foundations, the maximum lateral displacement at the center of gravity of the structure (Δ_{max}) can then obtained by,

$$\Delta_{max} = \theta_{peak}.h \tag{2.13}$$

Note also that the sliding displacement of the foundation is not considered in this study, because it has been shown that as long as h/L > 1.0, the rocking motion dominates and sliding displacements are negligible (Gajan and Kutter, 2009).

2.4.3. Permanent settlement

It is hypothesized (also found from experimental evidence) that the rocking induced total permanent settlement of the foundation (S_{tot}) could be a function of two parameters, C_r and I_a, as they incorporate the effects of foundation geometry, aspect ratio of the structure, soil parameters, and intensity of the earthquake, i.e.,

$$S_{tot} = f(C_r, I_a) \tag{2.14}$$

The other parameters that could potentially affect S_{tot} include θ_{peak} and L. The normalized total permanent settlement is defined as,

$$\frac{S_{tot}}{L} = f\left(C_r, I_a, \theta_{peak}\right) \tag{2.15}$$

It is well known that S_{tot} also depends on the vertical stiffness of the soil-foundation system (K_v). It is assumed that the effect of K_v on S_{tot} is indirectly included through FS_v and/or A/A_c and hence through C_r (as strength and stiffness are typically correlated for common soil types).

2.4.4. Energy dissipation

As shearing of soil beneath the foundation dissipates seismic energy through friction during rocking, the amount of energy dissipation (E) can be calculated primarily from the area

enclosed by the hysteresis loops in the cyclic moment-rotation (M - θ) relationship of the soil-foundation system,

$$E = \int_0^{\theta_{fin}} M.d\theta \tag{2.16}$$

A non-dimensional normalized energy dissipation (E_{nor}) is then obtained by normalizing E by the weight of the structure (V or P_{st}) and the dimension of the footing in the direction of shaking (L),

$$E_{nor} = \frac{E}{V.L} \tag{2.17}$$

As the amount of energy dissipation in foundation soil mainly depends on the foundations ability to rock and the magnitude of shaking, it was hypothesized that E is primarily a function of three key parameters discussed earlier, C_r, a_{max}, and I_a.

$$E_{nor} = f(C_r, a_{max}, I_a) \tag{2.18}$$

As rotation causes energy dissipation and resulting settlement, in general, both the amount of energy dissipation and total settlement increase as the magnitude of rotation increases. Since these three mechanisms are inter-related, it can also be postulated that,

$$E_{nor} = f\left(C_r, \theta_{peak}, \frac{S_{tot}}{L}\right) \tag{2.19}$$

2.4.5. Self-centering ability

Permanent tilt or rotation (θ_{perm}) of the foundation is one of the important parameters that needs to be investigated at the end of the earthquake to determine the severity of the damage and the self-centering ability of rocking foundations. It was found that θ_{perm} can be correlated to maximum rotation during shaking and the intensity of the earthquake,

$$\theta_{perm} = f(\theta_{peak}, I_a) \tag{2.20}$$

For relatively rigid structures supported by rocking foundations, the permanent lateral displacement at the height of center of gravity of the structure (Δ_{per}) can then obtained by,

$$\Delta_{per} = \theta_{perm}.H \tag{2.21}$$

Two new ratios have been defined to quantify the self-centering capability and the stability against tipping over failure of rocking foundations. The first one is self-centering ratio (SCR) of a rocking foundation and it is be defined as,

$$SCR = \left[1 - \frac{\theta_{perm}}{\theta_{peak}}\right] \tag{2.22}$$

If $\theta_{perm,}$ is zero at the end of the shake, SCR is equal to one, indicating a perfectly self-centering rocking system, and if θ_{perm} is equal to θ_{peak} (when the foundation does not rebound back from the maximum rotation it has experienced during shaking), SCR is equal to zero, indicating a perfectly non-self-centering rocking system.

2.4.6. Tipping-over stability

Critical rotation of the structure (θ_{crit}) can be defined as the magnitude of rotation that would possibly cause tipping-over failure of the structure-foundation system during earthquake. Using static equilibrium conditions on the verge of tipping-over failure, the maximum horizontal displacement at the center of gravity of the structure (Δ_{crit}) during earthquake that would cause tipping over failure can be given by

$$\Delta_{crit} = \frac{L - L_c}{2} \tag{2.23}$$

where L_c is the critical contact length of the footing with the soil (in the direction of shaking) that is required to support applied vertical loads (Deng et al., 2012). For rectangular and square footings, the L_c and L terms are proportional to A_c and A, respectively. The critical rotation (θ_{crit}) can then be correlated to C_r as,

$$\theta_{crit} = tan^{-1}\left[\frac{\Delta_{crit}}{h}\right] = tan^{-1}(C_r) \tag{2.24}$$

The tipping-over stability ratio (TSR) of a rocking foundation can be defined as,

$$TSR = \left[1 - \frac{\theta_{peak}}{\theta_{crit}}\right] \tag{2.25}$$

If θ_{peak} is zero during the shake, TSR is equal to one, indicating a perfect stability against tipping over failure (e.g., fixed-based system), and if θ_{peak} is equal to θ_{crit}, TSR is equal to zero, indicating that the structure is on the verge of tipping-over failure. It is not advocated here that TSR be close to either zero or one. It is shown, in the later sections, that the beneficial effects of foundation rocking can be achieved while keeping TSR in between zero and one.

3. EXPERIMENTAL ANALYSES OF CENTRIFUGE AND SHAKE TABLE TESTS

3.1. Introduction

In this chapter, an extensive analysis of experimental results are carried out to explore the possible correlations between the rocking capacity parameters, performance parameters and demand parameters using 142 centrifuge and shake table tests subjected to dynamic loading. Also, the energy dissipation – total settlement – rotation relation is compared with different rocking coefficient values and presented in this chapter.

3.2. Experimental Details

The results obtained from five series of centrifuge tests and four series of shaking table tests (altogether 142 individual experiments) conducted in several facilities independently in US, Greece and Japan have been considered for the experimental analysis. Major details of these test series, including the type of soil used, are presented in Table 3.1.

Table 3.1

Test series, test type, soil type and references of the experiments

Test series	Test type	References	Soil type
T1	Centrifuge test	Gajan and Kutter (2008a)	Dry Nevada sand
T2	Centrifuge test	Gajan and Kutter (2008a)	Dry Nevada Sand
T3	Centrifuge test	Deng et al. (2012)	Dry Nevada Sand
T4	Centrifuge test	Deng and Kutter (2012)	Dry Nevada Sand
T5	Centrifuge test	Hakhamaneshi et al. (2012)	Clay and Nevada sand
T6	1g shake table test	Tsatsis and Anastasopoulos (2015)	Dry Longstone sand
T7	1g shake table test	Drosos et al. (2012)	Dry Longstone sand
T8	1g shake table test	Antonellis et al. (2015)	Washed concrete sand
T9	1g shake table test	Anastasopoulos et al. (2013)	Dry Longstone sand

Table 3.2 presents the details of the types of structures and foundations, including the depth of embedment, used in all the experiments, while Table 3.3 presents the ranges of rocking

system parameters varied in all the experiments. As can be seen from Table 3.1, Table 3.2, and Table 3.3, the 142 experimental results analyzed and summarized in the study covers a wide range of soil, foundation, and structure types, a wide range of rocking system parameters (C_r, A/A_c, FS_v), and a wide range of the intensity of earthquakes.

Table 3.2

Details of structures and foundations used in the experiments

Test series	Structure details	Length of footing (m)	Width of footing (m)	Depth of footing (m)
T1	Rigid shear wall	2.8	0.65	0.7
T2	Rigid shear wall	2.8	0.65	0
T3	SDOF - Lollipop	6.7	4.28	2.24
T4	SDOF - Lollipop	7.35	4.7	2.24
T5	SDOF - Lollipop	1.6-6.66	1.67-10.6	0.15-0.6
T6	Slender bridge pier	3	3	0
T7	Bridge pier	7-11	1.14-1.7	0
T8	Bridge column	1.52	1.52	0.66
T9	Bridge pier	7-11	1.4-1.7	0

Table 3.3

Range of rocking system parameters

Test series	A/A_c	FS_v	C_r	PGA (g)	h/L
T1	7.1-10	7.2-11.5	0.235-0.236	0.12-0.90	1.78-1.89
T2	2.2-3.2	2.6-4	0.147-0.176	0.12-0.90	1.78-1.89
T3	14	15	0.303	0.62-0.95	`1.624
T4	10	11	0.353	0.218-0.882	1.267
T5	3.01-17.14	3.4-19.1	0.226-0.314	0.1-0.7	1.365-1.488
T6	1.9-8.04	2.5-14	0.082-0.183	0.072-1.25	0.356-0.424
T7	2.05-5.21	2.3-7.3	0.13-0.34	0.15-0.5	1.2-1.9
T8	11.3-13.5	23.2-24.5	0.25-0.29	0.40-0.95	1.74
T9	2.75-5.21	3.3-6.9	0.17-0.34	0.46-0.82	1.2-1.9

The experimental details such as footing and structural dimensions, soil type, PGA, FS_v, A/A_c and C_r of centrifuge test and shake table test of all series are shown in the following figures. Figure 3.1 (a) presents an example experimental set up of one centrifuge experiment in T1 - SSG03 series of shear wall structure. Figure 3.1 (b) presents an example experimental set up of one centrifuge experiment in T2 - SSG04 series of shear wall structure.

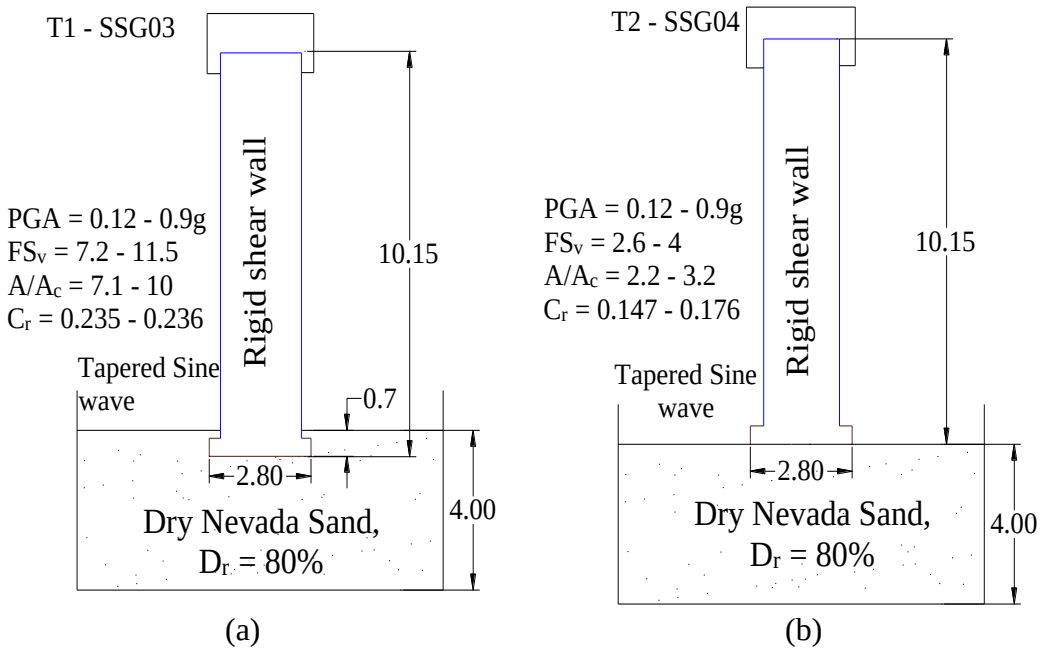

Figure 3.1. (a) Test set up of T1 - SSG03 (b) Test set up of T2 – SSG04 (Gajan and Kutter 2008a)

Figure 3.2 (a) presents an example experimental set up of one centrifuge experiment in T3 – LJD01 series of SDOF structure with notched column. Figure 3.2 (b) presents an example experimental set up of one centrifuge experiment in T4 - LJD03 series.

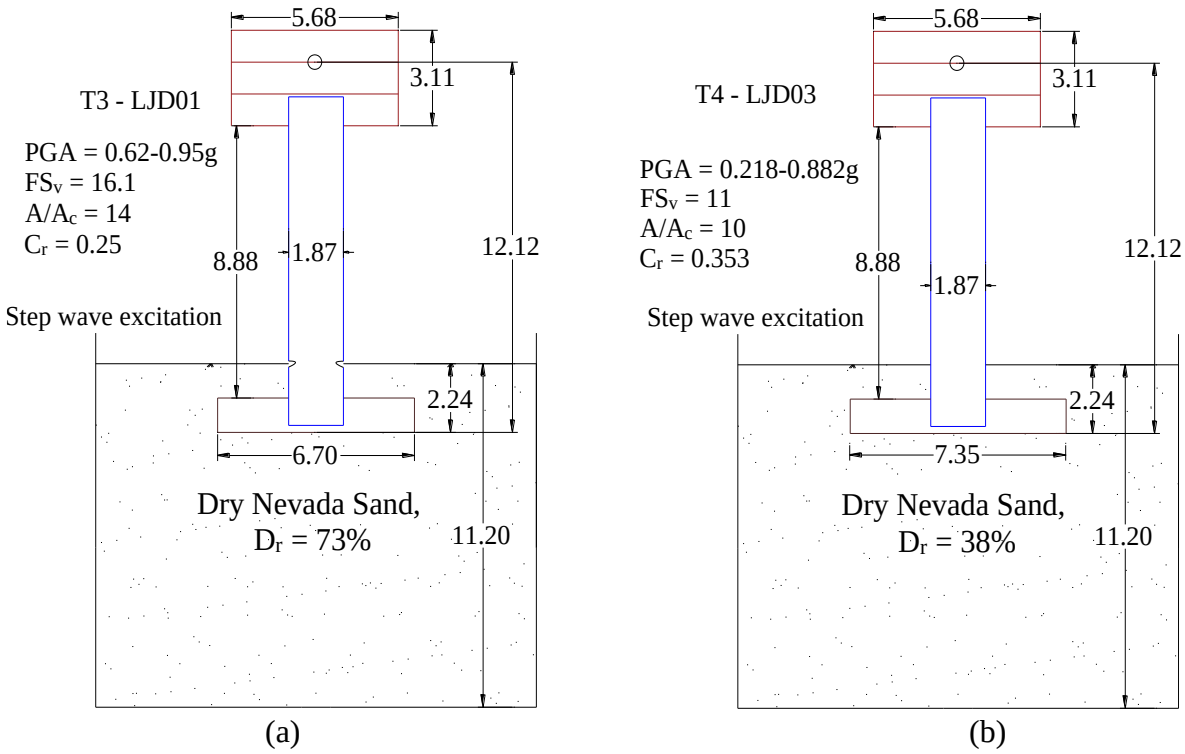

Figure 3.2. (a) Test set up of T3 – LJD01 (Deng et al, 2012) (b) Test set up of T4 – LJD03 (Deng and Kutter, 2012)

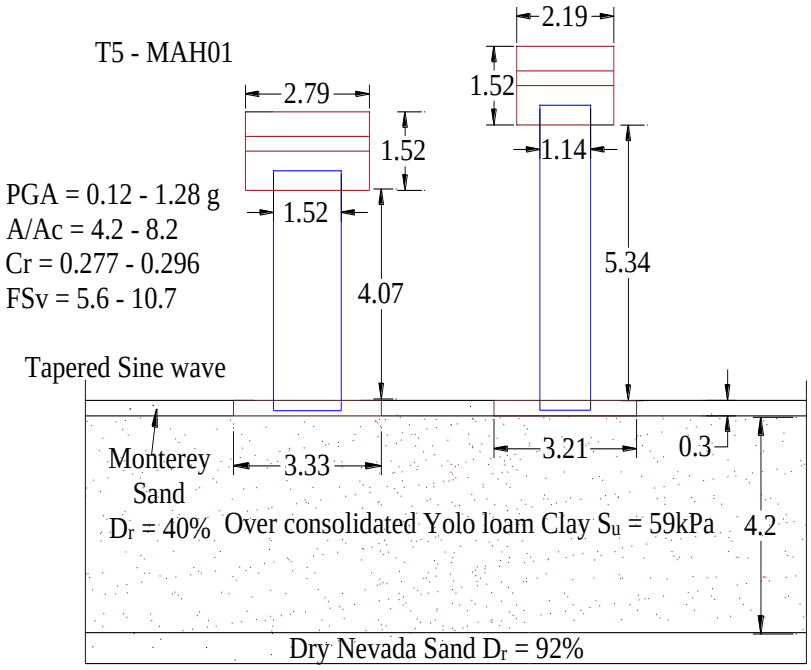

Figure 3.3. Test set up of T5 – MAH01 (Hakhamaneshi et al, 2012)

Figure 3.3 presents an example experimental set up of one centrifuge experiment in T5 – MAH01 series conducted on clay soil with S_u = 59kPa.

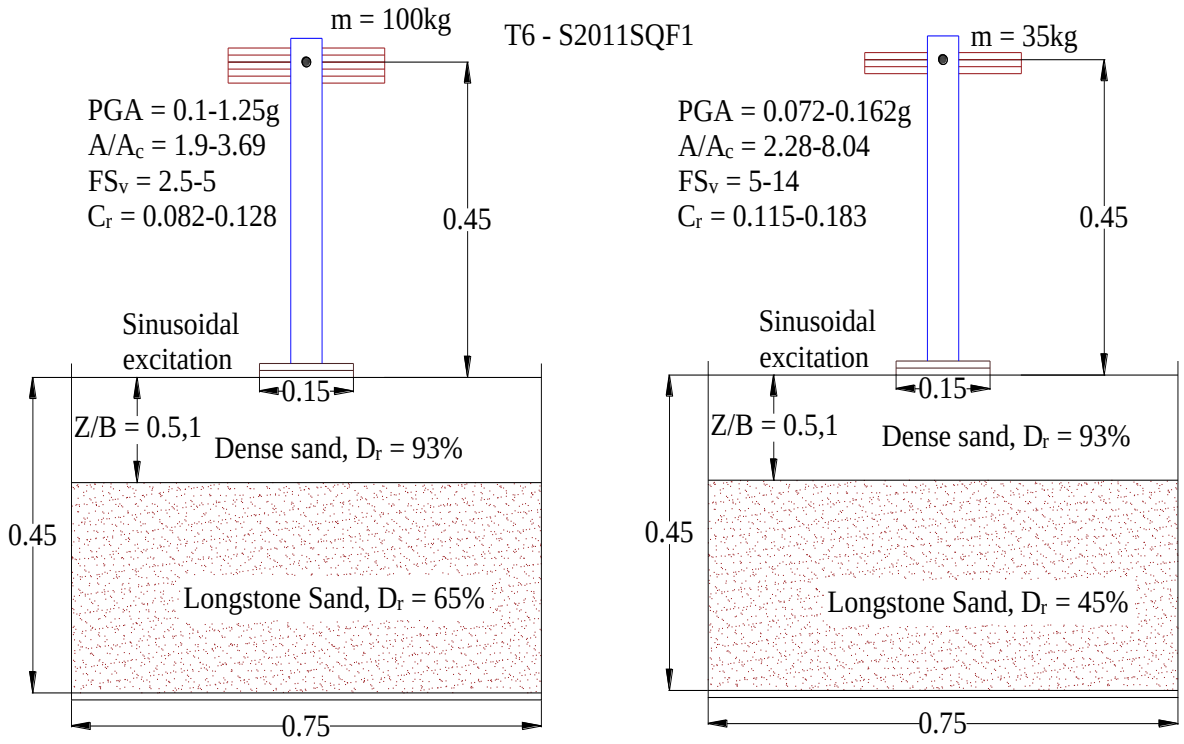

Figure 3.4. Test set up of T6 – S2011SQF1 (Tsatsis and Anastasopoulos, 2015)

Figure 3.4 presents an example experimental set up of one shake table test in T6 – S2011SQF1 series. Figure 3.5 presents an example experimental set up of one shake table test in T7 series.

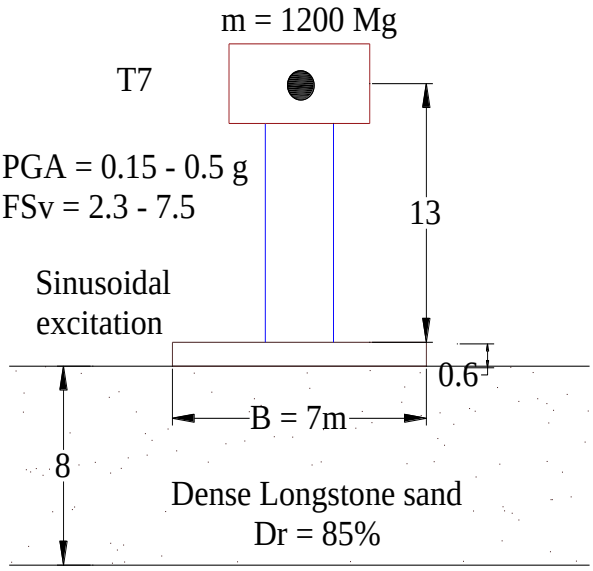

Figure 3.5. Test set up of T7 – (Drosos et al, 2012)

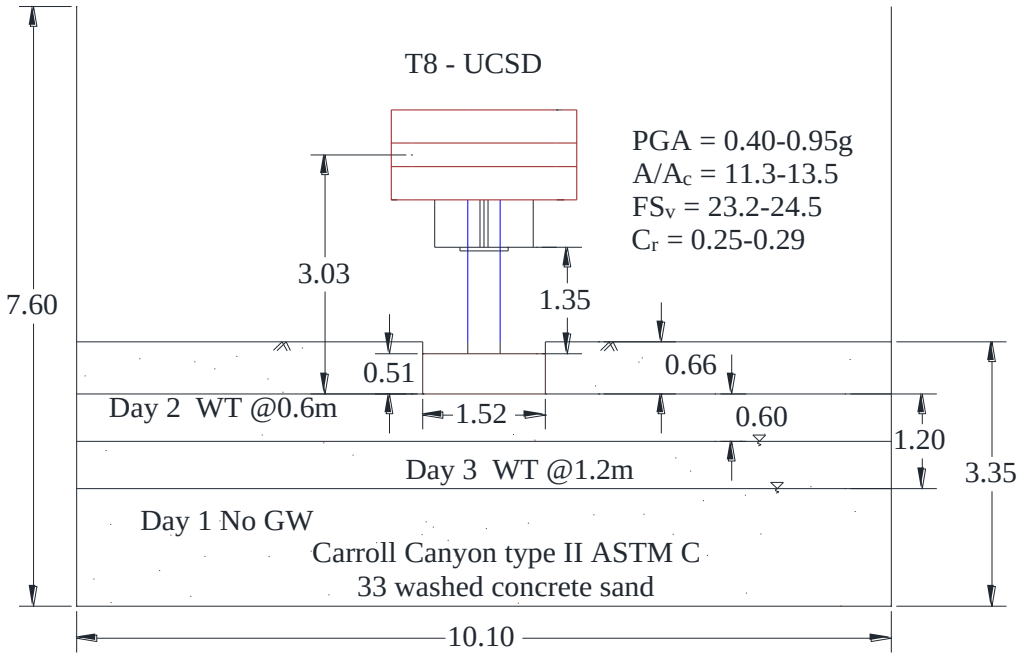

Figure 3.6. Test set up of T8 – UCSD (Antonellis et al, 2015)

Figure 3.6 presents an example experimental set up of one shake table test in T8 series and Figure 3.7 presents an example experimental set up of one shake table test in T9 series.

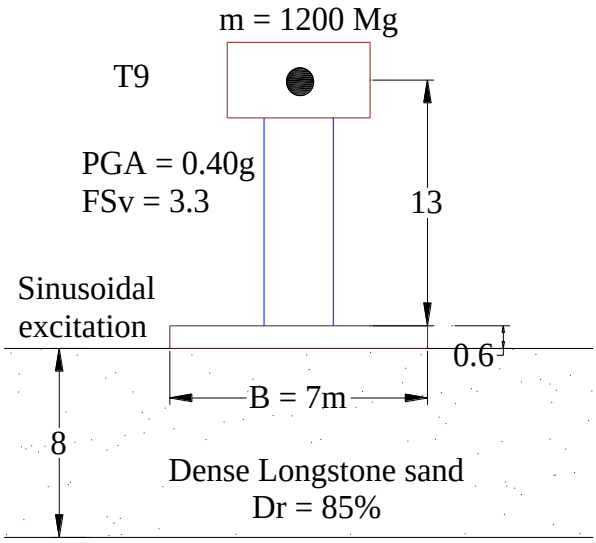

Figure 3.7. Test set up of T9 (Anastasopoulos, 2013)

3.3. Experimental Results from Each Test Series

The base horizontal acceleration of one experiment from each test series is given in Figure 3.8. The input acceleration of test series T2, T3, T4 and T6 are shown in Figure 3.8 (a). The input acceleration of one experiment from test series T1, T5 and T8 are shown in Figure 3.8 (b).

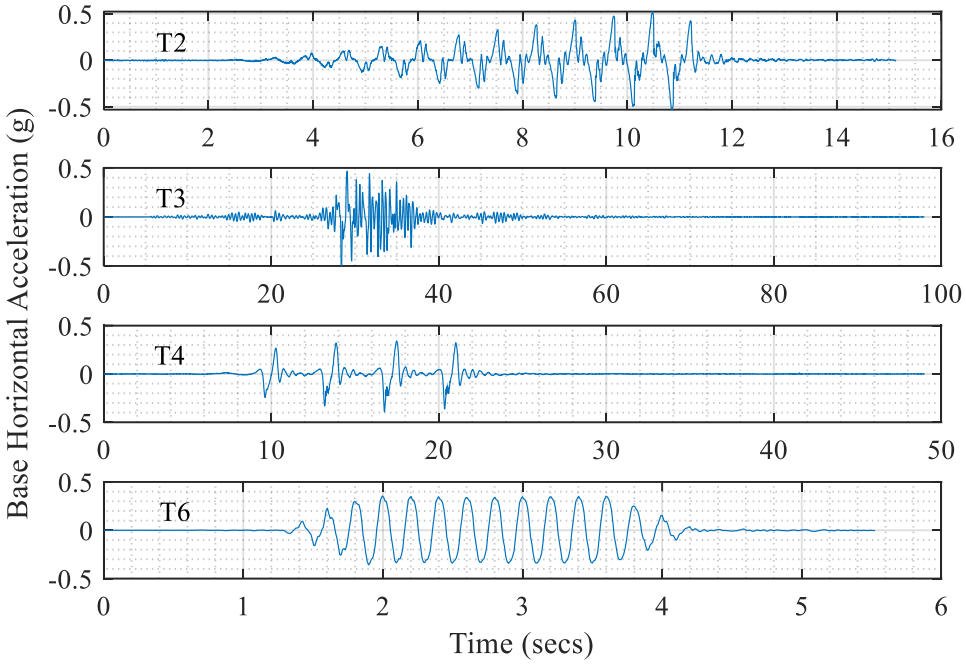

(a)

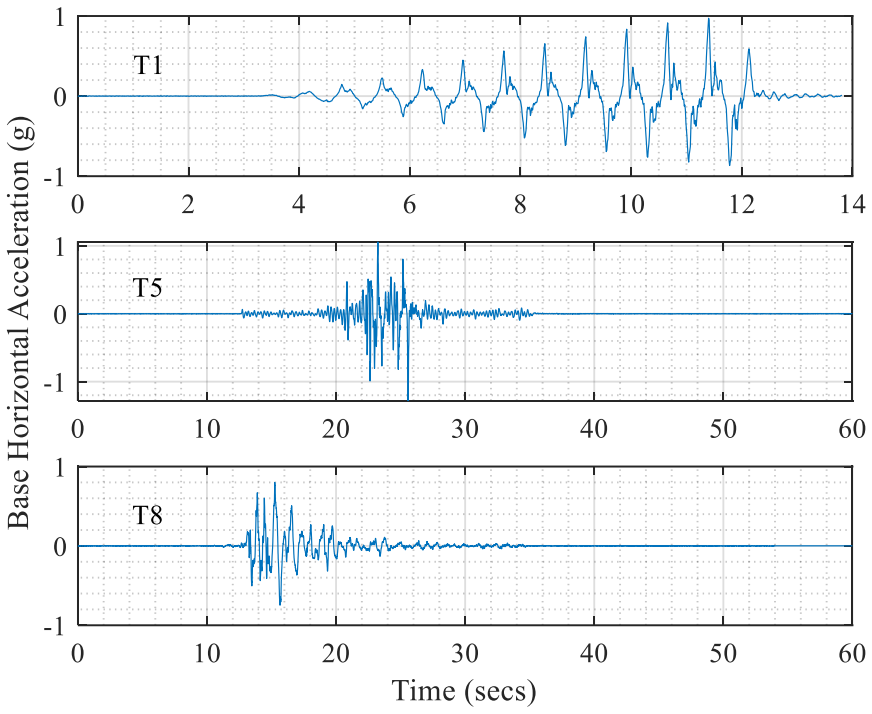

(b)

Figure 3.8. (a) Base acceleration – time period of one experiment from test series T2, T3, T4 and T6; (b) Input acceleration of one experiment from test series T1, T5 and T8

An example moment-rotation and settlement-rotation results of one of the experiments from test series based on the input acceleration in Figure 3.8 (a) and Figure 3.8 (b) is given below. The direction of shaking is along the length of the foundation in all the test series considered in this analysis. Figure 3.9 shows the moment – rotation and settlement – rotation of one experiment from dynamic test SSG03. The hysteresis loop in the moment-rotation plot gives the seismic energy dissipated below the foundation during each cycle of dynamic base shaking. It can be observed that, as the magnitude of the rotation increases, the seismic energy dissipation also increases. The settlement-rotation plot shows instantaneous uplift of the footing, gap closure, and permanent settlement at the end of the shake (~ 85mm in this case).

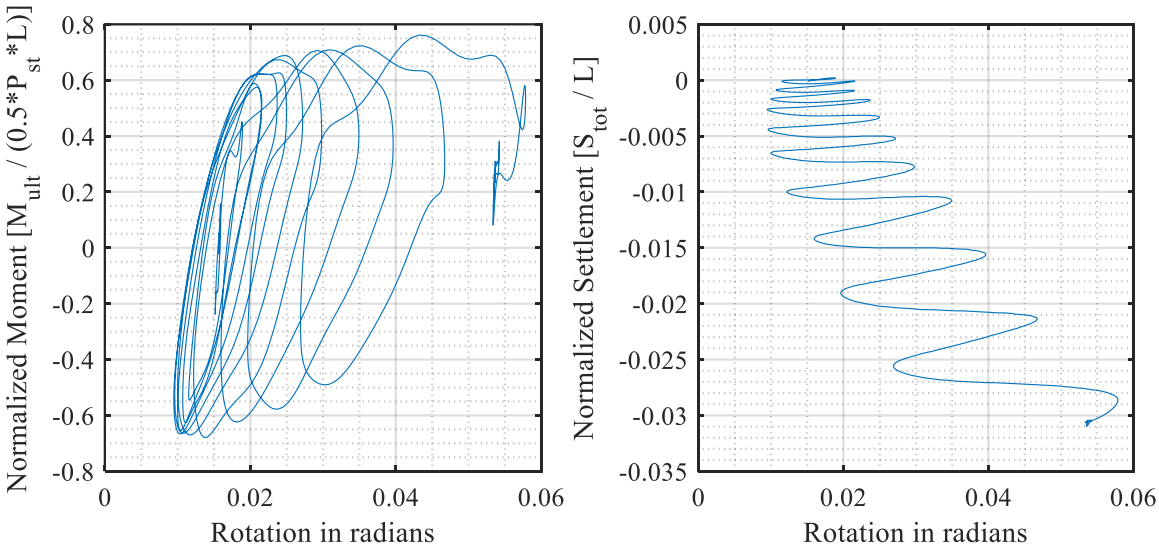

Figure 3.9. Load-displacement results of dynamic test SSG03: Sand, Dr = 80%, L = 2.8 m, B = 0.65 m, D = 0.7 m, FS_v = 7.2, M/(H.L) = 1.78, PGA = 0.972g; P_{st} = 569 kN

Figure 3.10 shows the moment – settlement – rotation relation of one experiment from dynamic test SSG04. In this case, the footing is placed on the surface of the ground with no embedment and the vertical factor of safety is 4. The rotational stiffness degrades with number of cycles and amplitude of rotation, while the moment capacity does not degrade but does show ductile behavior. Similarly, the moment – settlement – rotation plot for bridge pier models of the

test series T3, T4, T5, T6 and T8 are given in Figure 3.11, Figure 3.12, Figure 3.13, Figure 3.14, and Figure 3.15 respectively. From all the figures it can be observed that the rotational stiffness degrades with increase in amplitude of rotation. Note that all these quantities are calculated at the base center point of the foundation.

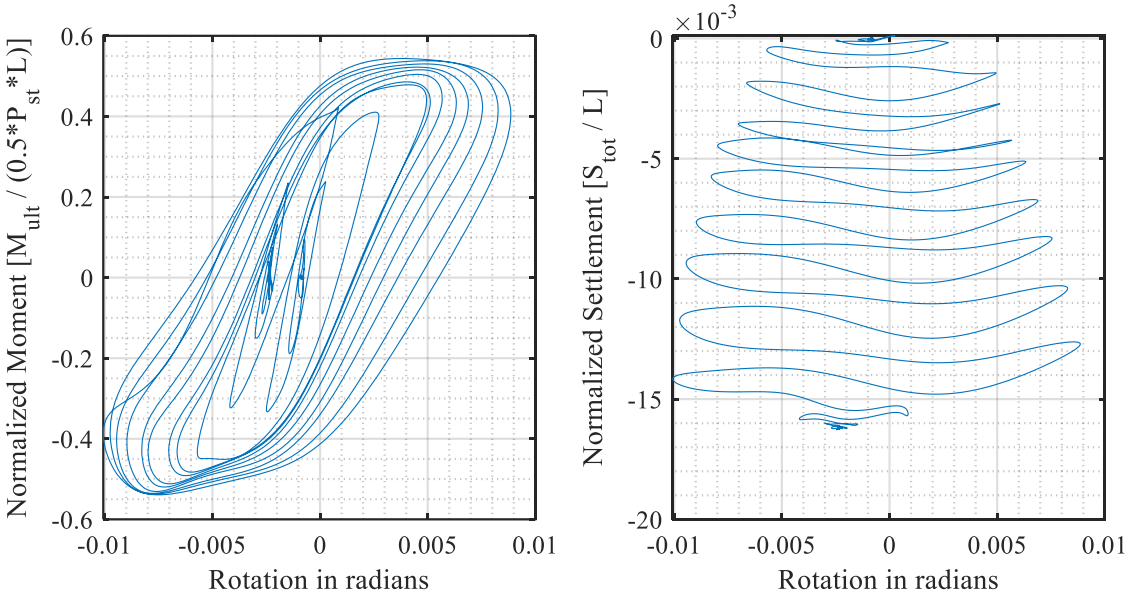

Figure 3.10. Load-displacement results of dynamic test SSG04: Sand, Dr = 80%, L = 2.8 m, B = 0.65 m, D = 0 m, FS_v = 4.0, M/(H.L) = 1.80, PGA = 0.532g; P_{st} = 361 kN

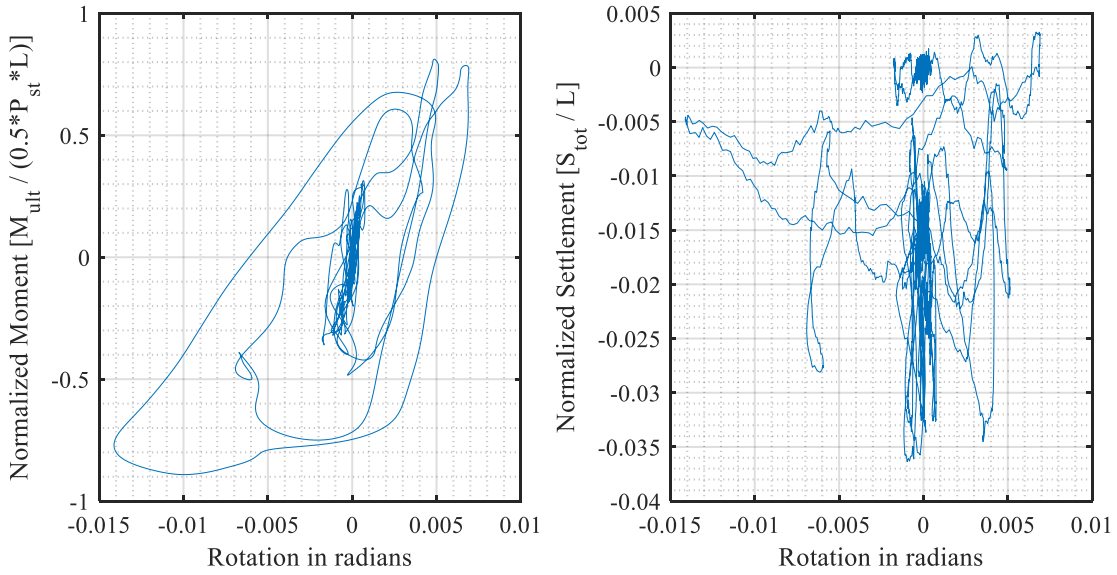

Figure 3.11. Load-displacement results of dynamic test LJD01: Sand, Dr = 73%, L = 6.7 m, B = 4.28 m, D = 2.24 m, FS_v = 16.1, M/(H.L) = 1.44, PGA = 0.620g; P_{st} = 6619 kN

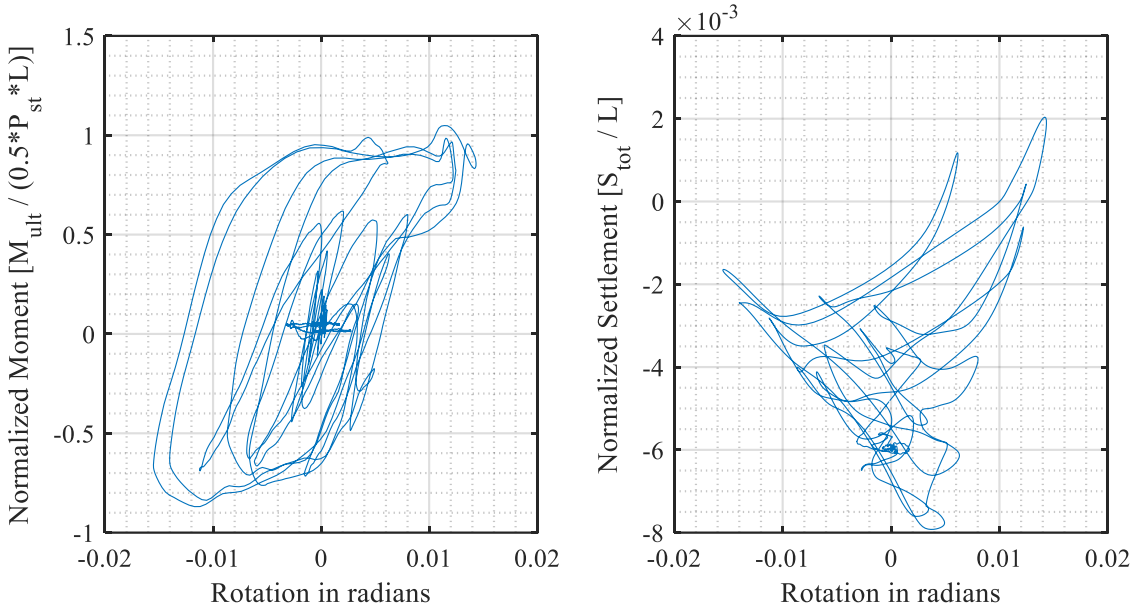

Figure 3.12. Load-displacement results of dynamic test LJD03: Sand, Dr = 38%, L = 7.35 m, B = 4.7 m, D = 2.24 m, FS_v = 11, M/(H.L) = 1.27, PGA = 0.407g; P_{st} = 6858 kN

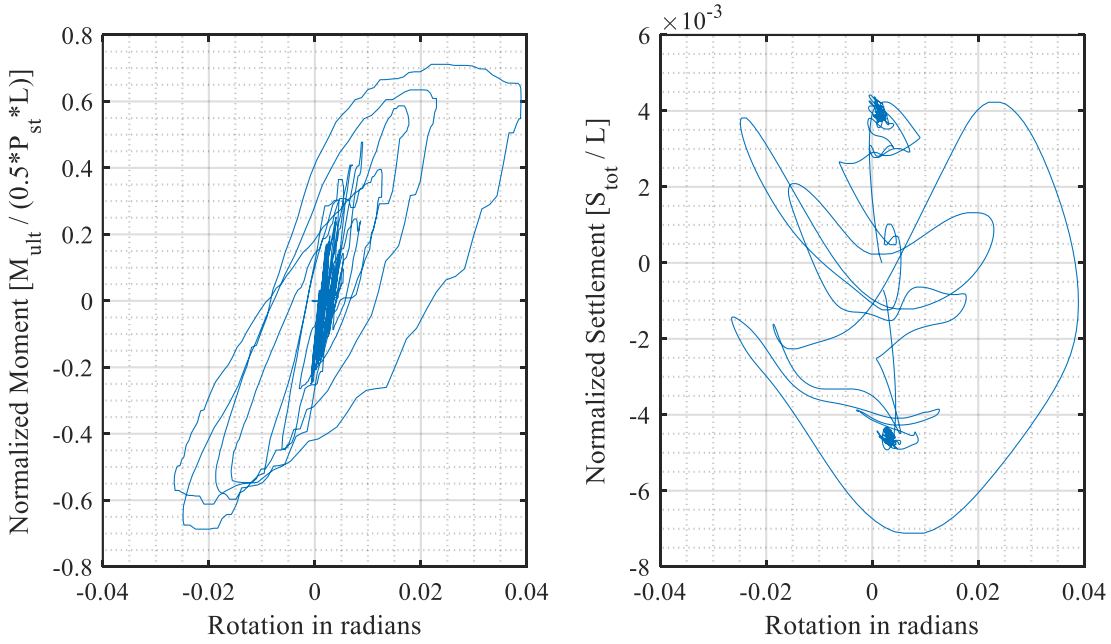

Figure 3.13. Load-displacement results of dynamic test MAH01: Clay, S_u = 59kPa, L = 6.66 m, B = 6.66 m, D = 0.6 m, FS_v = 3.4, M/(H.L) = 1.37, PGA = 0.641g; P_{st} = 5832 kN

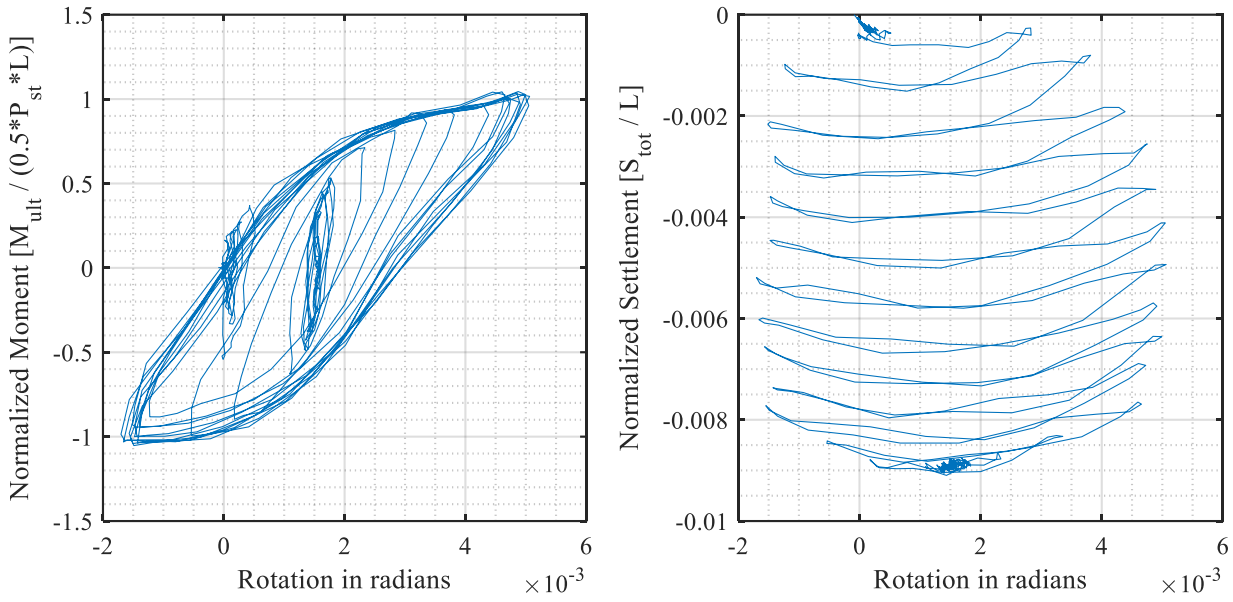

Figure 3.14. Load-displacement results of dynamic test S2011SQF1: Sand, Dr = 65%, L = 3 m, B = 3 m, D = 0 m, FS_v = 13.9, M/(H.L) = 2.37, PGA = 0.250g; P_{st} = 2773 kN

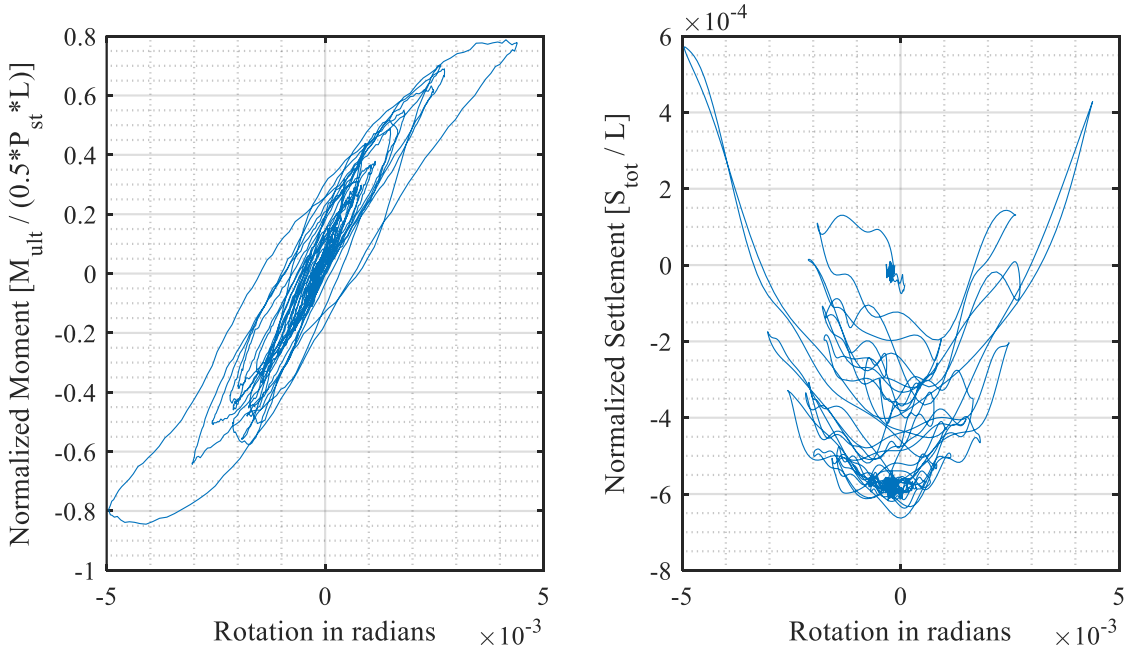

Figure 3.15. Load-displacement results of dynamic test UCSD: Sand, Dr = 85%, L = 1.52 m, B = 1.52 m, D = 0.66 m, FS_v = 23.2, M/(H.L) = 1.74, PGA = 0.329g; P_{st} = 292 kN

3.4. Correlation of Capacity – Demand – Performance Parameters

3.4.1. Seismic energy dissipation and permanent settlement

In order to analyze the seismic performance of rocking foundations in terms of energy dissipation and permanent settlement, rocking coefficient (C_r) is chosen as the capacity parameter of rocking system and Arias intensity of the earthquake (I_a) is chosen as the demand parameter. As C_r incorporates the combined effects of footing dimensions, slenderness ratio of structure, soil properties, and weight of the structure (incorporated in A/A_c), it is chosen as the capacity parameter (i.e., a rocking system with relatively small C_r value has relatively high tendency to rock).

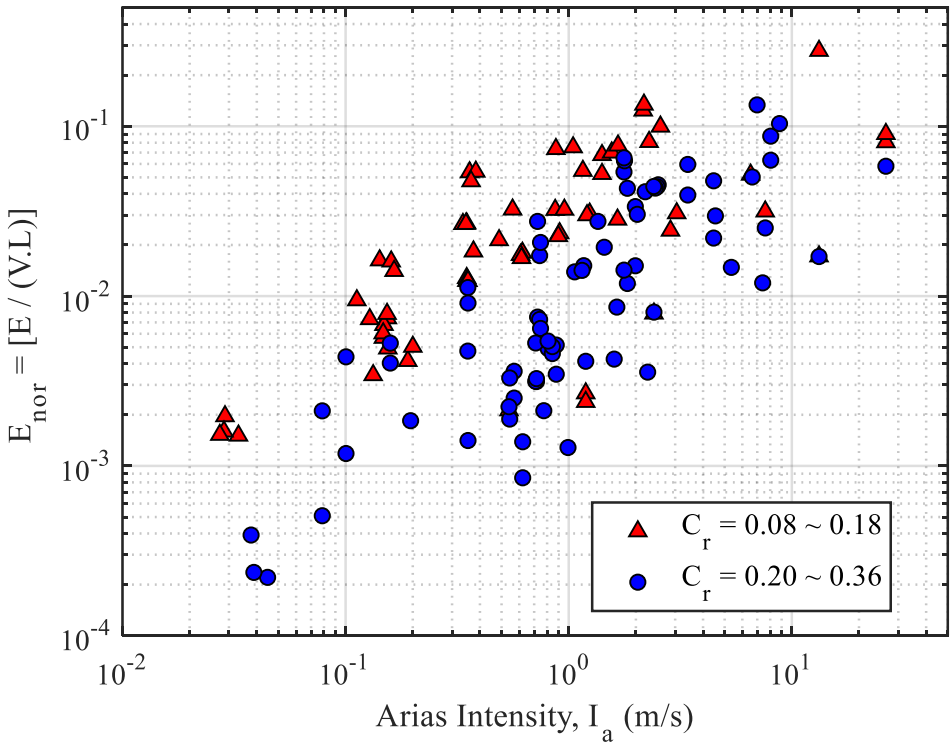

Figure 3.16. Variation of seismic energy dissipation with intensity of earthquake shaking and rocking coefficient of foundation

Since both seismic energy dissipation and permanent settlement depend on the magnitude, duration, frequency content, and number of cycles of loading, I_a is chosen as the earthquake demand parameter here (rather than peak ground acceleration or displacement).

Figure 3.16 plots variation of the normalized seismic energy dissipation ($E_{nor} = E/(V.L)$) with I_a for rocking systems with two different sets of C_r ranges. As expected, for a given range of C_r, E_{nor} increases as the intensity of the earthquake (I_a) increases. For a given Ia, E_{nor} increases as C_r decreases. This is also intuitive as systems with small C_r values have more tendency to rock and hence more energy dissipation.

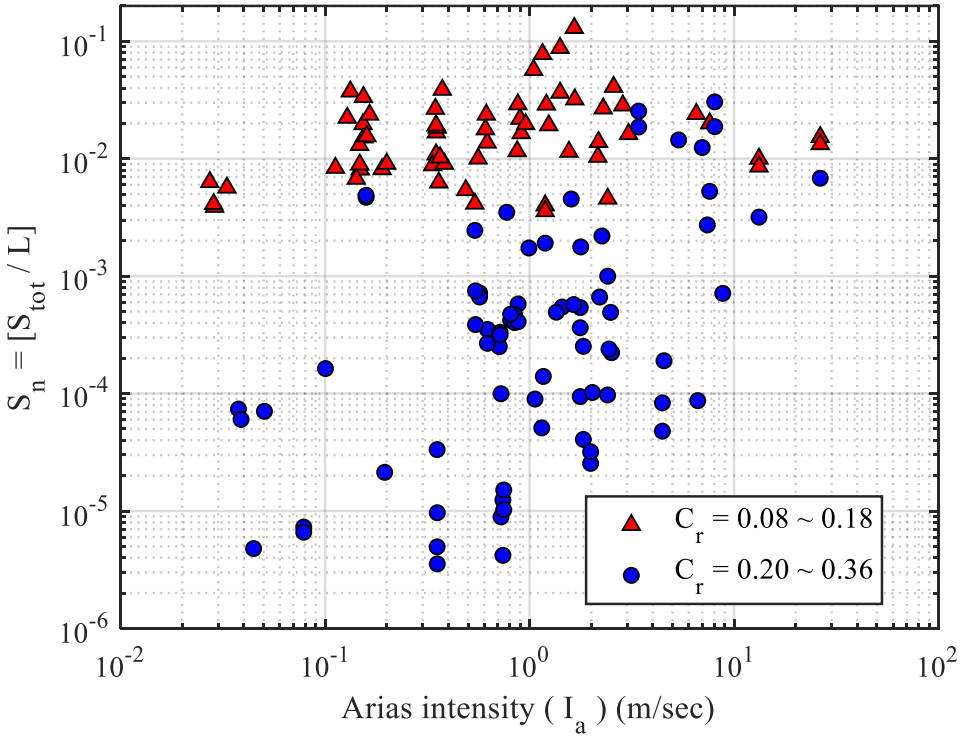

Figure 3.17. Variation of permanent settlement with intensity of earthquake shaking and rocking coefficient of foundation

Figure 3.17 presents variation of the normalized permanent settlement ($S_n = S_{tot}/L$) with I_a for different sets of C_r ranges (same sets of experiments as in Figure 3.16). Though the data is scattered for a given I_a, for most of the cases, as C_r increases, S_n decreases. This is intuitive

because as C_r decreases, vulnerability of the footing to rocking increases and hence more rocking induced settlement.

Normalized energy dissipation and normalized permanent settlement are compared with different ranges of C_r (Figure 3.18 (a) and Figure 3.18 (b)). As expected, for a given C_r range, S_n increases as the intensity of the earthquake (I_a) increases. These trends are consistent with the seismic energy dissipation results presented in Figure 3.16. Since plastic permanent settlement is a consequence of energy dissipation, settlement increases as energy dissipation increases. It should be noted that the rocking induced permanent settlement is smaller than 10% of the footing dimension, even for rocking systems having relatively smaller values of C_r and during relatively high intensity earthquake loading.

Figure 3.18 (a) shows an increase in settlement value for C_r value in the range of 0.08 – 0.25 and also depicts less permanent settlement with increased energy dissipation value for C_r in the range 0.27 – 0.36. In order to obtain an optimum range of C_r to reduce the settlement and increase the seismic energy dissipation, Figure 3.18 (b) is presented to show the variation of E_{nor} and S_n with different ranges of C_r. From Figure 3.18 (b), it can be observed that for C_r in the range 0.27 – 0.31, for most of the points there is a maximum energy dissipation with less permanent settlement.

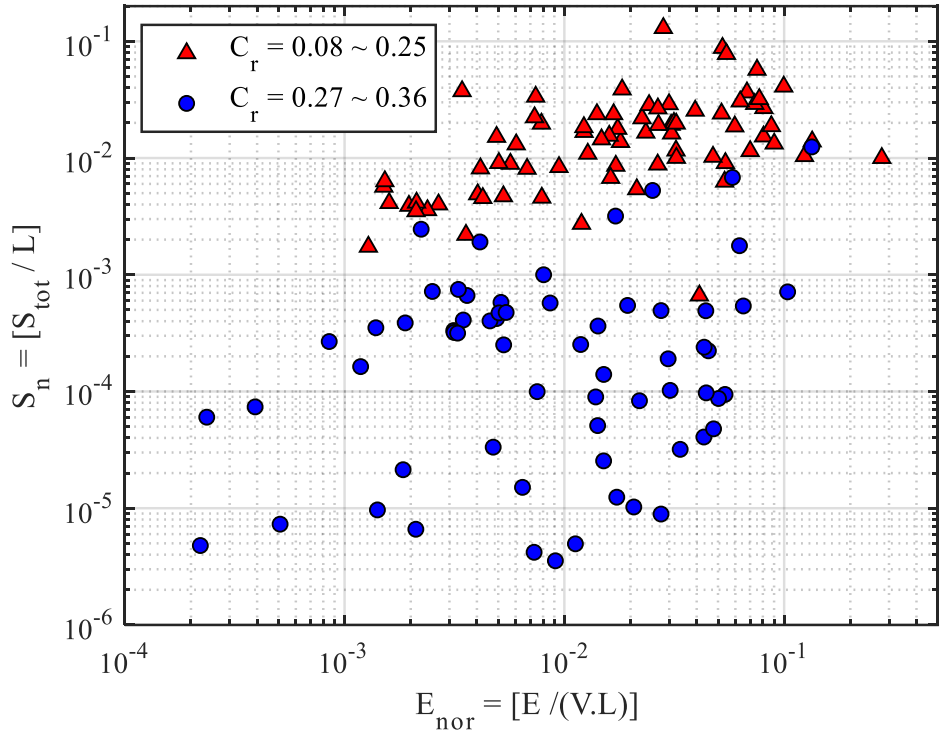

(a)

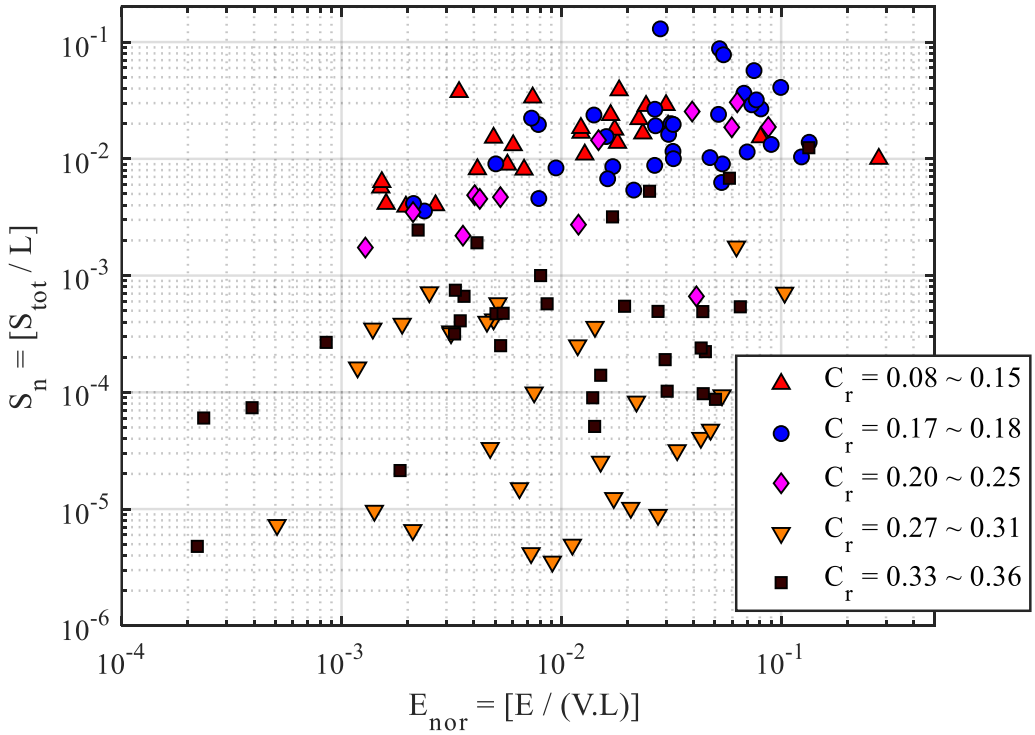

(b)

Figure 3.18. (a) Variation of permanent settlement with energy dissipation and rocking coefficient of foundation with two ranges; *(b)* Variation of permanent settlement with energy dissipation for different range of rocking coefficient of foundation

3.4.2. Self-centering ability and stability against tipping over failure

The ability to self-center at the end of the shake and the stability against tipping over failure during shaking are determined using the peak and permanent rotations of rocking systems during shaking and at the end of shaking, respectively. For this purpose, the peak ground acceleration of the earthquake (a_{max}) is chosen as the seismic demand parameter, as peak rotation is most likely caused by the maximum acceleration spike. In addition to C_r, the other single parameter that correlates the rocking induced rotation is the slenderness ratio of the rocking system (h/L). Figure 3.19 (a) and Figure 3.19 (b) show the variation of a_{max} with the peak rotation (θ_{peak}) with different ranges of h/L.

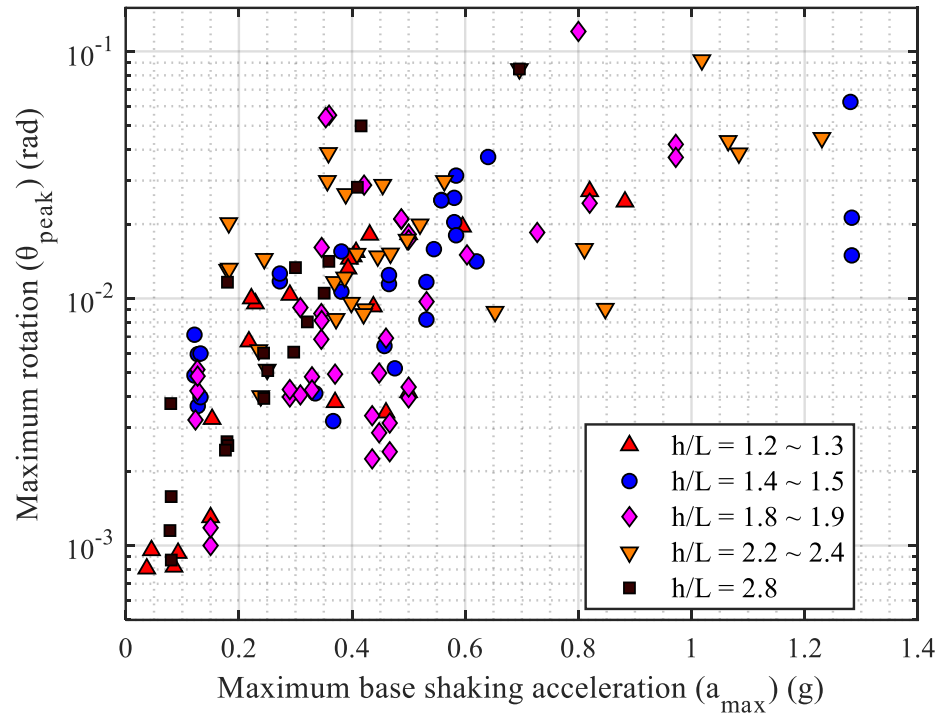

(a)

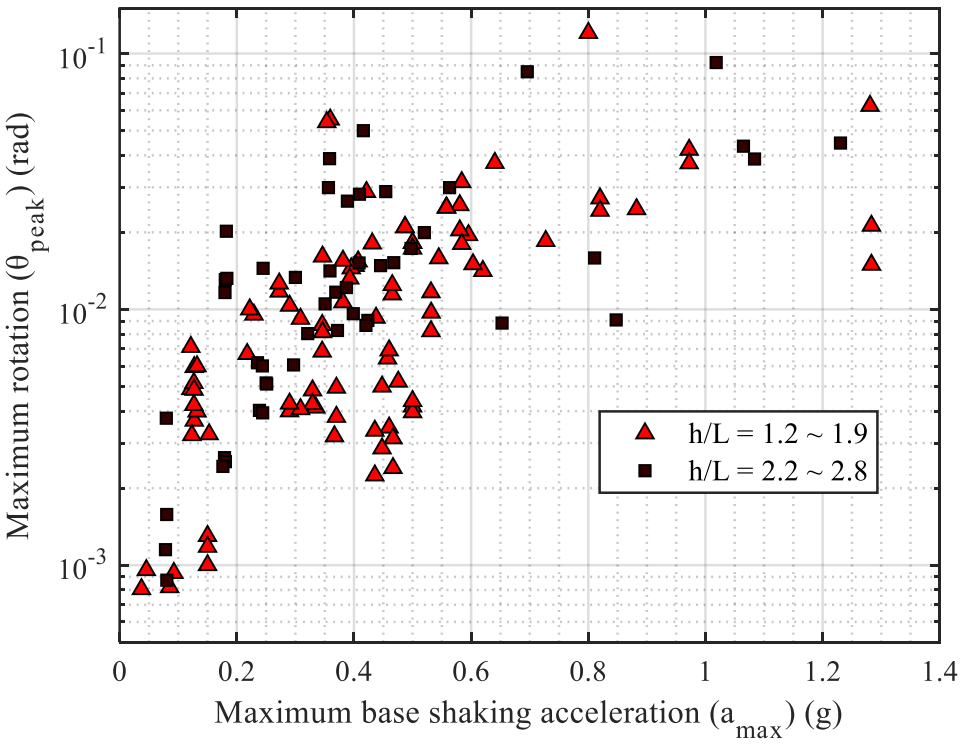

(b)

Figure 3.19. (a) Variation of peak rotation with maximum base acceleration and aspect ratio of the rocking system with different ranges of h/L; *(b)* Variation of peak rotation with maximum base acceleration and aspect ratio of the rocking system with two ranges of h/L

While permanent settlement and seismic energy dissipation are cumulative, the peak rotation (θ_{peak}) of a rocking system is instantaneous (due to the reversing nature of the seismic shaking and the self-centering characteristic of rocking shallow foundation). From Figure 3.19 (a) and Figure 3.19 (b), it is evident that, θ_{peak} increases as a_{max} increases. Though the data show some scattering, in general, higher aspect ratio structure-footing systems rotate more than their lower counterparts indicates the ability of slender structures to rock more than shorter structures. Though the structures experienced a higher maximum rotation during the earthquake, their permanent rotation at the end of the earthquake is smaller than their maximum rotation is. This indicates the self-centering ability of rocking foundations. Figure 3.20 presents variation of the permanent rotation with peak rotation and arias intensity of the base shaking.

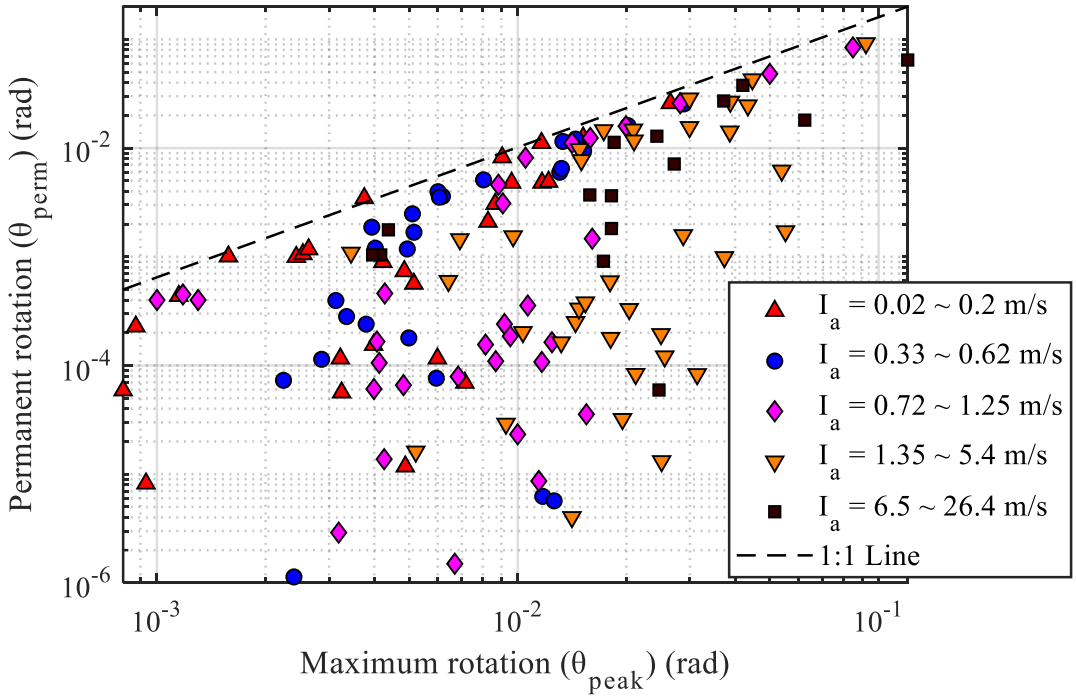

Figure 3.20. Variation of permanent rotation with peak rotation and arias intensity of base shaking

The maximum rotation and permanent rotation are comparatively less with lower intensity of dynamic shaking. However, from Figure 3.20, it can be observed that, for the

intensity between 0.72 – 1.25 m/s, most of the data points show less permanent settlement and peak rotation.

Figure 3.21 (a) plots variation of the self-centering ratio (SCR) of rocking foundations with θ_{peak} and Arias intensity and Figure 3.21 (b) shows variation of the SCR with θ_{peak} and C_r. From Figure 3.21 (a), it is evident that, even with high intensity of earthquake, the SCR values are observed to be greater than 0.7 for most of the events. Also, from Figure 3.21 (b) it can be seen that rocking systems with relatively higher C_r values have SCR values close to 1.0 regardless of the maximum rotation during shaking, indicating excellent self-centering ability.

For rocking systems with relatively smaller C_r values, though there is scattering in the data, it can be seen in general that SCR increases as θ_{peak} decreases. However, it is important to note that any of the structure-footing systems used in all of these 142 experiments have not tipped over regardless of the magnitude of shaking. Figure 3.22 presents variation of tipping-over stability ratio (TSR) during the earthquake as a function of maximum acceleration (a_{max}) of the earthquake for different sets of aspect ratios (h/L) of the structure-footing systems. From Figure 3.22, it can be seen that, irrespective of high base shaking, all data points possess a high tip-over stability value of 0.75 and above.

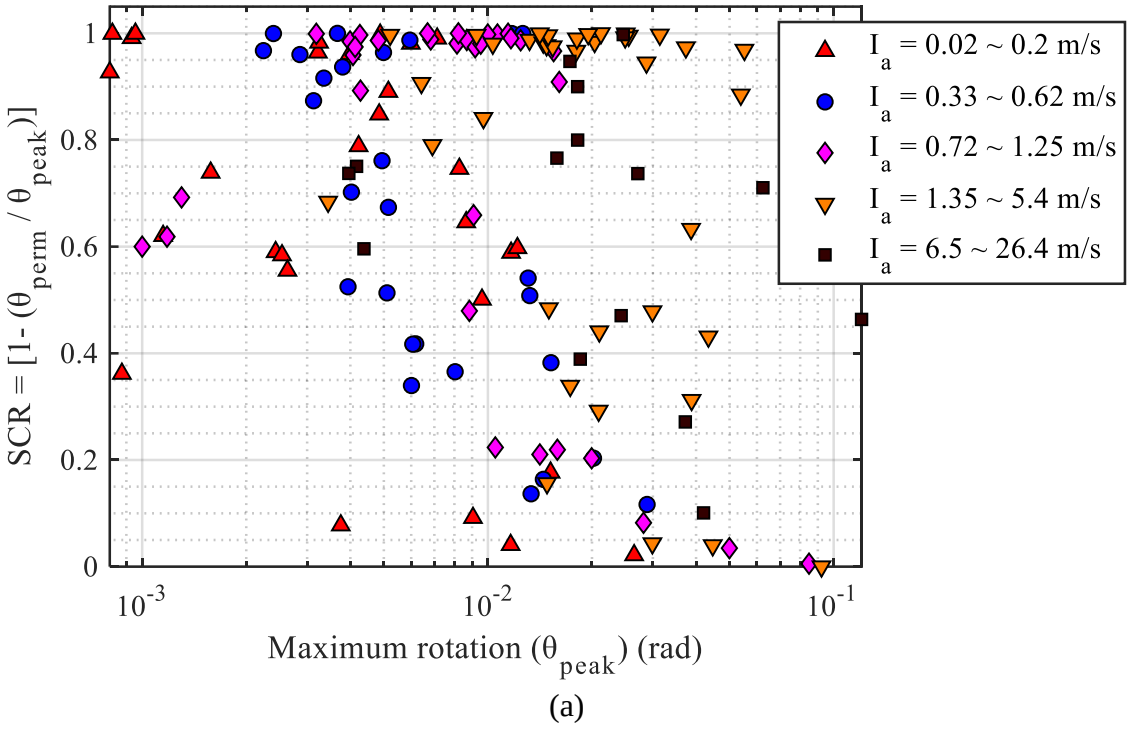

(a)

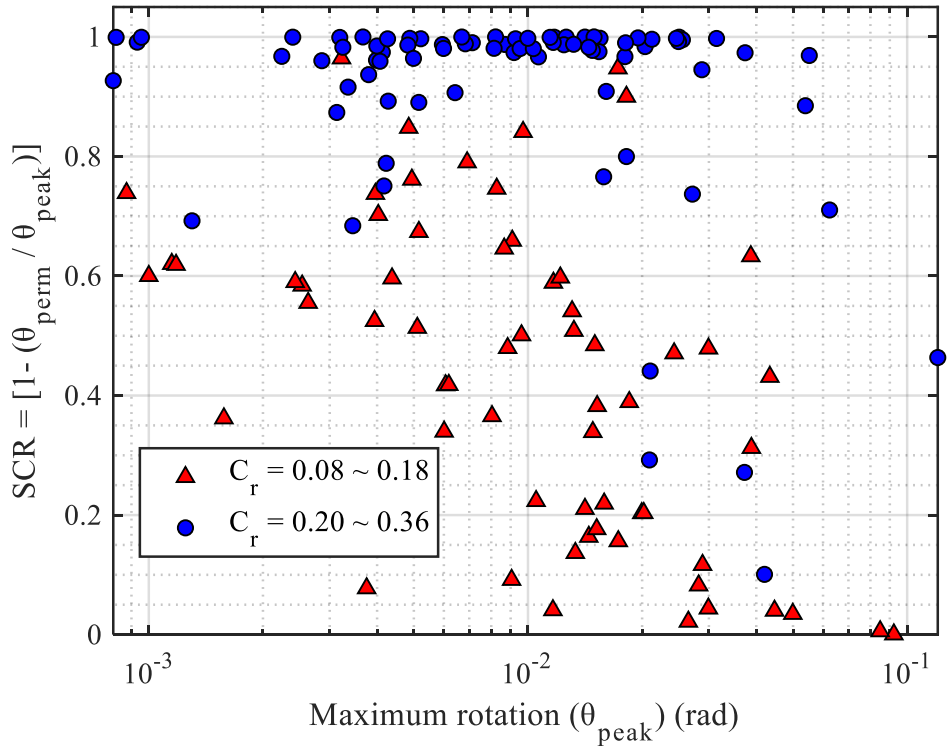

(b)

Figure 3.21. (a) Variation of self-centering ratio with peak rotation and arias intensity; (b) Variation of self-centering ratio with peak rotation and rocking coefficient

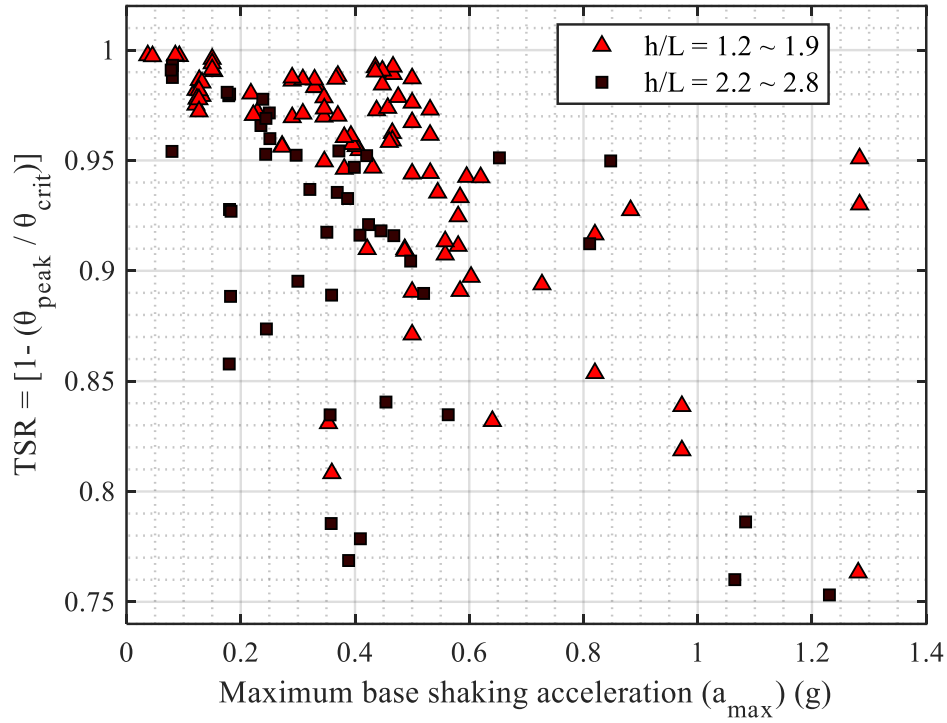

Figure 3.22. Variation of tip-over stability ratio with maximum acceleration and aspect ratio of rocking system

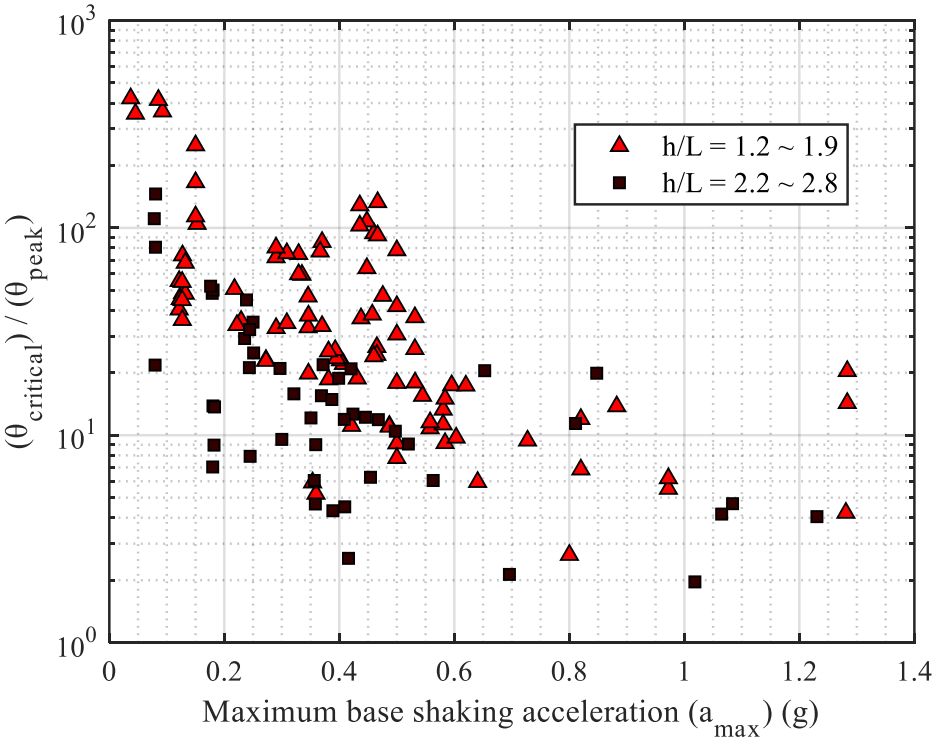

Figure 3.23. Variation of tip-over stability factor with maximum acceleration with two sets of aspect ratio of the rocking system

The peak and critical rotation of the rocking system (the magnitude of rotation that would cause tipping over failure) is compared with maximum base acceleration and aspect ratio of the structure-foundation system and shown in Figure 3.23.

It should be noted that TSR can be considered as the stability factor (factor of safety) against tipping-over failure of structure during the earthquake. As can be seen from Figure 3.23, the higher tendency of rocking of taller structures produces smaller ratios of TSR values, and as expected, TSR decreases as the intensity of the earthquake increases. However, TSR is as high as 200 for smaller magnitude earthquakes and 2 for high intensity earthquakes, indicating excellent stability of rocking foundations against tipping-over failure.

3.4.3. Ultimate moment capacity versus A/A_c

The variation of normalized ultimate moment capacity versus A/A_c for both ultimate moment theoretical value and maximum moment in experimental data with different ranges of a_{max} is shown in Figure 3.24.

From Figure 3.24, it can be observed that for $a_{max} < 0.2g$, the maximum moment experienced by rocking foundation is less than the theoretical ultimate moment, whereas, for relatively higher intensity earthquake the maximum moment is observed to be closer to the theoretical ultimate moment which shows that the foundation did not mobilize the theoretical ultimate moment during relatively smaller magnitude of earthquake.

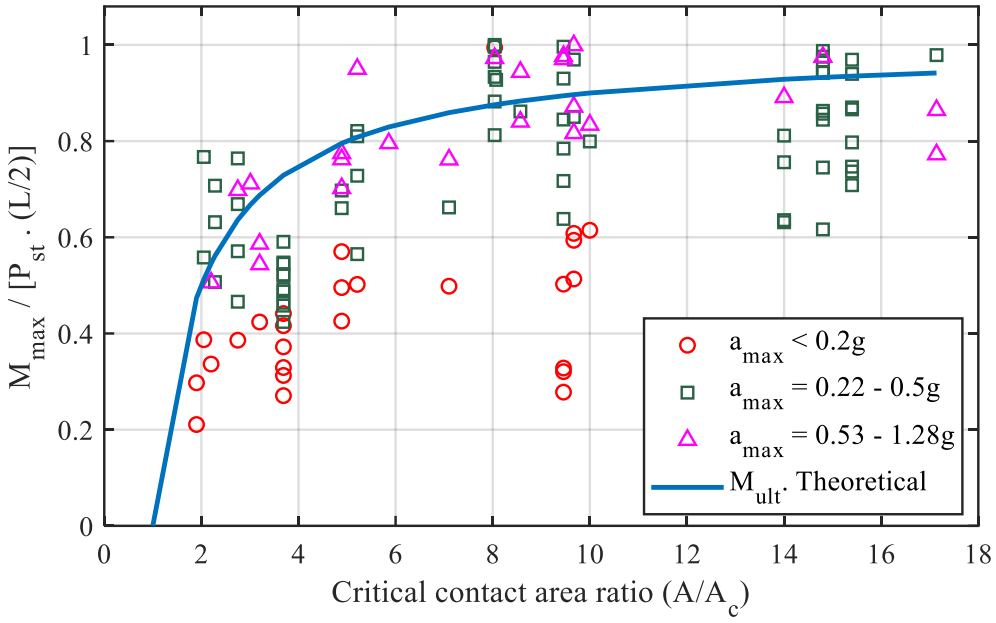

Figure 3.24. Variation of ultimate moment capacity with A/A_c for both theoretical and experimental data with different range of a_{max}

3.5. Effects of Rocking Coefficient on Moment Capacity and Permanent Settlement

The normalized moment [M_{ult} / (P_{st} x (L/2))] and normalized settlement (S_{tot}/L) are compared for a high C_r value, a medium C_r value, and a low C_r values among all 142 events and shown in Figure 3.25. From Figure 3.25, it can be observed that, the normalized moment value is close to 0.9 for the high C_r value. The footing details for the C_r value of 0.358 case are L = 1.52m, B = 1.52m, vertical load (P_{st}) of 292.1kN, and maximum acceleration of 0.290g. For the medium C_r value of 0.226, the normalized moment was close to 0.7 which is less than the normalized moment observed in the high C_r value. The footing details of the C_r of 0.226 case are L = 6.66m, B = 6.66m, P_{st} = 5830kN, and maximum acceleration of 0.641g.

In case of low C_r value of 0.082, the normalized moment is close to 0.2 which is very less compared to normalized moment of the high C_r value and the medium C_r value. The footing details of the low C_r value case are L = 0.15m, B = 0.15m, P_{st} = 0.986kN, and maximum acceleration of 0.080g. Therefore, the moment capacity value increases as the C_r value goes

higher which validates the results discussed in the correlation of rocking coefficient with energy dissipation. And for low C_r value of 0.082, the settlement value was less compared to the settlement obtained in C_r value of 0.226 which also validates the correlation results presented for the rocking coefficient and the permanent settlement.

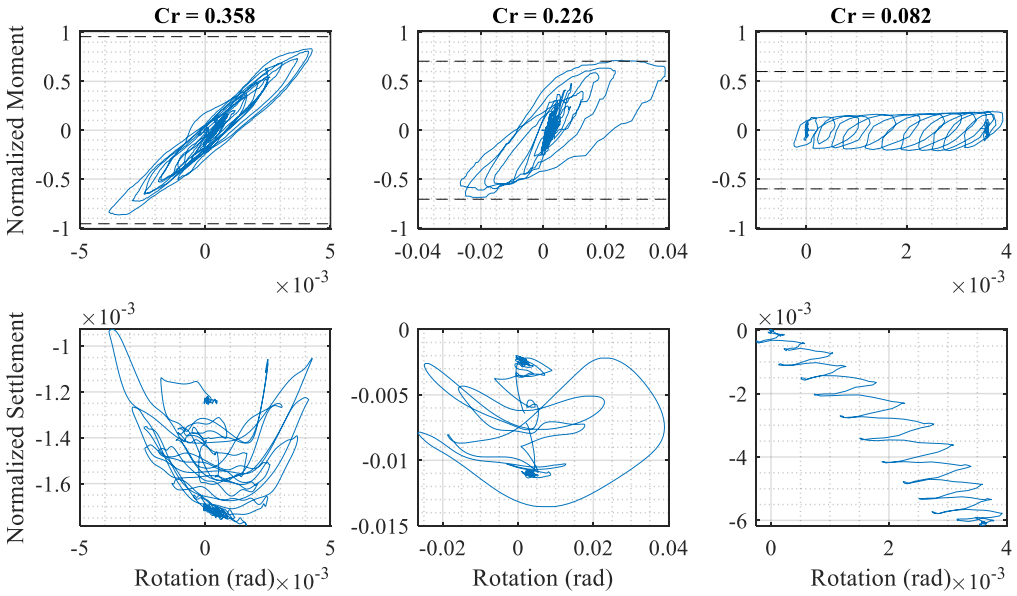

Figure 3.25. Effects of C_r in moment capacity and permanent settlement

4. NUMERICAL ANALYSIS AND VALIDATION OF MODELS

4.1. Introduction

The numerical analysis is being performed for the shear wall and bridge pier models used in the centrifuge and shake table tests. The results obtained for selected models are validated against experimental results. The input parameters used for the structure, soil, and foundation of all models are discussed in this chapter, and their results are presented.

4.2. Contact Interface Model

The soil-footing interface and the zone of influence are considered as a macro-element in the contact interface model (CIM). The finite element software OpenSees (Open System for Earthquake Engineering Simulation) is adopted for modeling CIM by tracking the geometry of the soil surface beneath the footing.

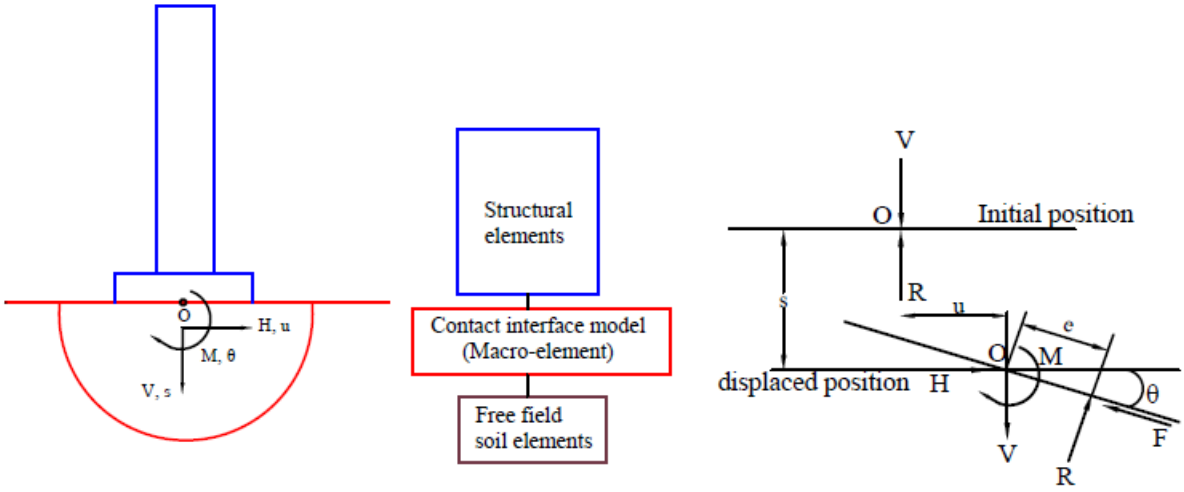

Figure 4.1. The concept of contact interface model (adopted from Gajan and Kutter, 2009a)

From Figure 4.1, it can be observed that CIM is placed at the soil-footing interface which replaces the rigid foundation and the zone of influence. As the incremental load is applied to the macro-element model, the corresponding displacements are obtained from the model and vice-versa. CIM is defined by seven user-defined input parameters and output the performance

parameters such as energy dissipation, permanent settlement, stiffness degradation, and permanent inclination.

4.2.1. Critical contact area ratio

Tracking the gap between the foundation and the underlying soil is the main feature in CIM. Therefore, to track foundation-soil contact, critical contact area ratio is used. Critical contact area ratio (A/A_c) is the ratio of area of the footing (A) to area of the footing required to have contact with soil to support the vertical and shear loads (A_c). For two-dimensional model, A/A_c equals footing length ratio (L/L_c). From Figure 4.2, it can be observed that, as the gap is formed between footing and the soil supporting the footing, the L_c value reduces. The pressure distribution in this critical area is assumed uniform and the resultant soil reaction occurs at the maximum eccentricity, $e_{max} = (L - L_c/2)$.

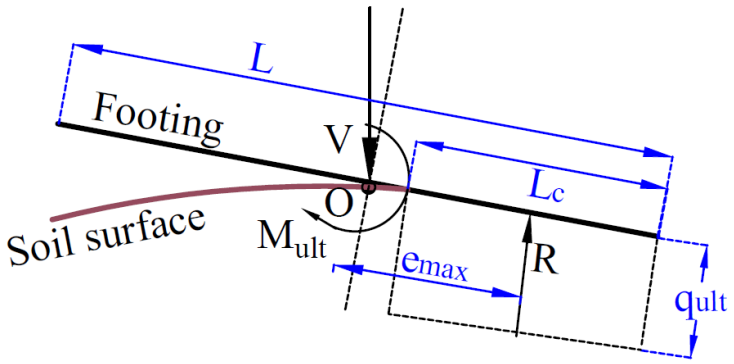

Figure 4.2. Definition of critical contact area ratio (adopted from Gajan and Kutter, 2009); (q_{ult} – ultimate bearing pressure, M_{ult} – ultimate moment capacity)

4.2.2. Pressure distribution and V-H-M space

The pressure distribution captured by CIM during rocking is shown in Figure 4.3. As rocking occurs at the soil below foundation, rounding of soil happens below the rigid foundation. From Figure 4.3, it can be observed that the CIM captures the contact of rigid foundation with rounding of soil in soil_min (surface between a and d) and soil_max (surface between b and c) and also the forces acting at the interface.

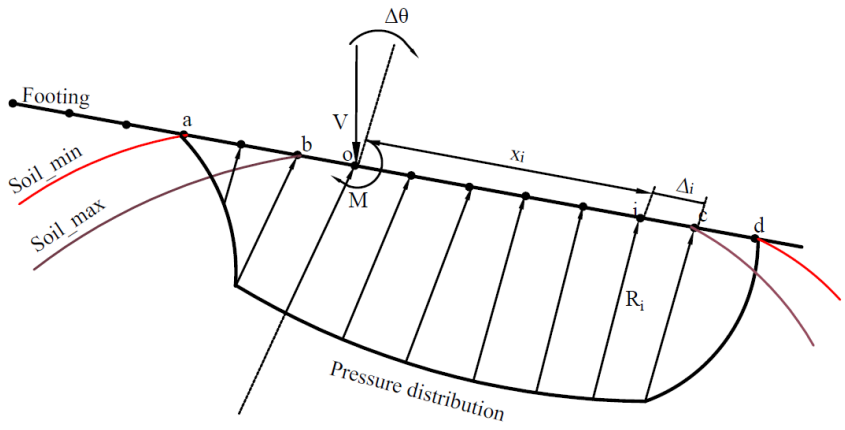

Figure 4.3. Pressure distribution in CIM during rocking behaviour (adopted from Gajan and Kutter, 2009); (R_i – normalized bearing pressure parameter at node i; $\Delta\theta$ – incremental rotation; Δ_i – spacing between nodes; x_i – distance of node i from footing base center point O)

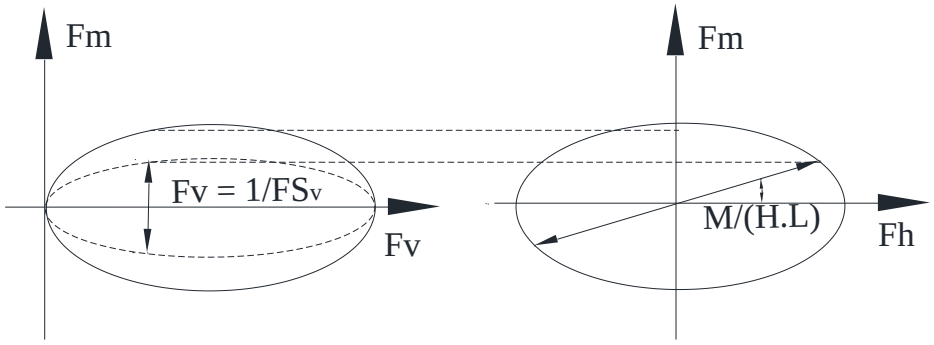

Figure 4.4. Load path for cyclic moment loading in normalized V-H-M space (adopted from Gajan and Kutter, 2009); (Fm = normalized moment force; Fv = normalized vertical load; Fh = normalized horizontal load)

The cross-section of the bounding surfaces in Fm – Fv and Fm – Fh and load path for cyclic moment loading in coupling V-H-M space is shown in Figure 4.4. The expression for normalized moment to shear ratio is given in Equation 2.12. From Figure 4.4, it can be observed that, the reduction in moment capacity occurs due to the coupling of vertical load and horizontal load.

4.2.3. User defined input parameters and equations

The seven user defined parameters of CIM are the following:

- Static factor of safety with respect to vertical load (FS_v) is calculated using the ratio of ultimate vertical load (V_{ult}) and applied total vertical load (V)
- Ultimate vertical load (V_{ult}) is the ultimate bearing capacity of the soil and it is calculated using the Meyerhof's bearing capacity formula (Das, 2011). The bearing capacity is comprised of bearing capacity factors, shape factors, and depth factors.
- Length of footing (L) is the dimension of footing along the direction of seismic load.

The formula used in computing q_{ult} for sand (4.2) and for clay (4.3) are given below,

$$V_{ult} = q_{ult}.B.L \tag{4.1}$$

$$q_{ult} = \gamma.D.N_q.F_{qs}.F_{qd} + \frac{1}{2}.\gamma.B.N_\gamma.F_{\gamma s}.F_{\gamma d} \tag{4.2}$$

$$q_{ult} = \gamma.D + S_u.N_c.F_{cs}.F_{cd} \tag{4.3}$$

Bearing capacity factors:

$$N_q = tan^2\left(45 + \frac{\phi}{2}\right).e^{\pi.tan\phi} \tag{4.4}$$

$$N_\gamma = 2\left(N_q + 1\right).\tan(\phi) \tag{4.5}$$

$$N_c = \pi + 2 = 5.14 \tag{4.6}$$

Shape factors:

$$F_{qs} = 1 + \frac{B}{L}.tan\phi \tag{4.7}$$

$$F_{\gamma s} = 1 - 0.4\,\frac{B}{L} \tag{4.8}$$

$$F_{cs} = 1 + \left\lfloor\frac{B}{L}\right\rfloor\left\lfloor\frac{N_q}{N_c}\right\rfloor \tag{4.9}$$

Depth factors:

If D ≤ B,

$$F_{qd} = 1 + 2\tan\phi\,.\,(1-\sin\phi)^2\,.\left(\frac{D}{B}\right) \tag{4.10}$$

$$F_{\gamma d} = 1 \tag{4.11}$$

$$F_{cd} = 1 + 0.4\left(\frac{D}{B}\right) \tag{4.12}$$

If D > B,

$$F_{qd} = 1 + 2\tan\phi\,.\,(1-\sin\phi)^2\,.\,atan\left(\frac{D}{B}\right) \tag{4.13}$$

$$F_{\gamma d} = 1 \tag{4.14}$$

$$F_{cd} = 1 + 0.4\;atan\left(\frac{D}{B}\right) \tag{4.15}$$

Using the V_{ult} value, FS_v can be calculated as,

$$FS_v = \frac{V_{ult}}{V} \tag{4.16}$$

- Initial vertical stiffness (K_v) and Initial horizontal stiffness (K_h). K_v and K_h are the initial vertical and horizontal stiffness of footing when it is fully in contact with the soil. The calculation of K_v and K_h are given in FEMA 356, which are

$$K_h = \left(\frac{GB}{2-\upsilon}\right)\left[3.4\left(\frac{L}{B}\right)^{0.65} + 1.2\right] \tag{4.17}$$

$$K_v = \left(\frac{GB}{1-\upsilon}\right)\left[1.55\left(\frac{L}{B}\right)^{0.75} + 0.8\right] \tag{4.18}$$

  The shear modulus G is calculated using the following formula (Kramer, 1996),

$$G = 218.8\,K_{2,max}.\,(\sigma')^{0.5} \tag{4.19}$$

  $K_{2,max}$ is determined from the relative density; σ' is the product of unit weight of soil (γ in kN/m^3) and length of footing (L) along the direction of seismic load.

  For embedded footing, the following correction factors are included,

$$\beta_h = \left(1 + 0.21\sqrt{\frac{D_f}{B}}\right)\left(1 + 1.6\left(\frac{hd(B+L)}{BL^2}\right)^{0.4}\right) \quad (4.20)$$

$$\beta_v = \left(1 + \frac{D}{21B}\left(2 + 2.6\frac{B}{L}\right)\right)\left(1 + 0.32\left(\frac{d(B+L)}{BL}\right)^{\frac{2}{3}}\right) \quad (4.21)$$

The K_h and K_v values for embedded footing are calculated using the formula given below,

$$K_{h\ embed} = \beta_h K_h \quad (4.22)$$

$$K_{v\ embed} = \beta_v K_v \quad (4.23)$$

The height of sidewall contacts between footing and soil are calculated based on Figure 4.5 (FEMA 356),

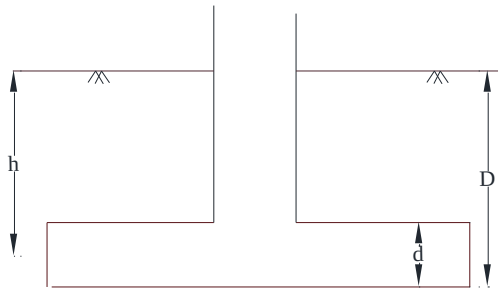

Figure 4.5. Definition of height of sidewall contacts (h and d) (adopted from FEMA 356)

- Rebounding ratio (Rv) is an empirical parameter that accounts for elastic rebound of the soil that exists after gap formation when footing rocks. Usually Rv value is in the range of 0.1 – 0.15 and for this study, Rv value of 0.1 is considered.
- Footing node spacing (deltaL) is the distance between footing nodes that are internally created in the model. The typical range of deltaL is 0.01 – 0.005 (Gajan and Kutter, 2009).

4.3. The Integrated Soil-Interface-Structure Numerical Model

The following procedure is adopted in OpenSees to implement CIM, structural and geotechnical model of the shear wall and the bridge-pier respectively.

4.3.1. Model builder

As OpenSees is a finite element software, the analysis starts by dividing the model into nodes and elements (OpenSees, 2008b).

- *model BasicBuilder -ndm $ndm <-ndf $ndf>* command is used to define the dimension of the model and the number of degrees of freedom at each node
- *node $nodeTag (ndm $coords)* is used to construct a node object with tag and nodal coordinates
- The element between the zone of influence and the ground surface is defined by *zeroLengthSection element* command.
- section soilFootingSection2d $Tag $FSv $Vult $L $kv $kh $Rv $delL command is used to define the CIM parameters
- The element of shear wall and the bridge column is defined by *elasticBeamColumn* command and their cross-sectional area, moment of inertia along z-axis and the elastic modules of the material are the arguments used in the command
- In this analysis, node 1 is fixed in all the directions and it is defined using the command *fix $node $x $y $z*
- The linear geometric transformation of beam stiffness and resisting force from the basic system to the global coordinate system is defined using the command *geomTransf Linear $transfTag*

- The gravity load at node 2 (superstructure) is applied using this *Pattern Plain* command for all the analysis.

4.3.2. Recorder object

During the analysis, the recorder object monitors the user defined parameters. The tracking of geometry is captured using recorder objects. When the incremental loads are given to the macro-element model, the corresponding incremental displacement is obtained and vice-versa. The displacements (vertical, horizontal and rotational) at nodes and the corresponding element force (axial, shear and moment) outputs are obtained using the following commands,

- recorder Node -file $fileName -node $n -dof 1 2 3 disp is used to give output displacements at nodes
- recorder Element -file $fileName -time -ele $n force is used to output the element forces

4.3.3. Analysis object

The analysis objects are used for performing the analysis. The analysis moves the model from state t to state t+dt. For the static analysis, the following analysis objects are used,

- *Norm Displacement Increment Test* is used to check the convergence of the model at the end of iteration step. The system of equations formed by the model is expressed as,

$$K\Delta U = R \tag{4.24}$$

Where K is the stiffness matrix, ΔU is the displacement increment, and R is the unbalanced force. The iteration is used to check whether $\sqrt{\Delta U^T \Delta U} < tol$, where tol is the tolerance criteria used in model convergence.

- *Newton Algorithm* is used to construct a Newton Raphson algorithm object and uses Newton Raphson method to advance to next step. In each iteration, the tangent is updated.
- *SparseGeneral SOE* is used to construct sparse system of equations which will be factored and solved using the superLU solver. The LU solver is a common tool to solve linear system of equations.
- *Plain Constraints* is used to enforce homogenous single point constraint such as fixed boundary conditions.
- *Plain Numberer* is used to assign the degrees of freedom to the nodes stored in the domain.
- *Static Analysis* is for static loading (executed once gravity loading is defined) and also solves $KU = R$ problem without the mass matrix or damping matrix.

For dynamic loading, along with Newton Algorithm and Plain Constraints, the following commands are used,

- *UmfPack General* is used to generate sparse system of equations which will be factored and solved using UmfPack solver
- *RCM Numberer* is used to assign the degrees of freedom to the nodes using the reverse Cuthill-McKee algorithm to ensure that the corresponding coefficient matrix has a narrow bandwidth
- *Energy Increment* is the convergence test that checks tolerance on the inner product of the unbalanced load and displacement increments at the current iteration

$$\frac{1}{2}\Delta U^T R < tol \tag{4.25}$$

- *Variable Transient Analysis* is used for transient analysis with variable time step. For each level the time step is further divided into sub steps to perform the analysis
- The dynamic loading at node 1(footing) is applied using *Uniform Excitation Pattern* command.
- *Newmark Integrator* is used to solve the transient problem. The following equations are used for time-stepping method (Newmark, 1959),

$$\dot{u}_{i+1} = \dot{u}_i + [(1-\alpha)\Delta t]\ddot{u}_i + (\alpha.\Delta t)\ddot{u}_{i+1} \tag{4.26}$$

$$u_{i+1} = u_i + (\Delta t)\dot{u}_i + [(0.5-\beta)(\Delta t)^2]\ddot{u}_i + [\beta(\Delta t)^2]\ddot{u}_{i+1} \tag{4.27}$$

Where u_i, $\dot{u}_i$, $\ddot{u}_i$ are the nodal displacement, nodal velocity and nodal acceleration respectively. The parameters α and β defines the variation of acceleration over time and determines the stability and accuracy of the method. Typically, α is 0.5 and β is 0.25 for the analysis.

The equation governing the dynamic analysis of structural nodes in relation with inertial forces is,

$$[M]\{\ddot{u}\} + [C]\{\dot{u}\} + [K]\{u\} = [F] \tag{4.28}$$

Where [M] is the structural mass matrix, [C] is the structural damping matrix, and [K] is the structural stiffness matrix. In OpenSees, the damping matrix is defined using Rayleigh damping which is specified as a combination of stiffness and mass proportional damping matrices.

$$[C] = \alpha[M] + \beta[K] \tag{4.29}$$

*D = $alphaM * M + $betaK * Kcurrent +$betaKinit * Kinit + $betaKcomm * KlastCommit* is the syntax used in OpenSees for damping. α and β are constants which are determined using the damping ratio for two modes of vibration. In $alphaM * M , M is the mass matrix used to calculate the Rayleigh damping. Kcurrent is the stiffness matrix at the current state used in

Rayleigh damping calculations. Kinit is initial stiffness matrix and KlastCommit is stiffness matrix at the last committed state that is used in Rayleigh damping calculations.

4.4. Shear Wall Model Validation

Among the test series discussed in Chapter 3, the shear wall structure in centrifuge test series T1 and T2 is adopted to verify the numerical model. The mesh used in CIM modeling for the shear wall is given in Figure 4.6

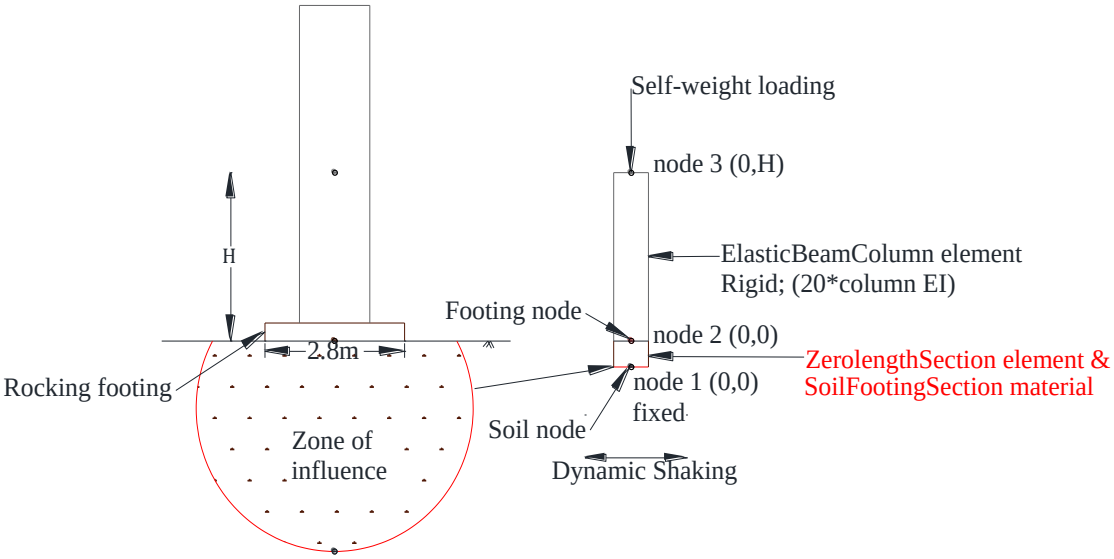

Figure 4.6. Mesh generation for CIM modeling of shear wall

The soil properties used in the numerical model are given in Table 4.1. For structural properties to be used in the model, the cross sectional area (A) of the shear wall and moment of inertia along z-direction (I) are calculated and given in Table 4.2 along with initial vertical stiffness, initial horizontal stiffness, and initial shear modulus values.

Table 4.1

Soil parameters of shear wall modeling

Test Series	L(m)	B(m)	D(m)	Φ (deg)	γ (kN/m^3)	q (kPa)	Dr (%)	P_{st} (kN)
SSG03	2.8	0.65	0.7	42	16.2	198 - 313	80	361 - 569
SSG04	2.8	0.65	0	42	16.2	198 - 313	80	361 - 569

Table 4.2

Rocking system parameters used for shear wall modeling

Test Series	FS_v	G (MN/m^2)	K_v (MN/m)	K_h (MN/m)	A (m^2)	I (m^4)
SSG03	7.2 – 11.5	92.51	856	813	0.95	0.495
SSG04	2.6 – 4.0	92.51	545	375	0.95	0.495

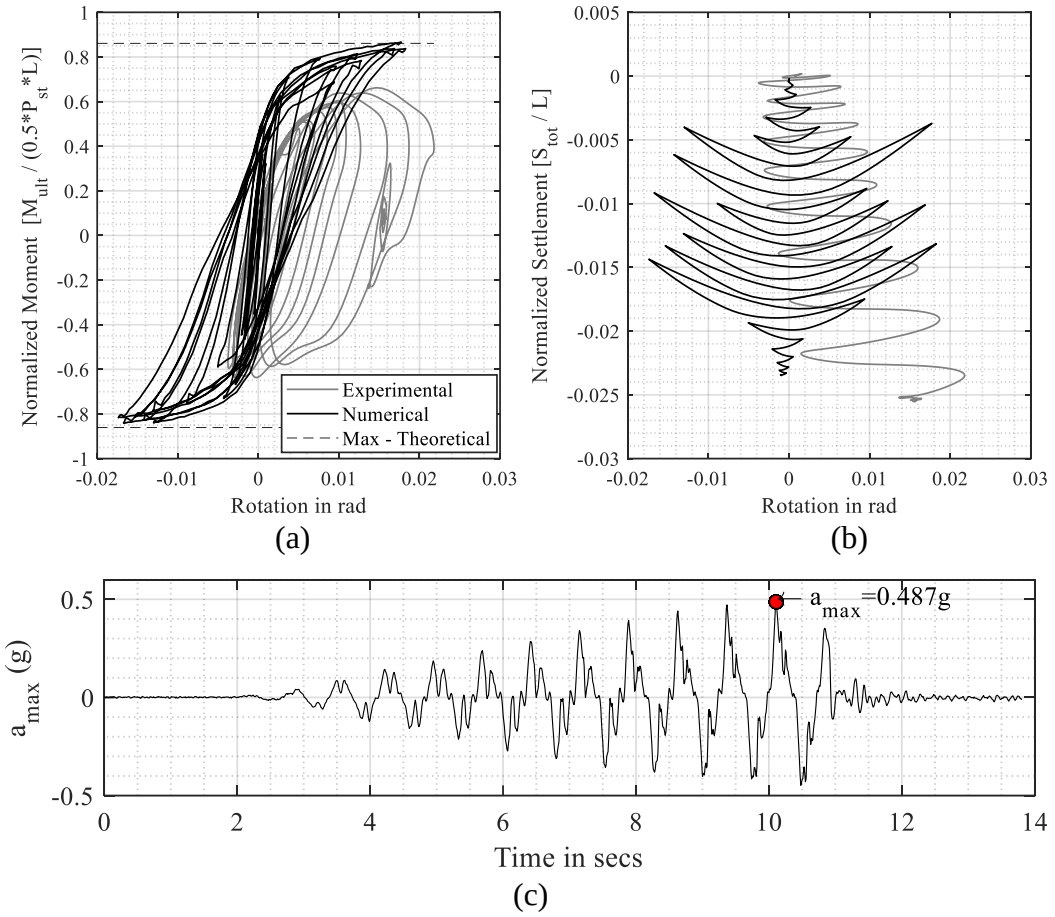

Figure 4.7. Validation of shear wall model SSG03 with experimental results (a) normalized moment capacity, (b) normalized permanent settlement, (c) input acceleration (g); FS_v = 7.2, P_{st} = 569kN, C_r = 0.236; A/A_c = 7.1; PGA = 0.487g

The CIM model is implemented in OpenSees to study the rocking behavior of rigid shear wall subjected to dynamic base shaking and also to validate the numerical modeling results with experimental results. Figure 4.7 shows the validation of numerical modeling of one event in

SSG03 test series with PGA of 0.487g, whereas Figure 4.8 shows the validation of one event in SSG04 test series with PGA of 0.727g.

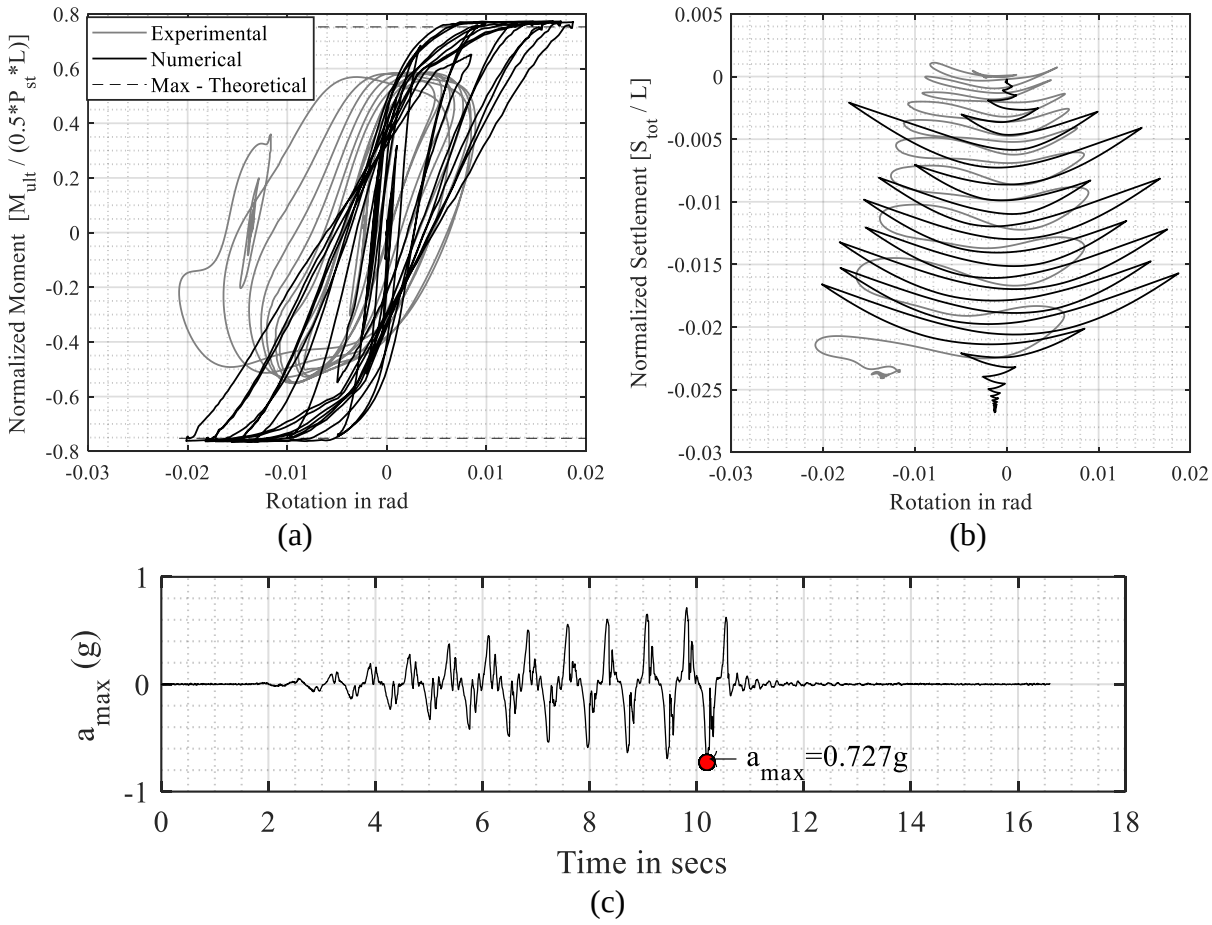

Figure 4.8. Validation of shear wall model SSG04 with experimental results (a) normalized moment capacity, (b) normalized permanent settlement, (c) input acceleration (g); FS_v = 4.0, P_{st} = 361kN, C_r = 0.176; A/A_c = 3.2; PGA = 0.727g

From Figure 4.7 and Figure 4.8, it can be observed that the moment capacity of numerical results is close to the theoretical moment capacity, as numerical modeling is based on the theoretical value. Also, the permanent settlement value in numerical model is 65.8mm in Figure 4.7 and 75mm in Figure 4.8 and these values are close to the experimental results which shows that CIM model effectively captures the rocking behavior of rigid shear wall subjected to dynamic base shaking. Furthermore, the SCR and TSR values are close to one as permanent rotation value is close to zero in numerical modeling and can be seen from Figure 4.7 and Figure

4.8 respectively. Hence, using the validated shear wall model, the energy dissipation, permanent settlement, and permanent rotation is evaluated for all events in SSG03 and SSG04 test series.

4.5. Bridge-Pier Model Validation

The bridge-pier model has a flexible column and a rigid foundation. The mesh used for the bridge-pier model is shown in Figure 4.9.

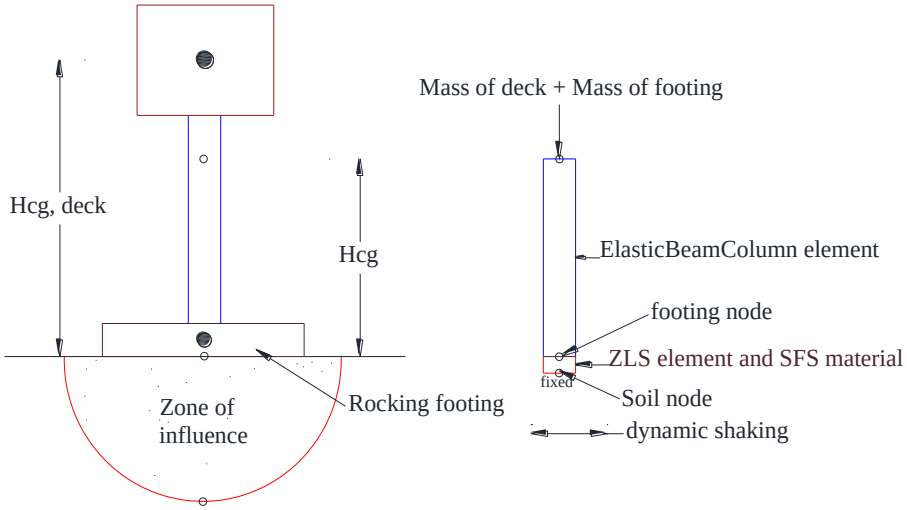

Figure 4.9. Mesh generation for CIM modeling of the bridge pier model

As can be seen from Figure 4.9, the bridge-pier model has a flexible column and rigid footing. For the analysis, the numerical modeling is developed for LJD01 and LJD03 test series. The soil properties considered in numerical modeling are given in Table 4.3 and rocking system parameters used in numerical modeling are given in Table 4.4 respectively.

Table 4.3

Soil parameters of bridge-pier modeling

Test Series	L(m)	B(m)	D(m)	Φ (deg)	γ (kN/m^3)	q (kPa)	Dr (%)	P_{st} (kN)
LJD01	6.7	4.28	2.24	36	16.243	209.3	73	6002
LJD03	7.35	4.7	2.24	32.7	15.018	179	38	6186

Table 4.4

Rocking system parameters used in bridge-pier modeling

Test Series	FS_v	G (MN/m^2)	K_v (MN/m)	K_h (MN/m)	A (m^2)	I (m^4)
LJD01	16.1	183.38	5474	5651	1.75	0.51
LJD03	11	113.61	3636	3696	1.75	0.51

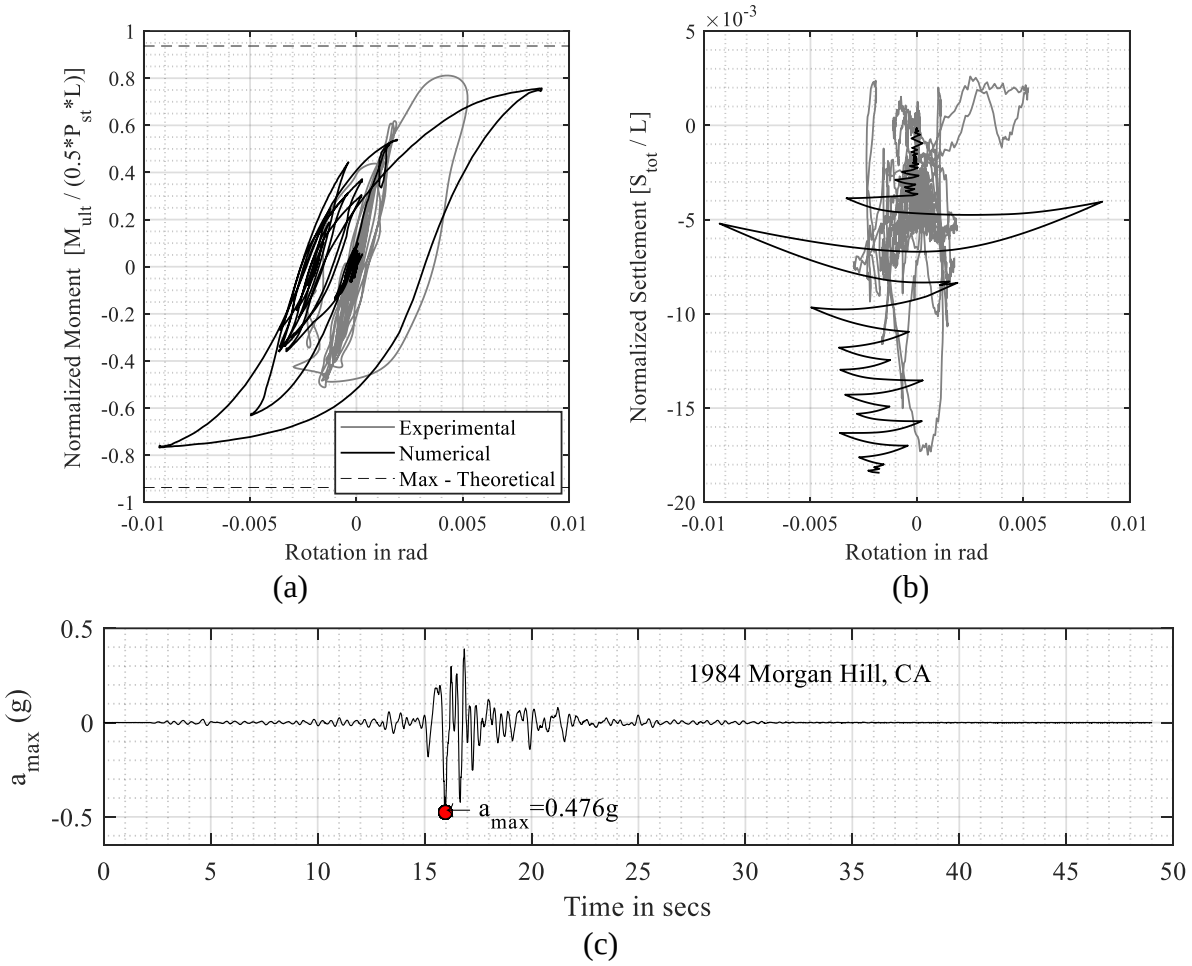

Figure 4.10. Validation of bridge – pier model (LJD01) with experimental results (a) moment capacity (N-m) (b) permanent settlement (m) and (c) input acceleration (g); FS_v = 16.1; P_{st} = 6002kN; C_r = 0.25; A/A_c = 14; PGA = 0.476g.

The validated bridge-pier modeling for one event in LJD01 test series is shown in Figure 4.10. In case of LJD01 test series, the Sanguinetti off-ramp located at I-105 was chosen as a prototype bridge and in case of LJD03 test series, CA-108 overcrossing the Sanguinetti Rd was

considered as a prototype bridge. The validated bridge-pier model for one event in LJD03 test series is shown in Figure 4.11. From Figure 4.10 (a) and Figure 4.11 (a), it can be observed that, there is a stiffness degradation as the rocking behavior dominates and the CIM model effectively captures the stiffness degradation with experimenta results. However, the permanent settlement seems to be higher than the experimental results in both Figure 4.10 (b) and Figure 4.11 (b).

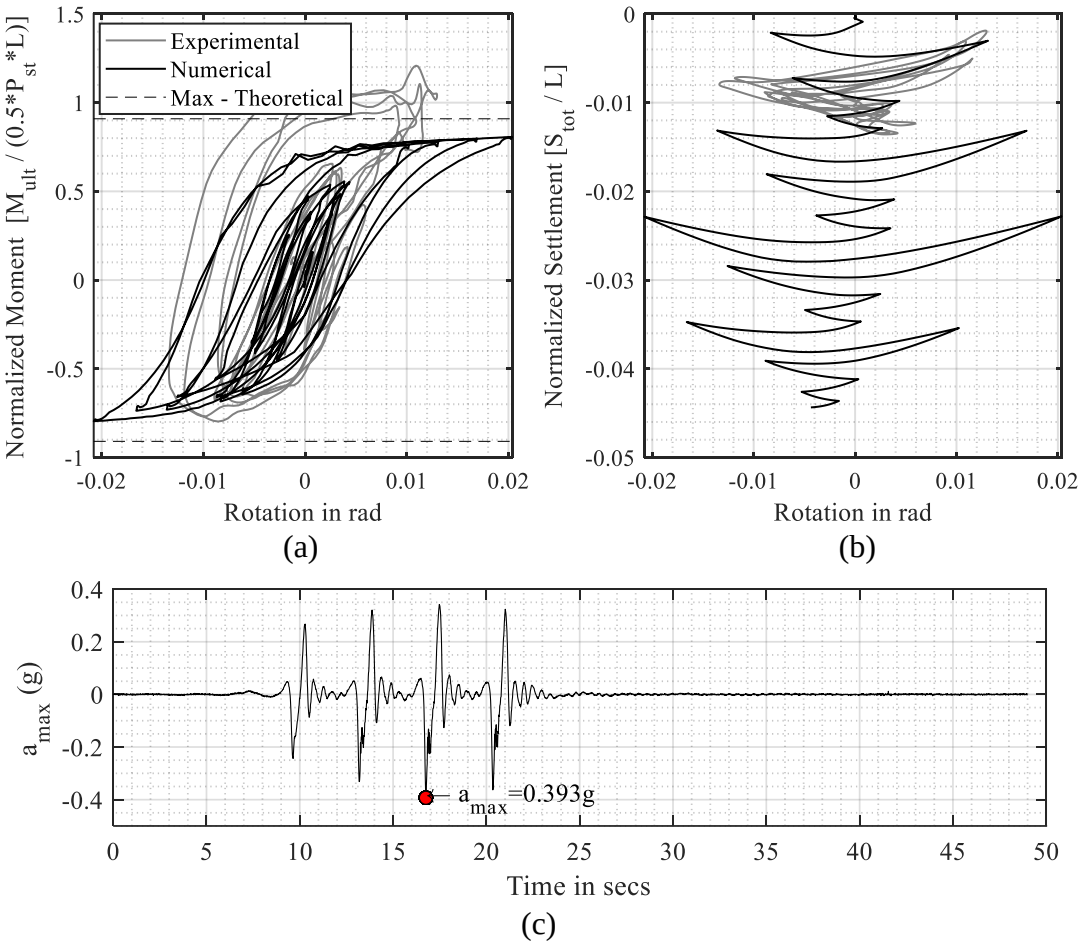

Figure 4.11. Validation of bridge – pier model (LJD03) with experimental results (a) moment capacity (N-m) (b) permanent settlement (m) and (c) input acceleration (g); $FS_v = 11$; $P_{st} = 6186kN$; $C_r = 0.353$; $A/A_c = 9.5$; PGA = 0.393g.

The maximum rotation value at the permanent settlement in Figure 4.10 (b) and in Figure 4.11 (b) are close to zero, hence the SCR and TSR values are close to one which shows an increase in self-centering characteristics of the brigde-pier model. Using the validated bridge-pier

model, the energy dissipation, permanent settlement and maximum rotation values are computed for other events in LJD01 test series and LJD03 test series.

4.6. Parameter Gaps in the Experimental Data

Using the validated shear wall model and the bridge – pier model, the performance parameters such as energy dissipation, permanent settlement, and permanent rotation are evaluated for the other experimental data. The computed performance parameters from the numerical model are plotted with the experimental results to fill the parameter gaps in the experimental data and also to check the accuaracy of the numerical model.

The variation of normalized energy dissipation with arias intensity and rocking coefficient is plotted for both experimental and numerical data, as shown in Figure 4.12. As can be seen from Figure 4.12, for most of the cases, the energy dissipation was higher for the numerical results than the experimental data and it also reinforces with experiemntal analyses that as the Cr value decreases, the energy dissipation value increases. For higher intensity earthquakes, energy dissipation for the numerical model is higher than the experimental results for Cr values from 0.25 – 0.353, which shows that the numerical model effectively captures the gap formation during rocking.

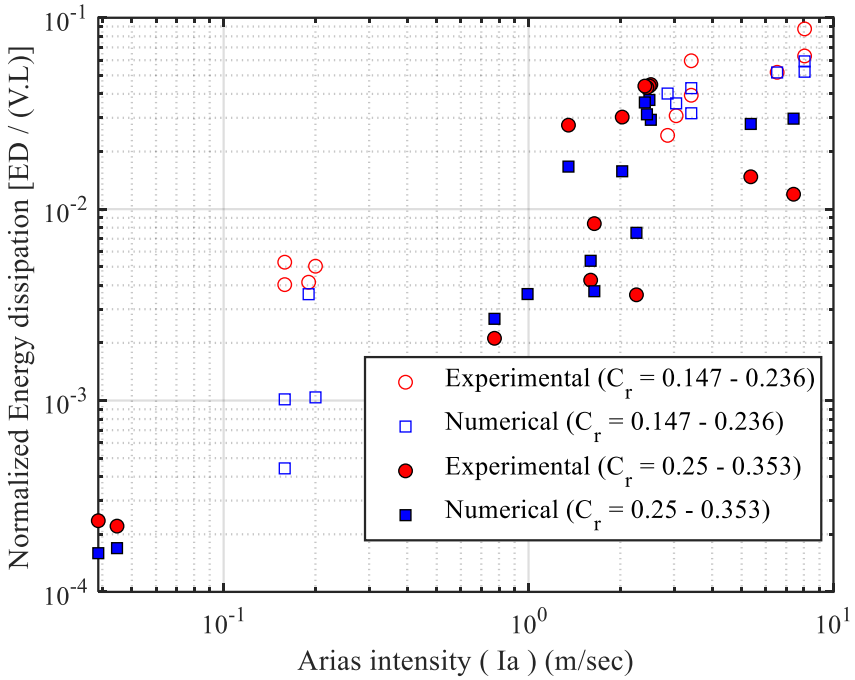

Figure 4.12. Variation of normalized energy dissipation with arias intensity for both numerical and experimental data

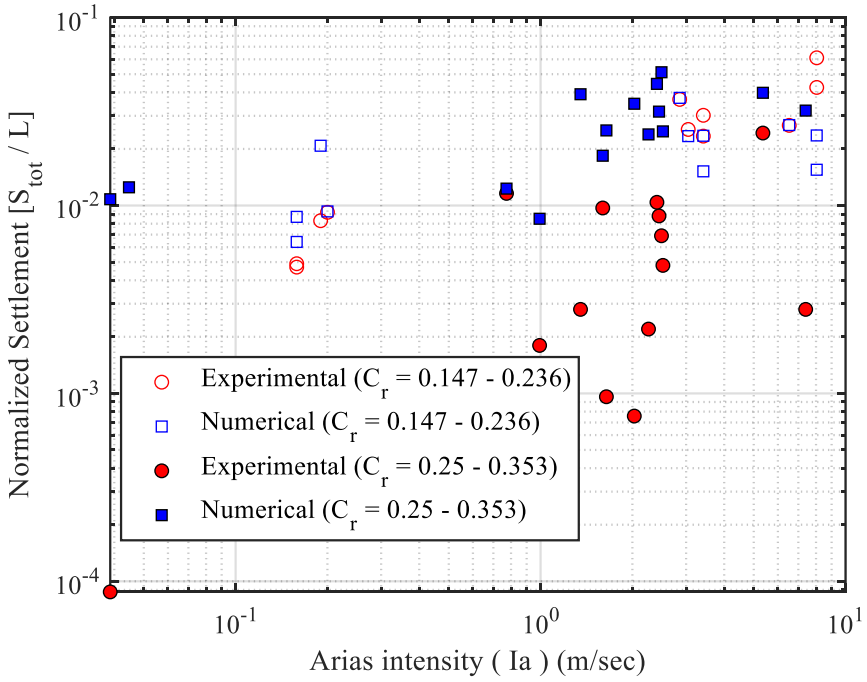

Figure 4.13. Variation of normalized settlement with arias intensity for both numerical and experimental data

Similarly, variation of the normalized permanent settlement is plotted with arias intensity and rocking coefficient for both numerical and experimental data and shown in Figure 4.13. From Figure 4.13, it can be observed that for most of the cases, permanent settlement for the numerical data is slightly higher than the permanent settlement for the experimental results since the moment capacity in numerical modeling is close to the theoretical moment capacity values.

Variation of the maximum rotation with maximum base acceleration and rocking coefficient for numerical data and experimental data is shown in Figure 4.14. Based on Figure 4.14, for most of the events, the numerical results predict higher maximum rotation for higher Cr values (0.25 – 0.353) than the experimental results, which enhances the rocking behavior and increases the self-centering ability of the soil-foundation system.

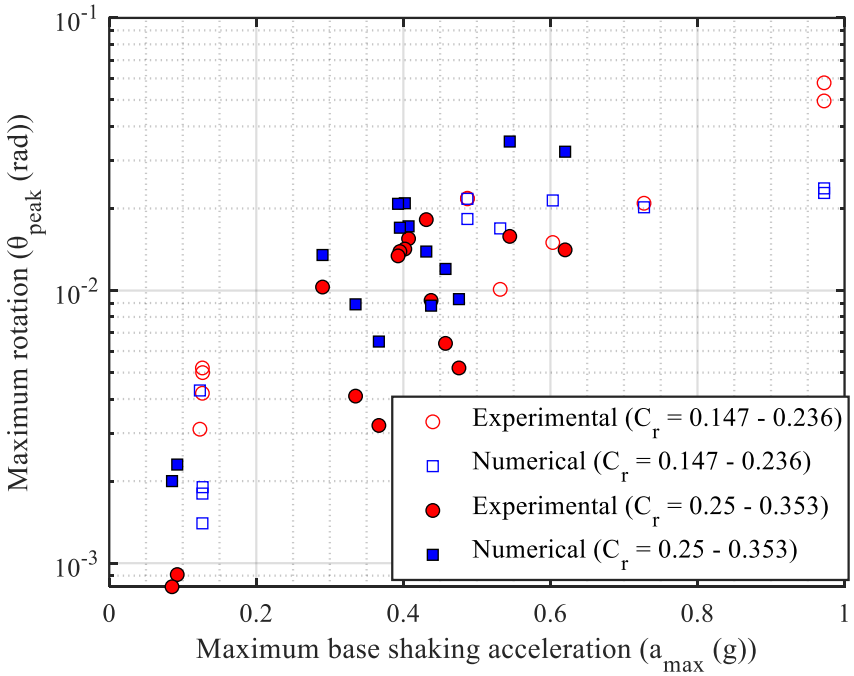

Figure 4.14. Variation of maximum rotation with maximum base acceleration for experimental and numerical results

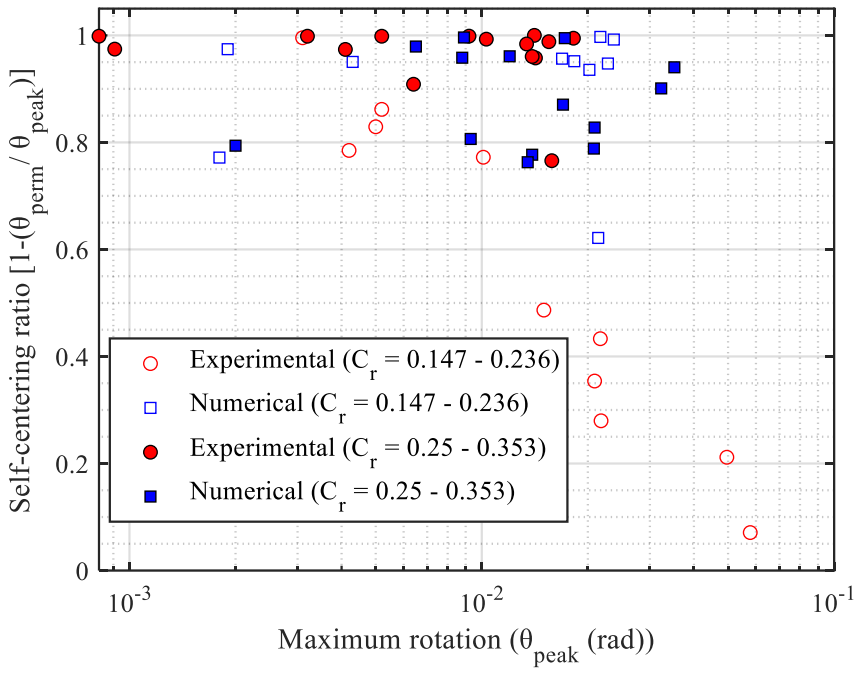

Figure 4.15. Variation of self-centering ratio with maximum rotation for experimental and numerical results.

Variation of the self-centering ratio with maximum rotation and rocking coefficient for experimental data and numerical results is shown in Figure 4.15. From Figure 4.15, it can be observed that, the self-centering ratio for numerical results are from 0.6 – 1 whereas for the experimental data, it varies from ~0.1 – 1. Hence, the numerical model predicts higher SCR values compared to the experimental results.

Variation of the tip-over stability ratio (TSR) with maximum base acceleration for both numerical data and experimental results is shown in Figure 4.16. From Figure 4.16, it can be observed that TSR value for numerical results is in the range of 0.85 – 1, and TSR for experimental data is 0.75 – 1, which indicates high stability against tip-over failure during rocking behavior.

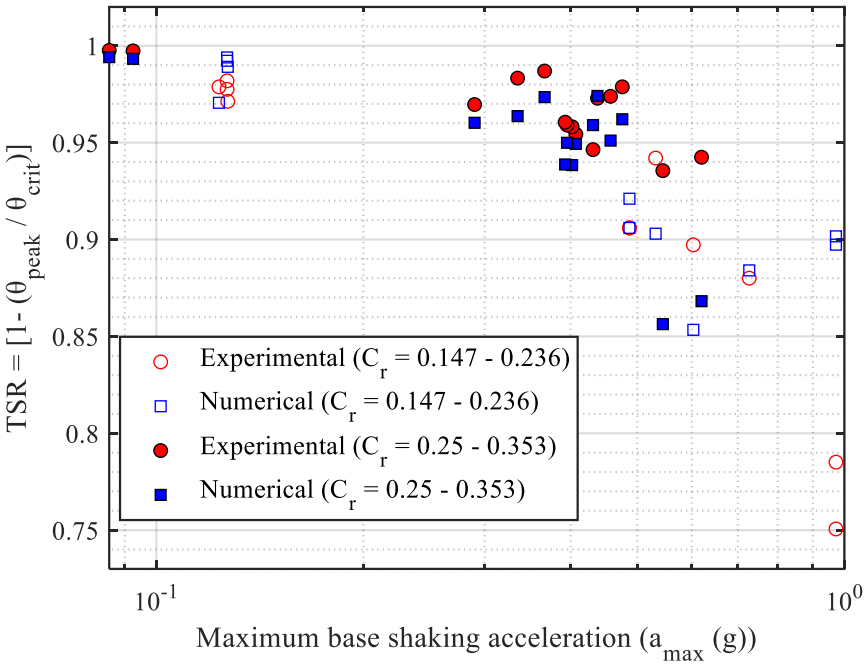

Figure 4.16. Variation of tip-over stability ratio with maximum base acceleration for experimental and numerical results.

4.6.1. Moment capacity vs A/A_c for experimental and numerical result

The maximum moment capacity versus A/A_c is compared for experimental and numerical results and shown in the Figure 4.17. From the Figure 4.17, it can be observed that, the maximum moment capacity for numerical results were closer to the ultimate theoretical moment capacity compared to the experimental results for most of the cases. The numerical model is able to capture effectively the nonlinear behavior of rocking foundation in case of relatively higher intensity of earthquake. Also, in most of the cases the maximum moment capacity of numerical data is higher than the maximum moment capacity of experimental data.

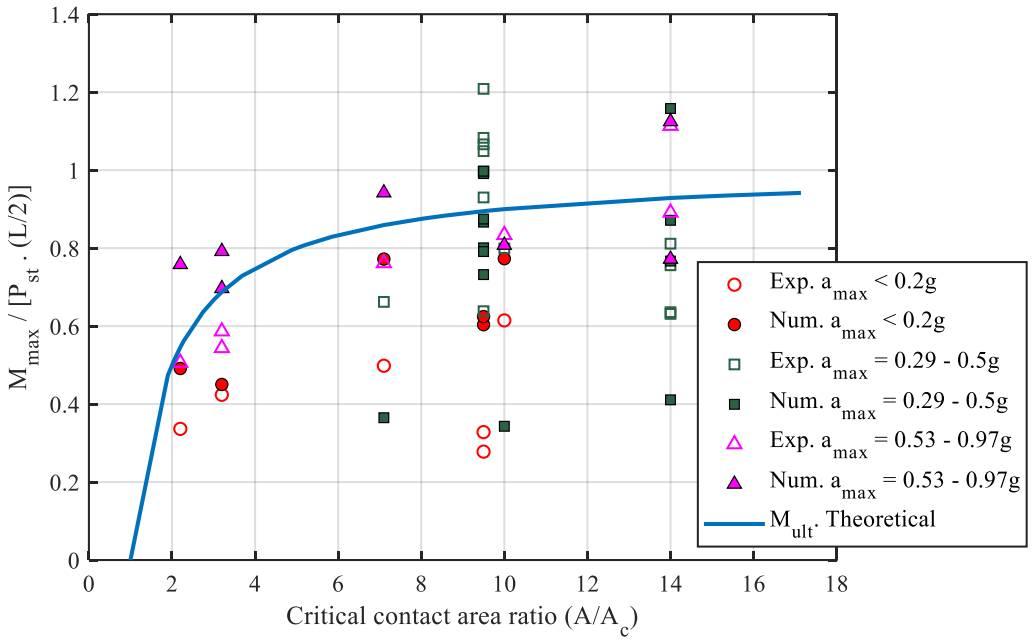

Figure 4.17. Moment capacity vs A/A_c for numerical and experimental results for 26 events

5. PARAMETRIC STUDY

5.1. Introduction

This chapter is used to analyse dependence of ultimate moment capacity on friction angle of sand or shear strength of clay, and the effects of initial vertical stiffness (K_v), peak ground displacement (d_{max}) and rocking coefficient (C_r) on permanent settlement. The range of the parameters is based on the table given in the appendix A for the shear wall and the bridge – pier model. The modeling results are presented and discussed.

5.2. Effect of Ultimate Moment Capacity on Soil Strength

The conventional bearing capacity for shallow foundation is computed based on the following soil properties such as friction angle (ϕ), unit weight of soil (γ), undrained shear strength (S_u), width of the footing (B), Depth of embedment (D), and Length of the footing (L). In rocking behavior of shallow rigid footing, the estimation of critical contact area and the ultimate moment capacity are emphasized, since the rocking of the footing is considered as a moving contact problem. And the moment capacity is obtained when contact area reaches Ac (Gajan and Kutter, 2008c).

The range of bearing capacity parameters considered for the analysis is given in Table 5.1. The mean, standard deviation and coefficient of variable variation for all 142 events are also given in Table 5.1.

Table 5.1

Bearing capacity parameters and their range

Parameter	Minimum	Maximum	Mean	Std.dev	CoV
L (m)	3	11	3.1	3.2	102.6%
B (m)	3	10.6	1.9	2	103.2%
D (m)	0	2.24	0.4	0.8	184.2%
H_{cg} (m)	0.356	13.3	4.6	4.4	95.2%
V (kN)	292.1	14400	4396	4321	98.3%
ϕ (deg)	32.7	46	40	5.4	13.54%
γ (kN/m^3)	14.2	18.19	15.81	1.22	7.7%
S_u (kPa)	53	70	61	8.62	14.2%

5.2.1. Effect of length of footing on FS_v, A/A_c, and moment capacity

The ultimate moment capacity, vertical factor of safety and critical contact area ratio for sand and clay are determined using the bearing capacity equation. The relationship between the length of footing and A/A_c, FS_v, and moment capacity is shown in Figure 5.1.

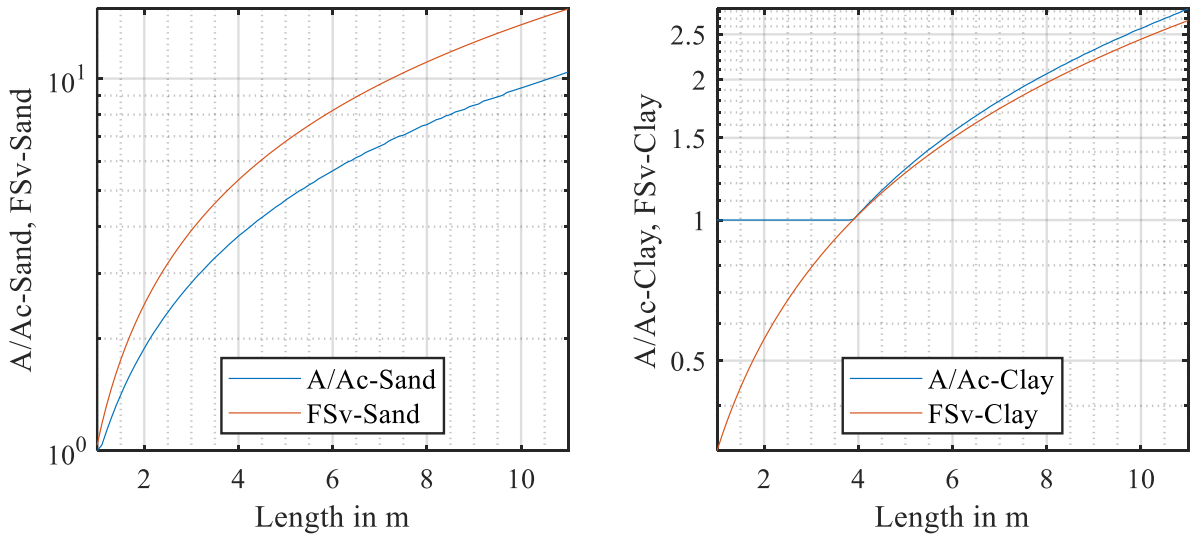

Figure 5.1. Effect of L on A/A_c, FS_v in sand and clay soil

The length of the footing given in Figure 5.1 is the dimension of footing along the direction of shaking and not necessarily the larger dimension of footing. The FS_v values were calculated based on the conventional bearing capacity equation given in Chapter 4 and initial

dimension of the footing. The critical contact area ratio is also calculated using the bearing capacity equation and the geometry of footing when contact length L is at its critical length L_c, using iterative procedure. From Figure 5.1, it can be observed that, the shape and size of the footing influence the FS_v and A/A_c values. Also, as the length increases, A/A_c for sand is about 1.5 times smaller than FS_v. In case of clay soil, the A/Ac is close to FS_v and it starts increasing slightly higher than FS_v when the length of the footing is 5m, because the bearing capacity equation for clay is not a direct function of L as can be seen from Equation 4.3.

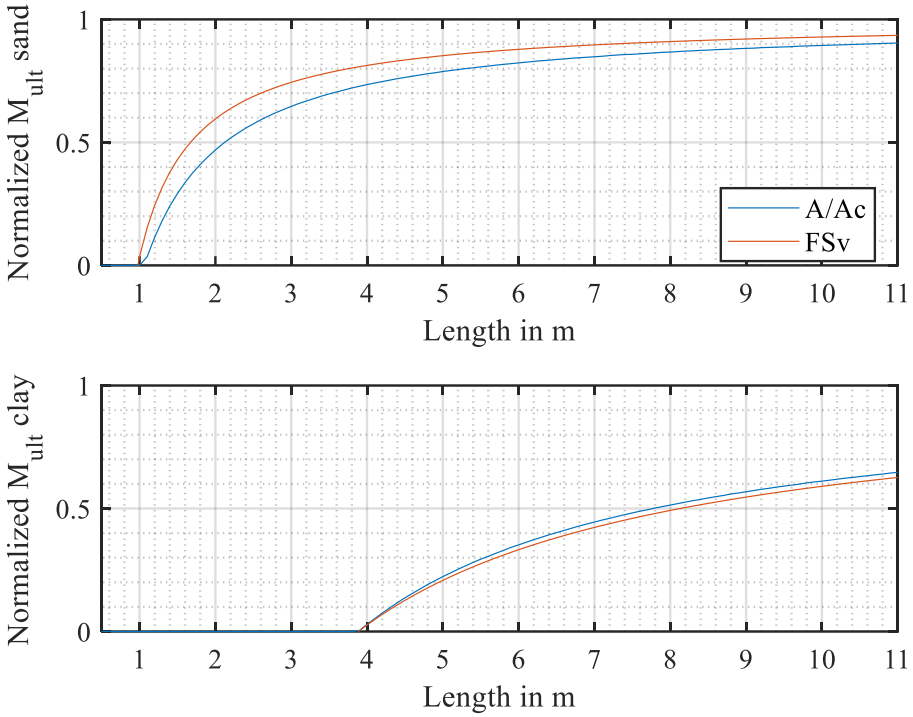

Figure 5.2. Effect of footing length on normalized moment capacity of sand and clay soil

The variation of normalized ultimate moment of sand and clay soil with length of the footing is shown in Figure 5.2. The calculation of ultimate moment capacity is given in Equation 2.1. From Figure 5.2, it can be observed that, difference in moment capacity calculated using FS_v and A/A_c decreases as length of the footing increases.

5.2.2. Effect of ϕ and S_u on moment capacity

The effect of moment capacity on soil strength is further evaluated by varying the friction angle of sand and shear strength of clay in moment capacity equation and bearing capacity equation. The variation of FS_v (conventional bearing capacity equation) and ultimate moment capacity for different ϕ and S_u values are shown in Figure 5.3. For this analysis, the friction angle is varied from 25 – 45 degrees, S_u is varied from 25 – 70 kPa, and other parameters are kept constant (mean values) as given in Table 5.1.

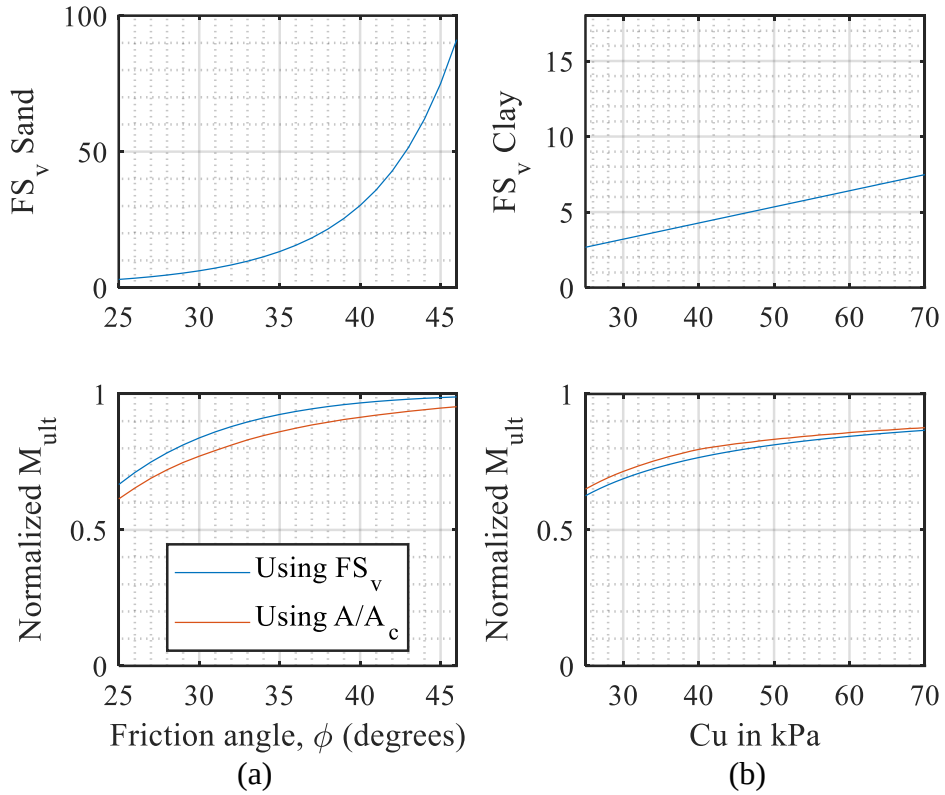

Figure 5.3. Variation of ultimate bearing capacity and ultimate moment capacity with (a) friction angle of sand and (b) shear strength of clay (S_u or C_u)

Since the bearing capacity factor N_q (Equation 4.4) is an exponential function of friction angle, the ultimate bearing capacity is more sensitive to friction angle of sand. Figure 5.3a shows FS_v value increases for sand as the friction angle increases. And, the plot in Figure 5.3a on variation of normalized ultimate moment capacity with friction angle shows that moment

capacity is less sensitive to the friction angle of sand. For example, when the friction angle of sand increases from 30 to 45 degrees, the FS_v of sand increases 92%, whereas the moment capacity increases only about 23%. Similarly, in Figure 5.3b, as S_u value increases, the FS_v of clay increases linearly since shear strength is proportional to the ultimate bearing capacity of clay. For example, when S_u varies from 30 – 70 kPa, the FS_v of clay increases 58%, whereas the moment capacity of clay increases only 18%. Hence, from Figure 5.3, it can be observed that, moment capacity is less sensitive for typical friction angle values of sand and typical shear strength values of clay.

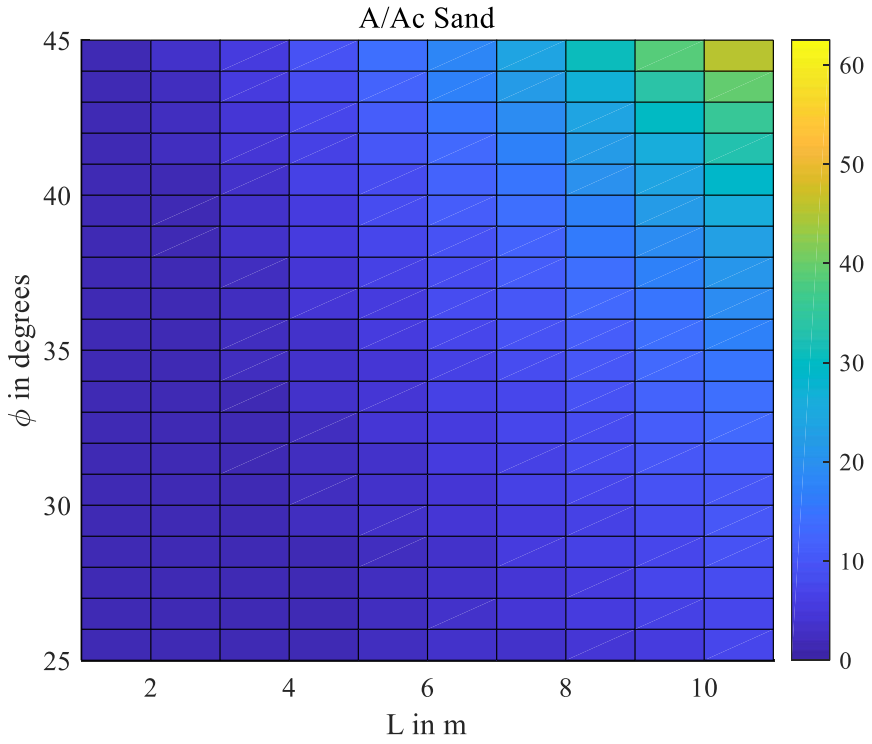

Figure 5.4. Variation of A/A_c with length of footing and friction angle of sand

The friction angle of sand is varied from 25 – 45 degrees and the length of footing is varied from 1 – 11m, to obtain the corresponding critical contact area ratio values. The obtained A/A_c values range from 1 – 60. For example, when L = 5m and friction angle is 43 degrees, the A/A_c was obtained as 12.35. The variation of A/A_c with length of footing and friction angle of

sand is shown in Figure 5.4. Using Figure 5.4, for the corresponding friction angle and length of footing, the A/A_c values can be predicted.

5.3. Effect of Initial Vertical Stiffness on Permanent Settlement

Based on numerical modeling of the shear wall and bridge-pier model, the initial vertical stiffness (K_v) was found to be a more influential parameter for permanent settlement. In order to obtain the relationship between permanent settlement and K_v, two earthquake data were used in the validated shear wall and bridge-pier models. The two earthquakes considered are Kobe (Hyogo-ken Nanbu) earthquake in 1995 and Gazli earthquake in 1976. The base horizontal acceleration versus time data of the two earthquakes are shown in Figure 5.6.

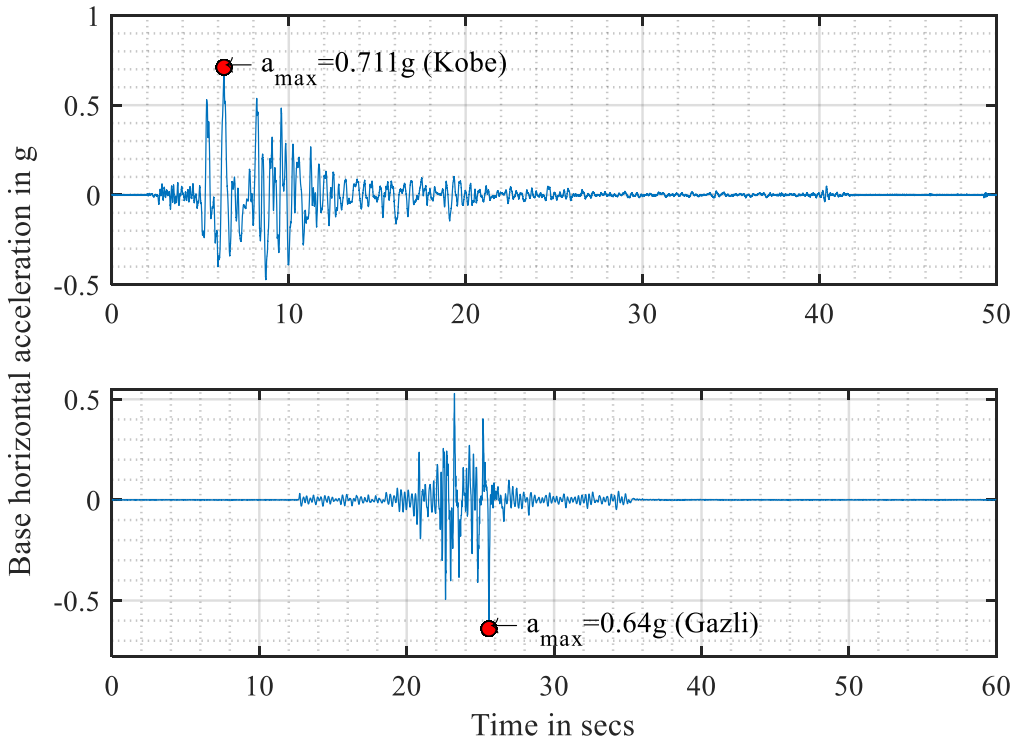

Figure 5.5. Base horizontal acceleration versus time for Kobe earthquake and Gazli earthquake

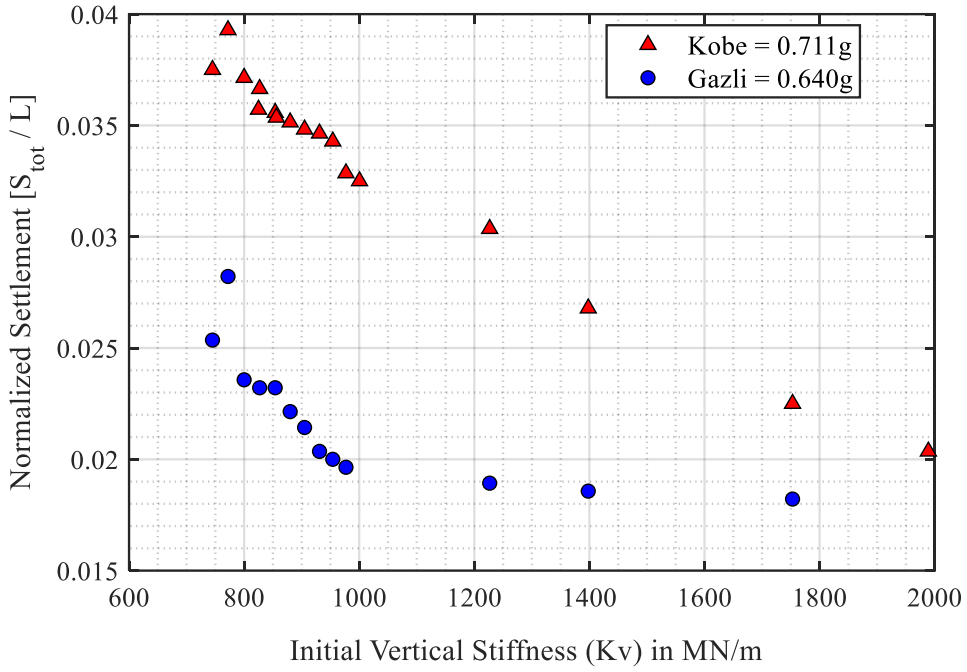

Figure 5.6. Variation of normalized settlement with different K_v values in Kobe and Gazli earthquake for the shear wall and the bridge-pier model

Variation of permanent settlement is obtained for different K_v values as shown in Figure 5.6. Since K_v is a function of shear modulus G, the G value is increased to obtain the corresponding permanent settlement for the shear wall and the bridge-pier model. From Figure 5.6, it can be observed that, the settlement value decreases as K_v value increases. Initially, the difference between settlements for the two acceleration history is more. As K_v value increases, the settlement values for the two events are close to each other. For example, the normalized settlement value for K_v of 1200 MN/m is 0.03 for Kobe earthquake and 0.019 for Gazli earthquake, the difference is 0.011. Whereas, for K_v value of 1800 MN/m, the normalized settlement value were 0.022 for Kobe earthquake and 0.018 for Gazli earthquake, the difference is 0.004. As the rigidity of the foundation increases, it enhances the rocking behavior of the footing and also the self-centering ability. Hence, the difference in normalized settlement values for the two events is observed to be very less as the stiffness increases. Moreover, the settlement

value increases for higher a_{max} values and reduces as the peak ground acceleration value reduces. For example, from Figure 5.6, it can be observed that for K_v value of 800 MN/m, the normalized settlement value is 0.037 for peak acceleration of 0.711g and 0.023 for peak acceleration of 0.640g.

The settlement is also computed with combined effects of rocking coefficient and peak ground displacement and shown in Figure 5.7. From Figure 5.7, it can be observed that settlement value reduces with increase in combined effects of K_v, C_r and d_{max}. Hence, settlement is directly proportional to the peak ground displacement (d_{max}) and inversely proportional to the combined effects of K_v, C_r and d_{max}.

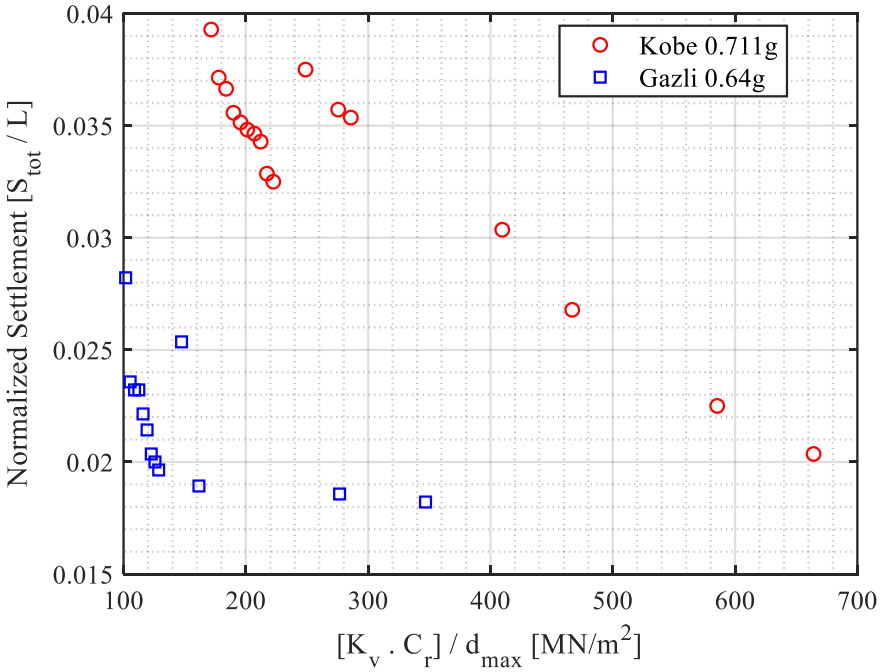

Figure 5.7. Combined effects of K_v, C_r and d_{max} on normalized settlement

6. SUMMARY AND CONCLUSIONS

6.1. Introduction

The summary of the research and conclusions derived from this research are presented in this chapter. The potential advantages of the rocking behavior of shallow foundations are highlighted from the experimental data analysis and numerical modeling analysis. The numerical model developed in this study captures most of the essential features of rocking behavior of shallow foundations supporting shear wall and bridge-pier structures. . The limitations of the current study and the recommendations for the future work are also discussed.

6.2. Summary

In this research, the nonlinear soil-foundation-structure interaction behavior of shallow foundations supporting shear wall and bridge-pier structures subjected to rocking motion is studied and analyzed using experimental data analysis and numerical modeling analysis. Further, a parametric analysis is carried out to study the effects of friction angle of sand and shear strength of clay on the moment capacity of rocking shallow foundations. The correlations involving rocking system capacity parameters, earthquake demand parameters, and performance parameters of foundation show that the seismic energy dissipation and permanent settlement are well correlated with rocking coefficient of foundation and the Arias intensity of earthquake, whereas the maximum moment and peak rotation of the foundation correlate well with peak ground acceleration. Numerical model is developed using contact interface model (CIM) as a primary component, available in OpenSees to capture the cyclic load-deformation behavior of rocking shallow foundations supporting shear wall and bridge-pier structures. The numerical simulation results are compared with experimental data to verify the accuracy of the numerical model developed in this study. Also, the parametric study clearly shows that moment capacity is

less sensitive to the friction angle of sand and shear strength of clay compared to the bearing capacity conforming the previous research findings. As expected, the settlement is inversely proportional to the initial vertical stiffness of soil-foundation system.

6.3. Conclusions

The following conclusions are derived based on the experimental data analysis of 142 earthquake shaking events, 26 numerical simulations of selected shear wall and bridge-pier models and a parametric study on effects of friction angle (shear strength) and initial vertical stiffness on settlement of rocking foundation respectively

6.3.1. Conclusions based on experimental analysis

- Experimental variables include a wide range of soil, foundation, and structure types and varying intensity of earthquake shakings. Rocking system performance parameters such as seismic energy dissipation in soil, permanent settlement, peak and permanent rotation are analyzed. These performance parameters are correlated with rocking system capacity parameters such as rocking coefficient, critical contact area ratio of the foundation and slenderness ratio of rocking systems and the earthquake demand parameters such as Arias intensity and peak ground acceleration.
- It is found that seismic energy dissipation and permanent settlement of rocking foundations correlate well with the Arias intensity of the earthquake (which includes the magnitude, duration, frequency content, and the number of cycles of loading), rather than peak ground acceleration or displacement of the earthquake motion.
- As opposed to total seismic energy dissipation and total settlement (which depend on the Arias intensity of the earthquake), the maximum moment experienced by the foundation is dictated by the peak ground acceleration of earthquake shaking.

- Rocking systems with relatively smaller values of C_r (< 0.2) dissipates considerable amount of seismic energy (as much as 10% of (V.L)), while permanent settlement is still smaller than 10% of the footing dimension even during relatively high intensity earthquake loading (where V is the total weight of the structure and L is the dimension of footing in the direction of earthquake shaking).
- A parameter called tipping over stability ratio (TSR) is defined, which is conceptually similar to factor of safety against tipping over failure. For all 142 experiments, TSR varies from about 200 for smaller magnitude earthquakes to as low as 2 for high intensity earthquakes, indicating excellent stability of rocking foundations against tipping-over failure. None of the structure-footing system used in 142 experiments has tipped over regardless of the magnitude of shaking.
- Maximum moment experienced by rocking foundations fall on or below the theoretical ultimate moment for most of the experiments. Foundations did not mobilize the theoretical ultimate moment during relatively smaller magnitude of shakings.

6.3.2. Conclusions based on numerical analysis and parametric study

- A reliable numerical model is developed using contact interface model (CIM) in OpenSees for both shear wall and bridge-pier structure-foundation-soil models. The developed numerical model is validated with experimental results for seismic energy dissipation, rotation and permanent settlement of foundations for the same base accelerations of earthquake motions.
- The numerical model is based on the theoretical ultimate moment capacity and hence the values predicted from the modeling is close to the theoretical value which is

further used to evaluate the performance parameters for other events considered for the analysis

- The numerical simulation results are compared with the experimental data to compute energy dissipation, permanent settlement, and permanent rotation, self-centering characteristics and tip-over stability ratio when mobilised moment equals the maximum moment capacity and also to highlight the accuracy of numerical modeling.
- Numerical model predictions for seismic energy dissipation of rocking foundations as a function of Arias intensity of the earthquake compare reasonably well with the corresponding experimental data. However, the numerical model seems to overpredict the permanent settlement, especially for foundations with relatively higher rocking coefficients ($C_r > 0.25$).
- Numerical model predictions for peak rotation of rocking foundation as a function of maximum base acceleration of the earthquake compare reasonably well with the corresponding experimental data. This conclusion is further strengthened by the comparisons of tipping-over stability ratio (TSR) obtained from numerical simulations with the corresponding TSR values obtained from experimental data.
- The friction angle of sand and shear strength of clay are less sensitive on moment capacity compared to the conventional bearing capacity which reinforces previous research findings.
- The settlement is inversely proportional to the initial vertical stiffness of the soil-foundation system

6.4. Recommendation for Future Work

6.4.1. Limitations of the numerical model developed in the study

The flexible column in the bridge-pier model is developed based on elastic beam column element. The developed model is computationally effective as it incorporates the vertical acceleration in terms of maximum static load, however, for performance authenticity, a real bridge scenario could be considered. Also, the simulations were performed considering the dry soil conditions below the rocking foundation on both shear wall model and bridge-pier model. Hence, the results obtained may be applicable only to those conditions.

6.4.2. Improvements for the future

The numerical model developed in this study is verified using selected experimental results. Therefore, more numerical simulations could be performed for other experimental test series (T5, T6 and T7) to further reinforce the results obtained in this study. Also, using the numerical model developed in this study, the theoretical gaps can be filled in the experimental data and propose future experiments based on the knowledge gap identified from the analysis.

REFERENCES

Anastasopoulos, I., Gazetas, G., Loli, M., Apostolou, M., and Gerolymos, N. (2010). "Soil failure can be used for seismic protection of structures",*Bulletin of Earthquake Engineering*, 8(2), 309-326.

Anastasopoulos, I., Loli, M., Georgarakos, T., and Drosos, V., (2013). "Shaking table testing of rocking-isolated bridge pier on sand", *J. Earthquake Eng*. 17, 1–32

Antonellis, G., Gavras, A. G., Panagiotou, M., Kutter, B. L., Guerrini, G., Sander, A. 547 C., and Fox, P. J., (2015). "Shake table test of large-scale bridge columns supported on rocking shallow foundations", *J.Geotech. Geoenviron. Eng*. 141, DOI: 10.1061/(ASCE)GT.1943-5606.0001284.

Das, B. M. (2015). *Principles of foundation engineering*, Cengage learning.

DeBeer, E. E. (1970). "Experimental determination of the shape factors and bearing equation factors of sand", *Geotechnique*, Vol. 20, No. 4, 387-411.

Deng, L., and Kutter, B. L., (2012). "Characterization of rocking shallow foundations using centrifuge model tests", *Earthquake Engng Struct. Dyn*. 41, 1043–1060.

Deng, L., Kutter, B. L., and Kunnath, S. K., (2012). "Centrifuge modeling of bridge systems designed for rocking foundations", *J. Geotech. Geoenviron. Eng*. 138, 335–344.

Drosos, V., Georgarakos, T., Loli, M., Anastsopoulos, I., Zarzouras, O., and Gazetas, G. (2012). "Soil-Foundation-Structure Interaction with Mobilization of Bearing Capacity: Experimental Study on Sand", *J.Geotech. Geoenviron*, 138(11), 1369–1386

FEMA 356 (2000), "Prestandard and Commentary for the Seismic Rehabilitation of Buildings", Federal Emergency Management Agency, Washington, DC

Gajan, S., and Kayser, M., (2017). “Quantification of the influence of subsurface uncertainties on the performance of rocking foundations during seismic loading”, *Soil Dyn. Earthq. Eng*. 116, 1–14.

Gajan, S., and Kutter, B. L., (2008a). “Capacity, settlement, and energy dissipation of shallow footings subjected to rocking”, *J. Geotech. Geoenviron. Eng*. 134, 1129–1141.

Gajan, S., and Kutter, B. L., (2008b). “Numerical simulations of rocking behavior of shallow footings and comparisons with experiments”, *Proc. British Geotechnical Association (BGA) International Conference on Foundations*. 24 – 27.

Gajan, S., and Kutter, B. L., (2008c). “Effect of critical contact area ration on moment capacity of rocking shallow footings”, in Proc, *Geotechnical Earthquake Engineering and Soil Dynamics IV*, ASCE.

Gajan, S., and Kutter, B. L. (2009a). “Contact Interface Model for Shallow Foundations Subjected to Combined Cyclic Loading”, *J. Geotech. Geoenviron*, 135(3), 407-419.

Gajan, S., and Kutter, B. L., (2009b). “Effects of moment-to-shear ratio on combined cyclic load displacement behavior of shallow foundation from centrifuge tests”, *J. Geotech. Geoenviron. Eng*.135, 1044–11055

Gajan, S., Kutter B. L., Phalen, J. D., Hutchinson, T. C. and Martin, G. R.,(2005). “Centrifuge modeling of load-deformation behavior of rocking shallow foundations”, *Soil Dyn. Earthq. Eng*. 25, 773–783.

Godagama, B.S., (2016). “Seismic Performance of Yielding Columns Supported by Rocking Foundations: A Computational Study”, *MS thesis*, Dept. of Civil and Environmental Engineering, North Dakota State University, Fargo, ND.

Hakhamaneshi, M., Kutter, B. L., Deng, L., Hutchinson, T. C., and Liu, W., (2012). "New findings from centrifuge modeling of rocking shallow foundations in clayey ground", in Proc, *GeoCongress 2012*, 25–29 March 2012, Oakland, CA.

Hansen, J. B. (1970). "A Revised and Extended Formula for Bearing Capacity", *Danish Geotechnical Institute*, Bulletin 28, Copenhagen.

Houlsby, G.T., Amorosi,A., and Rojas,E.(2005). "Elastic moduli of soils dependent on pressure: a hyperelastic formulation",. *Géotechnique* 55, 383–392.doi:10.1680/ geot.2005.55.5.383

Kramer, S. L. (1996). *Geotechnical earthquake engineering*, Pearson Education India.

Mergos, P.E., and Kawashima, K., (2005). "Rocking isolation of a typical bridge pier on spread foundation", *Journal of Earthquake Engineering*, pp. 395-414. doi: 10.1142/S1363246905002456

OpenSees (2008). "Open system for earthquake engineering simulation – development platform by peer."

Raychowdhury, P. and Hutchinson, T. (2008). "Nonlinear material models for Winkler-based shallow foundation response evaluation." In the Proc, *GeoCongress* 2008, New Orleans, Louisiana, March.

Terzaghi, K. (1943). "Theoretical soil mechanics", Wiley, New York, 1943

Tsatsis, A., Anastasopoulos, I., (2015). "Performance of rocking systems on shallow improved sand: shaking table testing", *Front. Built Environ*. 1:9. Doi: 10.3389/fbuil.2015.00009

APPENDIX A. THE SUMMARISED DATA OF 142 EVENTS USED FOR THE ANALYSIS

Event No	FSv	Cr	A/Ac	h/L	B(m)	L (m)	hcg (m)	D(m)	a_max (g)	Ia (m/s)	Sn (-)	En (-)	θmax (rad)	θperm (rad)	Δmax (m)	Pst or V (N)	q(kPa)
1	7.2	0.236	7.1	1.78	0.65	2.8	4.98	0.7	0.127	0.159	4.88E-03	4.03E-03	4.23E-03	8.94E-04	2.10E-02	5.69E+05	312.637
2	7.2	0.236	7.1	1.78	0.65	2.8	4.98	0.7	0.487	3.417	2.54E-02	3.94E-02	2.09E-02	1.48E-02	1.04E-01	5.69E+05	312.637
3	7.2	0.236	7.1	1.78	0.65	2.8	4.98	0.7	0.972	8.043	3.05E-02	6.31E-02	4.20E-02	3.78E-02	2.09E-01	5.69E+05	312.637
4	11.5	0.235	10.0	1.89	0.65	2.8	5.3	0.7	0.127	0.159	4.70E-03	5.28E-03	5.15E-03	5.65E-04	2.73E-02	3.61E+05	198.352
5	11.5	0.235	10.0	1.89	0.65	2.8	5.3	0.7	0.487	3.417	1.86E-02	5.96E-02	2.10E-02	1.17E-02	1.11E-01	3.61E+05	198.352
6	11.5	0.235	10.0	1.89	0.65	2.8	5.3	0.7	0.972	8.043	1.87E-02	8.74E-02	3.72E-02	2.71E-02	1.97E-01	3.61E+05	198.352
7	2.6	0.147	2.2	1.78	0.65	2.8	4.98	0	0.123	0.190	8.13E-03	4.15E-03	3.22E-03	1.16E-04	1.60E-02	5.69E+05	312.637
8	2.6	0.147	2.2	1.78	0.65	2.8	4.98	0	0.603	2.858	2.84E-02	2.43E-02	1.50E-02	7.74E-03	7.47E-02	5.69E+05	312.637
9	4.0	0.176	3.2	1.89	0.65	2.8	5.3	0	0.127	0.200	9.06E-03	5.03E-03	4.85E-03	7.37E-04	2.57E-02	3.61E+05	198.352
10	4.0	0.176	3.2	1.89	0.65	2.8	5.3	0	0.532	3.048	1.62E-02	3.08E-02	9.71E-03	1.54E-03	5.14E-02	3.61E+05	198.352
11	4.0	0.176	3.2	1.89	0.65	2.8	5.3	0	0.727	6.536	2.40E-02	5.19E-02	1.85E-02	1.13E-02	9.80E-02	3.61E+05	198.352
12	16.1	0.250	14.0	1.44	4.28	6.7	9.62	2.24	0.335	0.993	1.74E-03	1.28E-03	4.13E-03	1.06E-04	3.97E-02	6.62E+06	230.82
13	16.1	0.250	14.0	1.44	4.28	6.7	9.62	2.24	0.457	2.259	2.20E-03	3.57E-03	6.42E-03	5.99E-04	6.18E-02	6.62E+06	230.82
14	16.1	0.250	14.0	1.44	4.28	6.7	9.62	2.24	0.545	7.400	2.73E-03	1.20E-02	1.58E-02	3.71E-03	1.52E-01	6.62E+06	230.82
15	16.1	0.250	14.0	1.44	4.28	6.7	9.62	2.24	0.367	0.773	3.50E-03	2.11E-03	3.19E-03	2.90E-06	3.07E-02	6.62E+06	230.82
16	16.1	0.250	14.0	1.44	4.28	6.7	9.62	2.24	0.476	1.599	4.54E-03	4.25E-03	5.22E-03	1.61E-05	5.02E-02	6.62E+06	230.82
17	16.1	0.250	14.0	1.44	4.28	6.7	9.62	2.24	0.620	5.357	1.44E-02	1.48E-02	1.41E-02	4.02E-06	1.36E-01	6.62E+06	230.82
18	11.0	0.353	9.5	1.27	4.7	7.35	9.31	2.24	0.093	0.045	4.79E-06	2.21E-04	9.32E-04	8.20E-06	8.68E-03	6.86E+06	198.524
19	11.0	0.353	9.5	1.27	4.7	7.35	9.31	2.24	0.153	0.196	2.14E-05	1.85E-03	3.25E-03	5.64E-05	3.02E-02	6.86E+06	198.524
20	11.0	0.353	9.5	1.27	4.7	7.35	9.31	2.24	0.037	0.038	7.38E-05	3.92E-04	8.06E-04	5.90E-05	7.50E-03	6.86E+06	198.524
21	11.0	0.353	9.5	1.27	4.7	7.35	9.31	2.24	0.046	0.051	7.06E-05	1.05E-06	9.56E-04	6.05E-07	8.90E-03	6.86E+06	198.524
22	11.0	0.353	9.5	1.27	4.7	7.35	9.31	2.24	0.085	0.039	6.02E-05	2.36E-04	8.20E-04	6.31E-07	7.63E-03	6.86E+06	198.524
23	11.0	0.353	9.5	1.27	4.7	7.35	9.31	2.24	0.438	1.643	5.73E-04	8.61E-03	9.27E-03	2.91E-05	8.63E-02	6.86E+06	198.524
24	11.0	0.353	9.5	1.27	4.7	7.35	9.31	2.24	0.218	1.063	8.98E-05	1.39E-02	6.69E-03	1.50E-06	6.23E-02	6.86E+06	198.524
25	11.0	0.353	9.5	1.27	4.7	7.35	9.31	2.24	0.595	4.544	1.90E-04	2.97E-02	1.95E-02	3.22E-05	1.82E-01	6.86E+06	198.524
26	11.0	0.353	9.5	1.27	4.7	7.35	9.31	2.24	0.882	6.645	8.71E-05	5.03E-02	2.46E-02	5.95E-05	2.29E-01	6.86E+06	198.524
27	11.0	0.353	9.5	1.27	4.7	7.35	9.31	2.24	0.229	1.168	1.40E-04	1.51E-02	9.53E-03	1.86E-04	8.88E-02	6.86E+06	198.524
28	11.0	0.353	9.5	1.27	4.7	7.35	9.31	2.24	0.431	2.029	1.02E-04	3.03E-02	1.81E-02	1.79E-04	1.68E-01	6.86E+06	198.524
29	11.0	0.353	9.5	1.27	4.7	7.35	9.31	2.24	0.290	1.352	4.93E-04	2.75E-02	1.03E-02	2.03E-04	9.62E-02	6.86E+06	198.524
30	11.0	0.353	9.5	1.27	4.7	7.35	9.31	2.24	0.407	2.518	2.23E-04	4.52E-02	1.54E-02	3.80E-04	1.43E-01	6.86E+06	198.524
31	11.0	0.353	9.5	1.27	4.7	7.35	9.31	2.24	0.402	2.491	4.92E-04	4.40E-02	1.48E-02	3.34E-04	1.38E-01	6.86E+06	198.524
32	11.0	0.353	9.5	1.27	4.7	7.35	9.31	2.24	0.395	2.445	2.40E-04	4.32E-02	1.45E-02	2.51E-04	1.35E-01	6.86E+06	198.524
33	11.0	0.353	9.5	1.27	4.7	7.35	9.31	2.24	0.393	2.407	9.73E-05	4.42E-02	1.32E-02	1.63E-04	1.23E-01	6.86E+06	198.524
34	11.0	0.353	9.5	1.27	4.7	7.35	9.31	2.24	0.222	1.147	5.10E-05	1.42E-02	9.99E-03	2.33E-05	9.30E-02	6.86E+06	198.524
35	5.6	0.277	4.9	1.37	3.33	3.33	4.56	0.3	0.122	0.079	7.30E-06	5.09E-04	4.88E-03	1.18E-05	2.22E-02	7.29E+05	65.7504
36	5.6	0.277	4.9	1.37	3.33	3.33	4.56	0.3	0.272	0.353	3.33E-05	4.74E-03	1.17E-02	6.25E-06	5.35E-02	7.29E+05	65.7504
37	5.6	0.277	4.9	1.37	3.33	3.33	4.56	0.3	0.127	0.354	9.67E-06	1.41E-03	3.67E-03	5.51E-07	1.67E-02	7.29E+05	65.7504
38	5.6	0.277	4.9	1.37	3.33	3.33	4.56	0.3	0.132	0.100	1.63E-04	1.18E-03	3.99E-03	1.55E-04	1.82E-02	7.29E+05	65.7504
39	5.6	0.277	4.9	1.37	3.33	3.33	4.56	0.3	0.581	1.832	2.53E-04	1.19E-02	2.04E-02	3.30E-04	9.28E-02	7.29E+05	65.7504
40	3.4	0.226	3.0	1.37	6.66	6.66	9.13	0.6	0.641	2.202	6.64E-04	4.12E-02	3.74E-02	9.92E-04	3.41E-01	5.83E+06	131.483
41	10.0	0.314	8.6	1.37	1.67	1.67	2.28	0.15	0.465	0.741	4.19E-06	7.28E-03	1.14E-02	8.65E-06	2.61E-02	9.11E+04	32.676
42	10.0	0.314	8.6	1.37	1.67	1.67	2.28	0.15	0.531	0.748	1.51E-05	6.45E-03	8.21E-03	5.60E-07	1.87E-02	9.11E+04	32.676
43	10.0	0.314	8.6	1.37	1.67	1.67	2.28	0.15	1.283	4.462	8.33E-05	2.20E-02	1.49E-02	4.01E-07	3.41E-02	9.11E+04	32.676
44	5.6	0.277	4.9	1.37	3.33	3.33	4.56	0.3	0.381	0.725	9.97E-05	7.52E-03	1.07E-02	3.56E-04	4.86E-02	7.29E+05	65.7504
45	5.6	0.277	4.9	1.37	3.33	3.33	4.56	0.3	0.558	1.989	2.54E-05	1.51E-02	2.50E-02	1.32E-05	1.14E-01	7.29E+05	65.7504
46	5.6	0.277	4.9	1.37	3.33	3.33	4.56	0.3	0.584	1.769	3.64E-04	1.42E-02	1.80E-02	5.94E-04	8.22E-02	7.29E+05	65.7504

Event No	FSv	Cr	A/Ac	h/L	B(m)	L (m)	hcg (m)	D(m)	a_max (g)	Ia (m/s)	Sn (-)	En (-)	θmax (rad)	θperm (rad)	Δmax (m)	Pst or V (N)	q(kPa)
47	10.7	0.296	9.7	1.48	5.28	3.21	4.76	0.3	0.122	0.079	6.60E-06	2.11E-03	7.13E-03	6.93E-05	3.39E-02	5.48E+05	32.3327
48	10.7	0.296	9.7	1.48	5.28	3.21	4.76	0.3	0.272	0.353	4.95E-06	1.12E-02	1.26E-02	5.68E-06	6.00E-02	5.48E+05	32.3327
49	10.7	0.296	9.7	1.48	5.28	3.21	4.76	0.3	0.127	0.354	3.55E-06	9.10E-03	5.95E-03	7.64E-05	2.83E-02	5.48E+05	32.3327
50	10.7	0.296	9.7	1.48	5.28	3.21	4.76	0.3	0.132	0.100	5.61E-08	4.39E-03	5.99E-03	1.16E-04	2.85E-02	5.48E+05	32.3327
51	10.7	0.296	9.7	1.48	5.28	3.21	4.76	0.3	0.581	1.832	4.07E-05	4.31E-02	2.55E-02	1.21E-04	1.22E-01	5.48E+05	32.3327
52	6.4	0.270	5.9	1.48	10.6	6.42	9.53	0.6	1.281	8.806	7.13E-04	1.04E-01	6.24E-02	1.81E-02	5.95E-01	4.38E+06	64.4213
53	19.1	0.313	17.1	1.49	2.64	1.6	2.38	0.15	0.465	0.741	1.24E-05	1.73E-02	1.24E-02	1.64E-04	2.96E-02	6.85E+04	16.2145
54	19.1	0.313	17.1	1.49	2.64	1.6	2.38	0.15	0.531	0.748	1.02E-05	2.07E-02	1.17E-02	1.08E-04	2.77E-02	6.85E+04	16.2145
55	19.1	0.313	17.1	1.49	2.64	1.6	2.38	0.15	1.283	4.462	4.79E-05	4.77E-02	2.12E-02	8.35E-05	5.05E-02	6.85E+04	16.2145
56	10.7	0.296	9.7	1.48	5.28	3.21	4.76	0.3	0.381	0.725	8.91E-06	2.75E-02	1.55E-02	3.56E-05	7.37E-02	5.48E+05	32.3327
57	10.7	0.296	9.7	1.48	5.28	3.21	4.76	0.3	0.558	1.989	3.19E-05	3.36E-02	2.49E-02	1.94E-04	1.19E-01	5.48E+05	32.3327
58	10.7	0.296	9.7	1.48	5.28	3.21	4.76	0.3	0.584	1.769	9.43E-05	5.38E-02	3.14E-02	8.32E-05	1.50E-01	5.48E+05	32.3327
59	13.9	0.183	8.1	2.37	0.15	0.15	0.356	0	0.250	0.336	8.79E-03	2.66E-02	5.15E-03	1.68E-03	1.84E-03	3.47E+02	15.4089
60	13.9	0.183	8.1	2.37	0.15	0.15	0.356	0	0.445	1.410	3.64E-02	6.77E-02	1.48E-02	9.80E-03	5.28E-03	3.47E+02	15.4089
61	13.9	0.183	8.1	2.37	0.15	0.15	0.356	0	0.180	0.360	6.27E-03	5.36E-02	1.31E-02	6.00E-03	4.65E-03	3.47E+02	15.4089
62	13.9	0.183	8.1	2.37	0.15	0.15	0.356	0	0.356	2.158	1.04E-02	1.24E-01	2.99E-02	1.56E-02	1.07E-02	3.47E+02	15.4089
63	13.9	0.183	8.1	2.37	0.15	0.15	0.356	0	1.084	2.292	2.68E-02	8.09E-02	3.87E-02	1.42E-02	1.38E-02	3.47E+02	15.4089
64	13.9	0.183	8.1	2.37	0.15	0.15	0.356	0	0.468	0.487	5.40E-03	2.13E-02	1.52E-02	9.40E-03	5.42E-03	3.47E+02	15.4089
65	13.9	0.183	8.1	2.37	0.15	0.15	0.356	0	0.399	0.112	8.36E-03	9.45E-03	9.61E-03	4.80E-03	3.42E-03	3.47E+02	15.4089
66	13.9	0.183	8.1	2.37	0.15	0.15	0.356	0	0.369	0.142	6.75E-03	1.62E-02	1.17E-02	4.80E-03	4.15E-03	3.47E+02	15.4089
67	13.9	0.183	8.1	2.37	0.15	0.15	0.356	0	0.520	0.876	2.90E-02	7.35E-02	2.00E-02	1.59E-02	7.10E-03	3.47E+02	15.4089
68	13.9	0.183	8.1	2.37	0.15	0.15	0.356	0	0.811	0.870	1.16E-02	3.22E-02	1.59E-02	1.24E-02	5.65E-03	3.47E+02	15.4089
69	13.9	0.183	8.1	2.37	0.15	0.15	0.356	0	1.018	1.558	1.15E-02	7.00E-02	9.22E-02	9.22E-02	3.28E-02	3.47E+02	15.4089
70	4.9	0.115	2.3	2.37	0.15	0.15	0.356	0	0.245	0.374	3.86E-02	1.83E-02	1.45E-02	1.21E-02	5.15E-03	3.47E+02	15.4089
71	4.9	0.115	2.3	2.37	0.15	0.15	0.356	0	0.424	0.133	3.73E-02	3.42E-03	9.05E-03	8.22E-03	3.22E-03	3.47E+02	15.4089
72	4.9	0.115	2.3	2.37	0.15	0.15	0.356	0	0.389	0.154	3.35E-02	7.40E-03	2.65E-02	2.59E-02	9.43E-03	3.47E+02	15.4089
73	9.8	0.183	8.0	2.37	0.15	0.15	0.356	0	0.239	0.349	1.92E-02	2.68E-02	4.03E-03	1.20E-03	1.43E-03	3.47E+02	15.4089
74	9.8	0.183	8.0	2.37	0.15	0.15	0.356	0	0.497	1.410	8.77E-02	5.24E-02	1.73E-02	1.46E-02	6.16E-03	3.47E+02	15.4089
75	9.8	0.183	8.0	2.37	0.15	0.15	0.356	0	0.183	0.383	9.05E-03	5.40E-02	1.32E-02	6.50E-03	4.71E-03	3.47E+02	15.4089
76	9.8	0.183	8.0	2.37	0.15	0.15	0.356	0	0.358	2.174	1.39E-02	1.34E-01	3.88E-02	2.67E-02	1.38E-02	3.47E+02	15.4089
77	9.8	0.183	8.0	2.37	0.15	0.15	0.356	0	1.231	2.577	4.09E-02	9.96E-02	4.47E-02	4.29E-02	1.59E-02	3.47E+02	15.4089
78	9.8	0.183	8.0	2.37	0.15	0.15	0.356	0	0.454	0.560	1.00E-02	3.23E-02	2.89E-02	2.55E-02	1.03E-02	3.47E+02	15.4089
79	9.8	0.183	8.0	2.37	0.15	0.15	0.356	0	0.372	0.153	1.97E-02	7.86E-03	8.27E-03	2.10E-03	2.94E-03	3.47E+02	15.4089
80	9.8	0.183	8.0	2.37	0.15	0.15	0.356	0	0.387	0.160	1.55E-02	1.60E-02	1.22E-02	4.90E-03	4.33E-03	3.47E+02	15.4089
81	9.8	0.183	8.0	2.37	0.15	0.15	0.356	0	0.653	1.047	5.70E-02	7.52E-02	8.84E-03	4.60E-03	3.15E-03	3.47E+02	15.4089
82	9.8	0.183	8.0	2.37	0.15	0.15	0.356	0	0.848	0.956	1.97E-02	3.23E-02	9.09E-03	3.10E-03	3.24E-03	3.47E+02	15.4089
83	9.8	0.183	8.0	2.37	0.15	0.15	0.356	0	1.065	1.663	3.20E-02	7.71E-02	4.34E-02	2.47E-02	1.55E-02	3.47E+02	15.4089
84	7.1	0.183	8.0	2.37	0.15	0.15	0.356	0	0.235	0.346	2.66E-02	2.66E-02	6.18E-03	3.60E-03	2.20E-03	3.47E+02	15.4089
85	7.1	0.183	8.0	2.37	0.15	0.15	0.356	0	0.563	1.655	1.30E-01	2.82E-02	2.99E-02	2.86E-02	1.06E-02	3.47E+02	15.4089
86	7.1	0.183	8.0	2.37	0.15	0.15	0.356	0	0.182	0.365	1.02E-02	4.75E-02	2.02E-02	1.61E-02	7.19E-03	3.47E+02	15.4089
87	7.1	0.183	8.0	2.37	0.15	0.15	0.356	0	0.420	0.128	2.23E-02	7.32E-03	8.66E-03	3.07E-03	3.08E-03	3.47E+02	15.4089
88	7.1	0.183	8.0	2.37	0.15	0.15	0.356	0	0.409	0.165	2.37E-02	1.41E-02	1.52E-02	1.25E-02	5.40E-03	3.47E+02	15.4089
89	7.1	0.183	8.0	2.37	0.15	0.15	0.356	0	0.696	1.157	7.78E-02	5.47E-02	8.49E-02	8.44E-02	3.02E-02	3.47E+02	15.4089
90	4.9	0.128	3.7	2.83	0.15	0.15	0.424	0	0.080	0.029	3.89E-03	1.96E-03	1.58E-03	1.01E-03	6.69E-04	9.86E+02	43.8222
91	4.9	0.128	3.7	2.83	0.15	0.15	0.424	0	0.179	0.149	8.08E-03	6.77E-03	2.63E-03	1.17E-03	1.12E-03	9.86E+02	43.8222
92	4.9	0.128	3.7	2.83	0.15	0.15	0.424	0	0.251	0.349	1.09E-02	1.28E-02	5.11E-03	2.49E-03	2.16E-03	9.86E+02	43.8222

Event No	FSv	Cr	A/Ac	h/L	B(m)	L (m)	hcg (m)	D(m)	a_max (g)	Ia (m/s)	Sn (-)	En (-)	θmax (rad)	θperm (rad)	Δmax (m)	Pst or V (N)	q(kPa)
93	4.9	0.128	3.7	2.83	0.15	0.15	0.424	0	0.321	0.620	1.37E-02	1.80E-02	8.04E-03	5.10E-03	3.41E-03	9.86E+02	43.8222
94	4.9	0.128	3.7	2.83	0.15	0.15	0.424	0	0.359	0.910	1.65E-02	2.35E-02	1.41E-02	1.12E-02	5.99E-03	9.86E+02	43.8222
95	4.9	0.128	3.7	2.83	0.15	0.15	0.424	0	0.416	1.241	1.92E-02	3.06E-02	4.99E-02	4.82E-02	2.12E-02	9.86E+02	43.8222
96	2.5	0.082	1.9	2.83	0.15	0.15	0.424	0	0.080	0.033	5.68E-03	1.51E-03	3.75E-03	3.46E-03	1.59E-03	9.86E+02	43.8222
97	2.5	0.082	1.9	2.83	0.15	0.15	0.424	0	0.180	0.155	1.52E-02	4.92E-03	1.16E-02	1.12E-02	4.93E-03	9.86E+02	43.8222
98	4.0	0.128	3.7	2.83	0.15	0.15	0.424	0	0.081	0.029	4.11E-03	1.59E-03	8.74E-04	2.28E-04	3.70E-04	9.86E+02	43.8222
99	4.0	0.128	3.7	2.83	0.15	0.15	0.424	0	0.181	0.148	8.91E-03	5.68E-03	2.54E-03	1.06E-03	1.08E-03	9.86E+02	43.8222
100	4.0	0.128	3.7	2.83	0.15	0.15	0.424	0	0.244	0.350	1.67E-02	1.23E-02	3.94E-03	1.87E-03	1.67E-03	9.86E+02	43.8222
101	4.0	0.128	3.7	2.83	0.15	0.15	0.424	0	0.297	0.608	1.78E-02	1.75E-02	6.06E-03	3.53E-03	2.57E-03	9.86E+02	43.8222
102	4.0	0.128	3.7	2.83	0.15	0.15	0.424	0	0.351	0.898	2.19E-02	2.26E-02	1.05E-02	8.16E-03	4.45E-03	9.86E+02	43.8222
103	4.0	0.128	3.7	2.83	0.15	0.15	0.424	0	0.409	1.208	2.89E-02	2.99E-02	2.82E-02	2.59E-02	1.20E-02	9.86E+02	43.8222
104	3.1	0.128	3.7	2.83	0.15	0.15	0.424	0	0.078	0.027	6.32E-03	1.52E-03	1.15E-03	4.37E-04	4.87E-04	9.86E+02	43.8222
105	3.1	0.128	3.7	2.83	0.15	0.15	0.424	0	0.176	0.147	1.31E-02	6.04E-03	2.43E-03	9.98E-04	1.03E-03	9.86E+02	43.8222
106	3.1	0.128	3.7	2.83	0.15	0.15	0.424	0	0.244	0.353	1.84E-02	1.23E-02	6.01E-03	3.97E-03	2.55E-03	9.86E+02	43.8222
107	3.1	0.128	3.7	2.83	0.15	0.15	0.424	0	0.300	0.614	2.37E-02	1.68E-02	1.33E-02	1.15E-02	5.65E-03	9.86E+02	43.8222
108	24.5	0.296	14.8	1.74	1.52	1.52	2.64	0	0.467	0.622	3.51E-04	1.39E-03	3.13E-03	3.96E-04	8.27E-03	2.92E+05	126.428
109	24.5	0.296	14.8	1.74	1.52	1.52	2.64	0	0.329	0.879	5.80E-04	5.15E-03	4.82E-03	6.59E-05	1.27E-02	2.92E+05	126.428
110	24.5	0.296	14.8	1.74	1.52	1.52	2.64	0	0.346	0.717	3.33E-04	3.14E-03	8.69E-03	1.10E-04	2.29E-02	2.92E+05	126.428
111	24.5	0.296	14.8	1.74	1.52	1.52	2.64	0	0.359	1.778	1.77E-03	6.26E-02	5.52E-02	1.72E-03	1.46E-01	2.92E+05	126.428
112	24.5	0.330	14.8	1.74	1.52	1.52	2.64	0	0.448	0.569	6.64E-04	3.61E-03	4.99E-03	1.79E-04	1.32E-02	2.92E+05	126.428
113	24.5	0.330	14.8	1.74	1.52	1.52	2.64	0	0.309	0.845	4.71E-04	5.04E-03	9.19E-03	2.40E-04	2.42E-02	2.92E+05	126.428
114	24.5	0.330	14.8	1.74	1.52	1.52	2.64	0	0.346	0.711	2.51E-04	5.29E-03	1.61E-02	1.47E-03	4.25E-02	2.92E+05	126.428
115	24.5	0.330	14.8	1.74	1.52	1.52	2.64	0	0.421	1.443	5.46E-04	1.94E-02	2.87E-02	1.58E-03	7.59E-02	2.92E+05	126.428
116	24.5	0.330	14.8	1.74	1.52	1.52	2.64	0	0.354	1.770	5.40E-04	6.52E-02	5.39E-02	6.21E-03	1.42E-01	2.92E+05	126.428
117	24.5	0.330	14.8	1.74	1.52	1.52	2.64	0	0.800	6.986	1.24E-02	1.34E-01	1.20E-01	6.46E-02	3.18E-01	2.92E+05	126.428
118	24.1	0.296	14.8	1.74	1.52	1.52	2.64	0	0.436	0.544	3.87E-04	1.89E-03	2.24E-03	7.30E-05	5.92E-03	2.92E+05	126.428
119	24.1	0.296	14.8	1.74	1.52	1.52	2.64	0	0.290	0.808	4.21E-04	4.92E-03	3.99E-03	6.08E-05	1.05E-02	2.92E+05	126.428
120	24.1	0.330	15.4	1.74	1.52	1.52	2.64	0	0.467	0.622	2.68E-04	8.51E-04	2.40E-03	1.13E-06	6.33E-03	2.92E+05	126.428
121	24.1	0.330	15.4	1.74	1.52	1.52	2.64	0	0.329	0.879	4.09E-04	3.47E-03	4.26E-03	1.37E-05	1.13E-02	2.92E+05	126.428
122	24.1	0.330	15.4	1.74	1.52	1.52	2.64	0	0.346	0.717	3.16E-04	3.27E-03	6.83E-03	7.90E-05	1.80E-02	2.92E+05	126.428
123	23.2	0.317	15.4	1.74	1.52	1.52	2.64	0	0.448	0.569	7.19E-04	2.51E-03	2.86E-03	1.14E-04	7.55E-03	2.92E+05	126.428
124	23.2	0.317	15.4	1.74	1.52	1.52	2.64	0	0.309	0.845	4.02E-04	4.59E-03	4.07E-03	1.66E-04	1.07E-02	2.92E+05	126.428
125	23.2	0.317	15.4	1.74	1.52	1.52	2.64	0	0.346	0.711	3.20E-04	3.15E-03	8.14E-03	1.56E-04	2.15E-02	2.92E+05	126.428
126	23.2	0.358	15.4	1.74	1.52	1.52	2.64	0	0.436	0.544	7.49E-04	3.29E-03	3.35E-03	2.82E-04	8.85E-03	2.92E+05	126.428
127	23.2	0.358	15.4	1.74	1.52	1.52	2.64	0	0.290	0.808	4.75E-04	5.43E-03	4.28E-03	4.60E-04	1.13E-02	2.92E+05	126.428
128	7.3	0.337	5.2	1.20	1.7	11	13.2	0	0.150	1.192	1.91E-03	4.13E-03	1.30E-03	4.00E-04	1.72E-02	1.44E+07	768.021
129	3.5	0.167	2.8	1.90	1.4	7	13.3	0	0.150	1.192	3.57E-03	2.38E-03	1.00E-03	4.00E-04	1.33E-02	1.36E+07	1387.04
130	2.3	0.135	2.1	1.90	1.14	7	13.3	0	0.150	1.192	4.00E-03	2.68E-03	1.18E-03	4.50E-04	1.57E-02	1.34E+07	1683.71
131	7.3	0.337	5.2	1.20	1.7	11	13.2	0	0.500	13.240	3.18E-03	1.71E-02	4.17E-03	1.04E-03	5.50E-02	1.44E+07	768.021
132	3.5	0.167	2.8	1.90	1.4	7	13.3	0	0.500	13.240	8.57E-03	1.71E-02	3.96E-03	1.04E-03	5.27E-02	1.36E+07	1387.04
133	2.3	0.135	2.1	1.90	1.14	7	13.3	0	0.500	13.240	1.00E-02	2.78E-01	4.38E-03	1.77E-03	5.83E-02	1.34E+07	1683.71
134	7.3	0.337	5.2	1.20	1.7	11	13.2	0	0.500	26.400	6.82E-03	5.82E-02	1.82E-02	3.64E-03	2.40E-01	1.44E+07	768.021
135	3.5	0.167	2.8	1.90	1.4	7	13.3	0	0.500	26.400	1.33E-02	9.01E-02	1.82E-02	1.82E-03	2.42E-01	1.36E+07	1387.04
136	2.3	0.135	2.1	1.90	1.14	7	13.3	0	0.500	26.400	1.53E-02	8.06E-02	1.73E-02	9.10E-04	2.30E-01	1.34E+07	1683.71
137	3.3	0.167	2.8	1.90	1.4	7	13.3	0	0.370	0.540	4.14E-03	2.13E-03	4.94E-03	1.18E-03	6.57E-02	1.36E+07	1387.76
138	6.9	0.337	5.2	1.20	1.7	11	13.2	0	0.370	0.540	2.45E-03	2.23E-03	3.80E-03	2.40E-04	5.02E-02	1.44E+07	770.053

Event No	FSv	Cr	A/Ac	h/L	B(m)	L (m)	hcg (m)	D(m)	a_max (g)	Ia (m/s)	Sn (-)	En (-)	θmax (rad)	θperm (rad)	Δmax (m)	Pst or V (N)	q(kPa)
139	3.3	0.167	2.8	1.90	1.4	7	13.3	0	0.460	2.410	4.57E-03	7.90E-03	6.91E-03	1.45E-03	9.19E-02	1.36E+07	1387.76
140	6.9	0.337	5.2	1.20	1.7	11	13.2	0	0.460	2.410	1.00E-03	8.05E-03	3.45E-03	1.09E-03	4.55E-02	1.44E+07	770.053
141	6.9	0.337	5.2	1.20	1.7	11	13.2	0	0.820	7.600	5.27E-03	2.52E-02	2.71E-02	7.14E-03	3.58E-01	1.44E+07	770.053
142	3.3	0.167	2.8	1.90	1.4	7	13.3	0	0.820	7.600	2.00E-02	3.15E-02	2.43E-02	1.29E-02	3.23E-01	1.36E+07	1387.76

APPENDIX B. CALCULATION OF CIM PARAMETERS FOR SHEAR WALL

As an example, to illustrate the use of notations, Equation 4.1 – 4.23 are worked out for the following shear wall – footing model; L = 2.8m, B = 0.65m, D = 0.7m, $\Phi = 42^{\circ}$, γ = 16.255 kN/m^3 and the total vertical load acting on the footing is 569kN

Using Equation 4.1, Equation 4.2 (for dry sand) and also from 4.4 – 4.15, the value of N_q = 85.38; N_γ = 155.55; F_{qs} = 1.21; $F_{\gamma s}$ = 0.91; F_{qd} = 1.16; $F_{\gamma d}$ = 1 are obtained. Therefore, value of ultimate bearing capacity V_{ult} is computed as 4091kN. Using the Equation 4.16, factor of safety is calculated as 7.19 which matches with the experimental value that is FSv = 7.2.

The vertical and horizontal stiffness are calculated using the Equation 4.17 – Equation 4.23. The value of d is 0.7m and the value of h is 0.35m, and the value of $K_{2,max}$ is interpolated using the relative density and obtained as 62.67. Therefore, the shear modulus is computed as 92.51 MN/m^2 and the value of Kv and Kh are 856 MN/m and 813 MN/m respectively. The other CIM parameters Rv and deltaL are considered as 0.1 and 0.01 respectively.

APPENDIX C. OPENSEES CODE USED FOR VALIDATION OF SHEAR WALL

The following OpenSees code is used for the validation of shear wall model,

```
#validation of SSG04---- Sujitha
#T2-Gajan and Kutter, 2008
#units in N, m, sec, kg
#---------wipe out everything---------
wipe

#input dimension and DOF
model BasicBuilder -ndm 2 -ndf 3

set time 3102
set interval 0.00488
set pi [expr acos(-1)]

#strcutural properties (Shear wall)------------------------------------------------------------
set E 69e+9
set I 0.495
set A 0.95
set Hcg 5.039

#CIM parameters--------------------------------------------------------------------
set Rv 0.1
set delL 0.01
set L 2.8
set B 0.65
set Df 0
set Mtot 36800
set Vtot [expr $Mtot*9.81]
set rho 1657
set gamma [expr $rho*9.81]
set phi 42.4
set c 0
source FSv.txt

#stiffness calculation-------------------------------------------------------------
set gamma [expr $rho*9.81/1000]
set k 62.67
set nu 0.4
source stiffness_embed.txt

#define nodes and elements---------------------------------------------------
node 1 0 0
node 2 0 0
```

```
node 3 0 $Hcg

#elements
geomTransf Linear 1
section soilFootingSection2d 1 $FSv $Vult $L $kvembed $khembed $Rv $delL
element zeroLengthSection 1 1 2 1 -orient 0 -1 0 1 0 0
#rigid shear wall
element elasticBeamColumn 2 2 3 [expr $A*4] [expr $E*4] [expr $I*5] 1

#Boundary conditions
fix 1 1 1 1
fix 2 1 0 0
fix 3 0 0 0

#Static analysis starts----------------------------------------------------------
pattern Plain 1 Linear {load 3 0 -$Mtot 0}

test NormDispIncr 1e-10 800 1
algorithm Newton
system UmfPack
constraints Plain
numberer Plain
analysis Static
analyze 10

#recorders----------------------------------------------------------------------
set name "node"
for {set n 1} {$n <=3} {incr n 1} {
set fileName [join [list $name $n] {}]
recorder Node -file $fileName -node $n -dof 1 2 3 disp
}
set name "element"
for {set n 1} {$n <=2} {incr n 1} {
set fileName [join [list $name $n] {}]
recorder Element -file $fileName -time -ele $n force
}

#set time back to zero again before shaking
loadConst -time 0.0

#wipe gravity analysis objects
wipeAnalysis
puts "-------------End of static analysis-------------"

#dynamic analysis----------------------------------------------------------------
mass 3 $Mtot 0 0
```

```
test NormDispIncr 1e-12 1 1
algorithm Newton
system UmfPack
constraints Plain
numberer RCM
integrator Newmark 0.5 0.25
analysis VariableTransient
#Rayleigh damping for ED-------------------------------------------------------
source "Damping.txt"
rayleigh $alphaM $betaK $betaKinit $betaKcomm
#define ground motion characteristics
set dT $interval
set dTmin [expr $dT/150]
set dTmax $dT

#input-accleration-time history
set Series "Path -filePath input_motion.txt -dt $dT -factor 9.81"

#acceleration is applied in the fixed base node in the horizontal direction----------
pattern UniformExcitation 2 1 -accel $Series

set steps $time
set itr 500
for {set i 1} {$i < $steps} {incr i 1} {
test EnergyIncr 1e-5 $itr 0
set ok [analyze 1 $dT $dTmin $dTmax $itr]
if {$ok !=0} {
test EnergyIncr 1e-4 $itr 0
set ok [analyze 1 $dT $dTmin $dTmax $itr]
}
}
puts "------------------End of dynamic analysis-------------------------"

#print final node and element output on screen
for {set n 1} {$n <= 3} {incr n 1} {
print node $n
}
print ele
wipe
puts "------------cleared all----------------"
```

Damping.txt

```
puts "Damping is being applied"
set xDamp 0.05
```

```
set lambda [eigen -fullGenLapack 1]
puts "---lambda =$lambda---"
set omega {}
set f {}
set T {}
set pi [expr acos(-1)]
foreach lam $lambda {
lappend omega [expr pow($lam,0.5)]
lappend f [expr sqrt($lam)/(2*$pi)]
lappend T [expr (2*$pi)/(pow($lam,0.5))]
}
puts "---Tn = $T secs---"
set alphaM 0.0
set betaK 0
set betaKcomm [expr 2*$xDamp/$omega]
puts "-----betaKcomm $betaKcomm--------"
set betaKinit 0
```

APPENDIX D. OPENSEES CODE FOR BRIDGE-PIER MODEL VALIDATION

The OpenSees code used for bridge-pier validation is given below,

```
#validation of LJD01--- Sujitha
#units in N, m, sec, kg
#---------wipe out everything---------
wipe

#input dimension and DOF
model BasicBuilder -ndm 2 -ndf 3

#specify nodes
set hcg 10.31

node 1 0 0
node 2 0 0
node 3 0 $hcg

#local to global coordinates
geomTransf Linear 1

#input CIM details
#----------CIM---------
# 7 user defined paramters--FSv, Vult, L, kv, kh, Rv, del L
set L 6.698
set B 4.283
set Df 2.24

set Mdeck 515303
set Mfoot 96472
set Mtot [expr $Mdeck+$Mfoot]
set Vtot [expr $Mtot*9.81]

set rho 1655.8
set gamma [expr $rho*9.81]
set phi 36
set pi [expr acos(-1)]

source FSv.txt
set gamma 16.243
set k 58.07
set nu 0.4
source stiffness_embed.txt

set Rv 0.1
```

```
set delL 0.01
puts "CIM analysis starts"
section soilFootingSection2d 1 $FSv $Vult $L $kvembed $khembed $Rv $delL
puts "Ultimate V = $Vult"
#soil material, element (ZLS) - default
element zeroLengthSection 1 1 2 1 -orient 0 -1 0 1 0 0

#Bridge-column element (elastic BC)
set A 1.75
set E 6.9e+10
set I 0.51
element elasticBeamColumn 2 2 3 $A $E $I 1

#bottom end of CIM is fixed
fix 1 1 1 1
fix 2 1 0 0
fix 3 0 0 0


#define gravity loads
pattern Plain 1 Linear {
load 3 0 -$Mtot 0
}

#define analysis
test NormDispIncr 1e-8 40 1
algorithm Newton
system SparseGeneral
constraints Plain
numberer Plain
analysis Static
analyze 10

#recorders
set name "node"
for {set n 1} {$n <=3} {incr n 1} {
set fileName [join [list $name $n] {}]
recorder Node -file $fileName -node $n -dof 1 2 3 disp
}

set name "element"
for {set n 1} {$n <=2} {incr n 1} {
set fileName [join [list $name $n] {}]
recorder Element -file $fileName -time -ele $n force
}
```

```
#set time back to zero again before shaking
loadConst -time 0.0

#wipe gravity analysis objects
wipeAnalysis

puts "Dynamic analysis starts"
#define mass at node 3 in direction 1 (for seismic loading)
mass 3 $Mtot 0 0

#analysis objects for seismic loading
test EnergyIncr 1e-4 20 1
algorithm Newton
system UmfPack
constraints Plain
numberer RCM
integrator Newmark 0.5 0.25
analysis VariableTransient

#Rayleigh damping for ED
source "Damping.txt"
rayleigh $alphaM $betaK $betaKinit $betaKcomm


#define ground motion characteristics
set dT 0.0059805
set dTmin [expr $dT/150]
set dTmax $dT

#input-accleration-time history
set Series "Path -filePath input_motion.txt -dt $dT -factor 9.81"

#acceleration is applied in the fixed base node in the horizontal direction
pattern UniformExcitation 2 1 -accel $Series

#apply shaking
set steps 4182
set itr 90

for {set i 1} {$i < $steps} {incr i 1} {
test EnergyIncr 5e-4 $itr 0
set ok [analyze 1 $dT $dTmin $dTmax $itr]

if {$ok !=0} {
test EnergyIncr 1e-4 $itr 0
set ok [analyze 1 $dT $dTmin $dTmax $itr]
```

```
}
}

#print final node and element output on screen

for {set n 1} {$n <= 3} {incr n 1} {
print node $n
}

print ele

#--------all done (wipe out)---------
wipe
```

stiffness_embed.txt

```
# calculation of Kv and Kh -- Sujitha

set d $Df
set h [expr $Df/2]

#calculation of shear modulus

set sigma1 [expr $Vtot/($B*$L)]
set sigma [expr $sigma1/1000]


set G [expr 218.8*$k*pow($sigma,0.5)]
puts "------Shearmodulus = $G in kN/m2------"

#calculate stiffness
set kh [expr (($G*$B)/(2-$nu))*((3.4*pow(($L/$B),0.65))+1.2)]
set kv [expr (($G*$B)/(1-$nu))*((1.55*pow(($L/$B),0.75))+0.8)]

set betah [expr (1+(0.21*sqrt($Df/$B)))*(1+1.6*pow((($h*$d*($B+$L))/($B*$L*$L)),0.4))]

set tempv [expr ($d*($B+$L))/($B*$L)]
set tempv2 [expr pow($tempv,(0.67))]
set betav [expr (1+(($Df/(21*$B))*(2+(2.6*$B/$L))))*(1+(0.32*$tempv2))]

#embeded stiffness
set khembed [expr $kh*$betah*1000]
set kvembed [expr $kv*$betav*1000]

puts "------Kvembed = [expr $kvembed/1e+6] in MN/m-----"
```

```
puts "-----Khembed = [expr $khembed/1e+6] in MN/m-----"
```

APPENDIX E. THE SUMMARISED DATA OF G, K_v, K_h, BEARING PRESSURE OF STRUCTURE (q_b) FOR ALL THE EVENTS USED FOR THE ANALYSIS

Event No	q_b(kPa)	γ(kN/m3)	G (kN/m^2)	K_v (MN/m)	K_h (MN/m)
Shear wall model					
1	312.637	16.255	92509	856	813
2	312.637	16.255	92509	856	813
3	312.637	16.255	92509	856	813
4	198.352	16.255	92509	856	813
5	198.352	16.255	92509	856	813
6	198.352	16.255	92509	856	813
7	312.637	16.255	92509	545	375
8	312.637	16.255	92509	545	375
9	198.352	16.255	92509	545	375
10	198.352	16.255	92509	545	375
11	198.352	16.255	92509	545	375
Bridge-pier model					
12	230.82	16.243	132549	3660	3931
13	230.82	16.243	132549	3660	3931
14	230.82	16.243	132549	3660	3931
15	230.82	16.243	132549	3660	3931
16	230.82	16.243	132549	3660	3931
17	230.82	16.243	132549	3660	3931
18	198.524	15.018	89193	2657	2802
19	198.524	15.018	89193	2657	2802
20	198.524	15.018	89193	2657	2802
21	198.524	15.018	89193	2657	2802
22	198.524	15.018	89193	2657	2802
23	198.524	15.018	89193	2657	2802
24	198.524	15.018	89193	2657	2802
25	198.524	15.018	89193	2657	2802
26	198.524	15.018	89193	2657	2802
27	198.524	15.018	89193	2657	2802
28	198.524	15.018	89193	2657	2802
29	198.524	15.018	89193	2657	2802
30	198.524	15.018	89193	2657	2802
31	198.524	15.018	89193	2657	2802
32	198.524	15.018	89193	2657	2802
33	198.524	15.018	89193	2657	2802
34	198.524	15.018	89193	2657	2802
35	65.7504	19.163	11800	172.9	148.1
36	65.7504	19.163	11800	172.9	148.1

Event No	q_b(kPa)	γ(kN/m3)	G (kN/m^2)	K_v (MN/m)	K_h (MN/m)
37	65.7504	19.163	11800	172.9	148.1
38	65.7504	19.163	11800	172.9	148.1
39	65.7504	19.163	11800	172.9	148.1
40	131.483	19.163	14000	410.4	351.4
41	32.676	19.163	10600	77.9	66.68
42	32.676	19.163	10600	77.9	66.68
43	32.676	19.163	10600	77.9	66.68
44	65.7504	19.163	11800	172.9	148.1
45	65.7504	19.163	11800	172.9	148.1
46	65.7504	19.163	11800	172.9	148.1
47	32.3327	19.163	11800	215	182.6
48	32.3327	19.163	11800	215	182.6
49	32.3327	19.163	11800	215	182.6
50	32.3327	19.163	11800	215	182.6
51	32.3327	19.163	11800	215	182.6
52	64.4213	19.163	14000	511.26	434.17
53	16.2145	19.163	10600	96.5	81.94
54	16.2145	19.163	10600	96.5	81.94
55	16.2145	19.163	10600	96.5	81.94
56	32.3327	19.163	11800	215	182.6
57	32.3327	19.163	11800	215	182.6
58	32.3327	19.163	11800	215	182.6
59	15.4089	15.784	23567	13.845	10.163
60	15.4089	15.784	23567	13.845	10.163
61	15.4089	15.784	23567	13.845	10.163
62	15.4089	15.784	23567	13.845	10.163
63	15.4089	15.784	23567	13.845	10.163
64	15.4089	15.784	23567	13.845	10.163
65	15.4089	15.784	23567	13.845	10.163
66	15.4089	15.784	23567	13.845	10.163
67	15.4089	15.784	23567	13.845	10.163
68	15.4089	15.784	23567	13.845	10.163
69	15.4089	15.784	23567	13.845	10.163
70	15.4089	14.205	13733	8.068	5.923
71	15.4089	14.205	13733	8.068	5.923
72	15.4089	14.205	13733	8.068	5.923
73	15.4089	14.730	17065	10.026	7.359
74	15.4089	14.730	17065	10.026	7.359
75	15.4089	14.730	17065	10.026	7.359
76	15.4089	14.730	17065	10.026	7.359
77	15.4089	14.730	17065	10.026	7.359
78	15.4089	14.730	17065	10.026	7.359

Event No	q_b(kPa)	γ(kN/m3)	G (kN/m^2)	K_v (MN/m)	K_h (MN/m)
79	15.4089	14.730	17065	10.026	7.359
80	15.4089	14.730	17065	10.026	7.359
81	15.4089	14.730	17065	10.026	7.359
82	15.4089	14.730	17065	10.026	7.359
83	15.4089	14.730	17065	10.026	7.359
84	15.4089	14.205	13733	8.068	5.923
85	15.4089	14.205	13733	8.068	5.923
86	15.4089	14.205	13733	8.068	5.923
87	15.4089	14.205	13733	8.068	5.923
88	15.4089	14.205	13733	8.068	5.923
89	15.4089	14.205	13733	8.068	5.923
90	43.8222	15.784	23567	13.845	10.163
91	43.8222	15.784	23567	13.845	10.163
92	43.8222	15.784	23567	13.845	10.163
93	43.8222	15.784	23567	13.845	10.163
94	43.8222	15.784	23567	13.845	10.163
95	43.8222	15.784	23567	13.845	10.163
96	43.8222	14.823	17726	10.414	7.644
97	43.8222	14.823	17726	10.414	7.644
98	43.8222	15.130	19339	11.36	8.339
99	43.8222	15.130	19339	11.36	8.339
100	43.8222	15.130	19339	11.36	8.339
101	43.8222	15.130	19339	11.36	8.339
102	43.8222	15.130	19339	11.36	8.339
103	43.8222	15.130	19339	11.36	8.339
104	43.8222	14.823	17726	10.414	7.644
105	43.8222	14.823	17726	10.414	7.644
106	43.8222	14.823	17726	10.414	7.644
107	43.8222	14.823	17726	10.414	7.644
108	126.428	18.194	80543	479.5	351.98
109	126.428	18.194	80543	479.5	351.98
110	126.428	18.194	80543	479.5	351.98
111	126.428	18.194	80543	479.5	351.98
112	126.428	18.194	80543	479.5	351.98
113	126.428	18.194	80543	479.5	351.98
114	126.428	18.194	80543	479.5	351.98
115	126.428	18.194	80543	479.5	351.98
116	126.428	18.194	80543	479.5	351.98
117	126.428	18.194	80543	479.5	351.98
118	126.428	18.194	80543	479.5	351.98
119	126.428	18.194	80543	479.5	351.98
120	126.428	18.194	80543	479.5	351.98

Event No	q_b(kPa)	γ(kN/m3)	G (kN/m^2)	K_v (MN/m)	K_h (MN/m)
121	126.428	18.194	80543	479.5	351.98
122	126.428	18.194	80543	479.5	351.98
123	126.428	18.194	80543	479.5	351.98
124	126.428	18.194	80543	479.5	351.98
125	126.428	18.194	80543	479.5	351.98
126	126.428	18.194	80543	479.5	351.98
127	126.428	18.194	80543	479.5	351.98
128	768.021	15.497	189486	3805.6	2545.7
129	1387.04	15.497	151158	2110.1	1438.8
130	1683.71	15.497	151158	1966.2	1320.5
131	768.021	15.497	189486	3805.6	2545.7
132	1387.04	15.497	151158	2110.1	1438.8
133	1683.71	15.497	151158	1966.2	1320.5
134	768.021	15.497	189486	3805.6	2545.7
135	1387.04	15.497	151158	2110.1	1438.8
136	1683.71	15.497	151158	1966.2	1320.5
137	1387.76	15.497	151158	2110.1	1438.8
138	770.053	15.497	189486	3805.6	2545.7
139	1387.76	15.497	151158	2110.1	1438.8
140	770.053	15.497	189486	3805.6	2545.7
141	770.053	15.497	189486	3805.6	2545.7
142	1387.76	15.497	151158	2110.1	1438.8